PREPARATION AND CHARACTERIZATION OF PLASMA-FLUORINATED EPITAXIAL GRAPHENE

A Thesis
Presented to
The Academic Faculty

by
Sonam Dorje Sherpa

In Partial Fulfillment
of the Requirements for the Degree
Doctor of Philosophy in Chemical Engineering in the
School of Chemical and Biomolecular Engineering

Georgia Institute of Technology
May 2013

PREPARATION AND CHARACTERIZATION OF PLASMA-FLUORINATED EPITAXIAL GRAPHENE

Approved by:

Dr. Dennis W. Hess, Adviser
School of Chemical and Biomolecular Engineering
Georgia Institute of Technology

Dr. Elsa Reichmanis
School of Chemical and Biomolecular Engineering
Georgia Institute of Technology

Dr. Elisa Riedo
School of Physics
Georgia Institute of Technology

Dr. Michael A. Filler
School of Chemical and Biomolecular Engineering
Georgia Institute of Technology

Dr. Samuel Graham
School of Mechanical Engineering
Georgia Institute of Technology

Dr. Michael D. Williams
Department of Physics
Clark Atlanta University

Date Approved: March 5, 2013

ACKNOWLEDGEMENTS

My father firmly believed in the precedence of academic accomplishments and service to the society over the accumulation of wealth. It was his unwavering belief that inspired me toward a graduate school in lieu of more lucrative careers after completing my undergraduate studies in chemical engineering. Likewise, his emphasis on the value of delayed gratification enabled me to persevere when I was frustrated at the lack of progress during the various stages of my graduate research. I also take this opportunity to thank my mother for her unconditional love and invaluable life-lessons. Without the love, support, and guidance of my parents, I could not have succeeded in my academic endeavors. I am grateful to my parents for their sacrifices in raising me and my siblings in an environment that allowed us to fulfill our potential. Like every family, we have had our share of good and bad times. Grace and serenity with which my parents have faced the adversities of life has infused me with an indefatigable spirit that all challenges in life can be surmounted regardless of how bleak the situation may seem. As I approach the completion of my doctoral studies, I would like to tell my parents something that I have never had a chance to tell them personally

Your struggle is my strength

In the ten years I have been in the United States, I have experienced a lot of changes and I have realized that family is the only thing that stays constant in a life that changes so quickly. My siblings have always been an integral part of my life even though I have been away from home for more than a decade. We have been together through thick and thin of life and this thesis belongs to them as much as it belongs to me.

I express my sincere gratitude toward my thesis adviser, Dr. Dennis W. Hess, for giving me an opportunity to perform doctoral research under his supervision. His guidance and boundless

support encouraged me to explore diverse research topics without any fear of failure. I thank him specifically for his patience and enthusiasm in my growth as a scientist. I am also grateful to Dr. Galit Levitin for her support throughout my graduate education. Initial phase of graduate research is an overwhelming experience and I appreciate her assistance in getting me started with my thesis project. I cannot thank her enough for her insights and encouragement during the latter stages of my research and I continue to benefit from her career-related advices. Many thanks to Lester Li, Michael Casciatio, Tae-Seop Choi, and Zhenguan Tang for creating a friendly and jovial work environment. Former group members, Ashish Pande and Fangyu Wu, shared their experiences as graduate students and advised me on how to succeed in graduate school.

I am pleased to thank Baiqian Zhang and Andrei Savu from Walt de Heer group in School of Physics at Georgia Tech for their efforts in growing graphene samples for my studies. My first publication could not have been possible without Baiqian's kind cooperation. I learned a lot about graphene through interaction with the MRSEC community at Georgia Tech and some of the ideas for my research originated from the discussions during journal club meetings and seminars.

I would not have been able to perform a bulk of the studies that are described in this thesis without Walt Henderson's tireless efforts to maintain XPS/UPS system (Axis UltraDLD, Kratos Analytical) and XPS system (Thermo Scientific K-Alpha). I am also appreciative of the cleanroom staff for their efforts in ensuring the smooth operation of Plasma-Therm RIE and other equipments that were important for my research.

Finally, I would like to acknowledge my beautiful fiancée Nawang Chonzom Lama. Her presence in my life has been a blessing. She is my hope of a better tomorrow and I dedicate this thesis to the parts and parcels of life that await us.

TABLE OF CONTENTS

LIST OF TABLES

LIST OF FIGURES

LIST OF SYMBOLS AND ABBREVIATIONS

EG	Epitaxial graphene
GNR	Graphene nanoribbon
CNT	Carbon nanotube
HOPG	Highly oriented pyrolytic graphite
IUPAC	International Union of Pure and Applied Chemistry
GO	Graphene oxide
CVD	Chemical vapor deposition
QHE	Quantum Hall effect
FET	Field effect transistor
ALD	Atomic layer deposition
UHV	Ultra-high vacuum
CCS	Confinement-controlled sublimation
RIE	Reactive ion etch
RF	Radio frequency
XPS	X-ray photoelectron spectroscopy

UPS	Ultra-violet photoelectron spectroscopy
AFM	Atomic force microscopy
SKPM	Scanning Kelvin probe microscopy
LEED	Low energy electron diffraction
STM	Scanning tunneling microscopy
ITO	Indium tin oxide
OLED	Organic light emitting diode
SAM	Self-assembled monolayer
HUMO	Highest occupied molecular orbital
LUMO	Lowest occupied molecular orbital
HIB	Hole-injection barrier
E_F	Fermi energy
Φ	Work function
PTFE	Polytetrafluoroethyelene

SUMMARY

Fluorination of graphene enables control of its physical, chemical, and electronic properties. This thesis describes the results of our investigation of the fluorination of graphene using reactive ion etch (RIE) plasma and our subsequent efforts to elucidate the factors that control the work function of fluorinated graphene.

Our initial studies, described in chapter two, demonstrated the viability of sulfur hexafluoride plasmas to fluorinate epitaxial graphene (graphene grown on silicon carbide) as a safer alternative to the commonly reported techniques of fluorination that include exposures to fluorine and xenon difluoride gas. Incorporation of fluorine moieties on epitaxial graphene after SF_6 plasma-treatment was confirmed by x-ray photoelectron spectroscopy. Increase in work function of plasma-treated epitaxial graphene was determined by ultra-violet photoelectron spectroscopy. Raman spectroscopy and low-energy electron diffraction characterization of fluorinated epitaxial graphene suggest that the framework of sp^2-hybridized carbon atoms remains intact after the plasma-treatment.

Our earlier studies on the plasma-fluorination of epitaxial graphene revealed an increase in the work function of epitaxial graphene after an SF_6 plasma-treatment; however, the increase in work function did not correlate with the fluorine concentration. In chapter three, the findings of our subsequent investigation to controllably modify the work function of epitaxial graphene are described; we discovered that the work function of fluorinated epitaxial graphene is controlled by the polarity of carbon-fluorine bonds which depends upon the nature of the chemical bonds (ionic, semi-ionic, or covalent) between fluorine and carbon atoms.

Even though the dependence of the work function of fluorinated graphene on the polarity of carbon-fluorine bonds was established, the factors that determine the polarity of carbon-fluorine

bonds in fluorinated graphene were not apparent. Therefore, further studies to investigate the effect of the surface topography of epitaxial graphene on the work function of plasma-fluorinated epitaxial graphene were performed using scanning Kelvin probe microscopy (SKPM). In chapter four, the results of SKPM characterization of plasma-fluorinated epitaxial graphene are described; these results demonstrated that the increase in the work function of epitaxial graphene after plasma-treatment is independent of its surface topography. Surface damage due to the plasma-treatment is negligible, but the non-uniform fluorination may result from non-uniformities in plasma density.

The work described in this thesis has established plasma technology as a facile approach for the chemical functionalization of graphene without the disruption of its lattice and surface topography. The work function of graphene can be modified via plasma-fluorination and the increase in its work function depends upon the polarity of carbon-fluorine bonds in addition to its fluorine concentration.

CHAPTER 1: INTRODUCTION

1.1 Overview of graphene

Graphene is a single layer of sp^2-hybridized carbon atoms arranged in a hexagonal lattice. Graphene is therefore a 2D building block for graphitic material of all other dimensions as shown in Figure 1; that is, it is an unwrapped form of 0D fullerenes and an unrolled form of a 1D carbon nanotube (CNT) and more commonly known graphite (3D) is simply a stack of graphene monolayers.

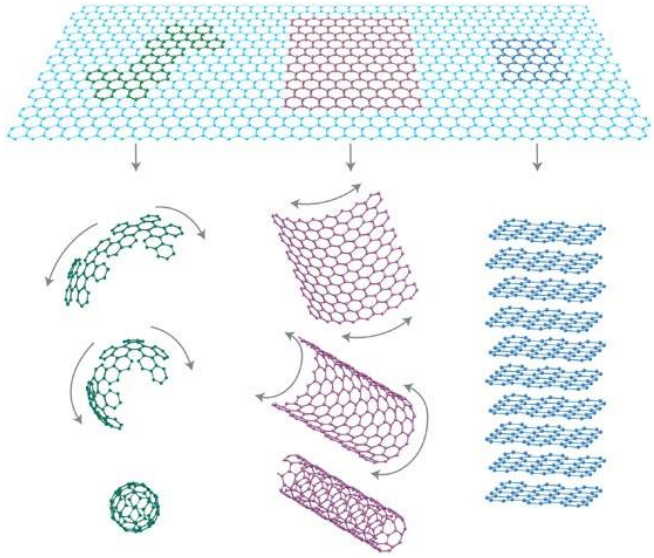

Fullerene (0D) CNT (1D) Graphite (3D)

Figure 1: Graphene as a 2D building block for graphitic materials of other dimensions[1]

As a result of sp^2 hybridization, each carbon atom in graphene contains three sp^2 orbitals and one π orbital. Each carbon atom in graphene is bonded to three neighboring carbon atoms via a σ bond between the sp^2 orbitals and bond length between the two carbon atoms in graphene is ~ 1.42 Å. The remaining π orbital contributes to a network of delocalized electrons as shown in Figure 2.

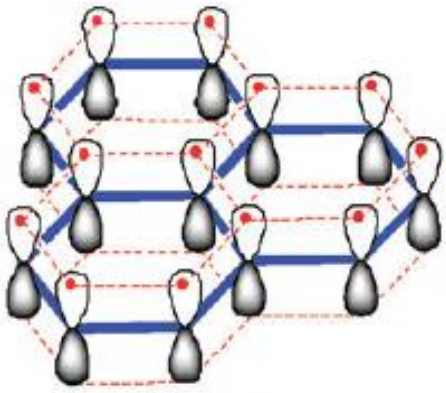

Figure 2: π-bonding system in graphene[2]

Prior to 1985, the term “graphene" has been used rather indiscriminately to refer to various materials that resemble graphitic structures. In 1985, a report published by a subgroup of the International Committee for Characterization and Terminology of Carbon and Graphite recommended the standardization of the term “graphene” — “the ending -ene is used for fused polycyclic aromatic hydrocarbons, even when the root of the name is of trivial origin, for example, naphthalene, anthracene, tetracene, coronene, ovalene. A single carbon layer of the graphitic structure would be the final member of infinite size of this series. The term graphene layer should be used for such a single carbon layer.[3]” In 1997, The International Union of Pure and Applied Chemistry (IUPAC) formalized these recommendations by incorporating them into their Compendium of Chemical Technology — “previously, descriptions such as graphite layers, carbon layers or carbon sheets have been used for the term graphene. Because graphite designates that modification of the chemical element carbon, in which planar sheets of carbon atoms, each atom bound to three neighbors in a honeycomb-like structure, are stacked in a three-dimensional regular order, it is not correct to use for a single layer a term which includes the term graphite, which would imply a three- dimensional structure. The term graphene should be

used only when the reactions, structural relations or other properties of individual layers are discussed.[4]"

1.2 History of graphene

In 1947, Wallace described the structure of the electronic energy bands and Brillouin zones for graphite by using graphene, which is referred as "single hexagonal layer" in his article, as a theoretical building block[5]. The first experimental observation of a material similar to graphene was reported in 1962 when Boehm et al. discovered that the chemical reduction of dispersions of graphite oxide in dilute alkaline media with hydrazine, hydrogen sulfide, or iron(II) salts resulted in thin, lamellar carbonaceous material that contained only small amounts of hydrogen and oxygen[6]. The number of layers in the lamellae was measured by densitometry against a set of standardized films of known thicknesses using transmission electron microscopy (TEM). The carbonaceous material exhibited a minimum thickness of 4.6 Å. Although the variations in thickness of the calibration standards and unevenness in the photographic emulsions contributed to a high degree of experimental error in the aforementioned electron-micrograph densitometry measurements, Boehm et al. concluded: "this observation confirms the assumption that the thinnest of the lamellae really consisted of single carbon layers.[6]" In 1968, Morgan and Somorjai investigated the adsorption of various gaseous organic molecules such as CO, C_2H_4, and C_2H_2 onto a Pt (100) surface at high temperature by using low energy electron diffraction (LEED)[7]. One year later, May analyzed these LEED patterns and proposed that single as well as multiple layers of a material that possess a graphitic lattice were present on the surface as a result of these adsorption processes[8]. Between 1970 and 1980, Blakely et al. reported an extensive series of studies on the surface segregation of single and multiple layers of carbon atoms from various crystalline faces of transition-metal substrates[9–11] such as Ni (100) and (111), Pt (111), Pd (100), and Co (0001). High temperature treatment resulted in the phase separation of the carbon atoms dissolved in these metals to form single or multiple layers of carbon atoms on the surface as

determined by LEED, Auger electron spectroscopy, and scanning tunneling microscopy (STM). In 1975, Van Bommel et al. reported that the surfaces of SiC (0001) are covered with a layer of graphite due to evaporation of silicon during the heat treatment [12]. At high temperatures under ultrahigh vacuum conditions ($P \approx 10^{-10}$ Torr), single-layered flakes of carbon atoms with graphitic structure were obtained as determined by LEED and Auger electron spectroscopy. Surface structure of SiC is preserved at temperatures below 800 °C whereas an increase in the temperature resulted in the appearance of "graphite rings" in the LEED pattern. Prior to the work of Van Bommel, Badami in 1965 had proposed that the three layers of residual carbon atoms collapse onto one another upon sublimation of the silicon to effectively form graphitic sheets[13]. This model is supported by x-ray diffraction studies that determined the C-C distance to be ~ 1.85 Å when only one or two layers of carbon atoms and ~ 1.42 Å upon the collapse of the third layer. This measurement is consistent with both theoretically and experimentally determined C-C bond lengths (1.41–1.43 Å) in graphene.

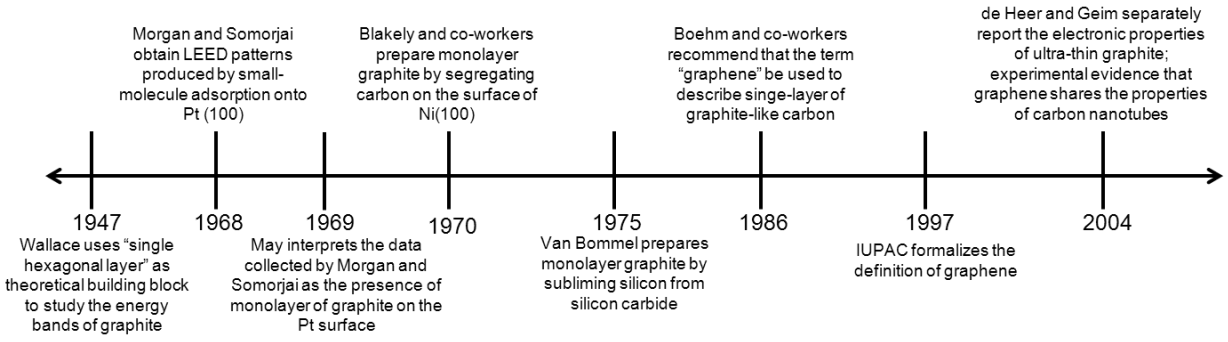

Figure 3: Timeline of major events in the history of graphene (adapted from Ref 14)

Although the inadvertent observations of graphene or graphene-like materials had been reported, the usefulness of graphene until 2004 was limited to being a theoretical building block used to study graphitic material of other dimensions (please see Figure 3 for the timeline of the major

events in the history of graphene[14]). Graphene began to attract the interest of the scientific community after Walt A. de Heer (Georgia Institute of Technology, USA) and Andrei Geim (University of Manchester, England) separately reported the results of their studies on the electronic properties of the ultra-thin graphite films. In 2004, de Heer et al. demonstrated the two-dimensional nature of electron transport in the ultra-thin graphite films (~ 3 atomic layers) grown by thermal decomposition on the (0001) surface of 6H-SiC and established the potential of these films as a new quantum Hall system[15] — quantum Hall effect (QHE) is the quantization of the Hall voltage (labeled as V_H in Figure 4) which is the potential created across a current-carrying electrical conductor when the conductor is placed in a magnetic field perpendicular to the current flow in the conductor.

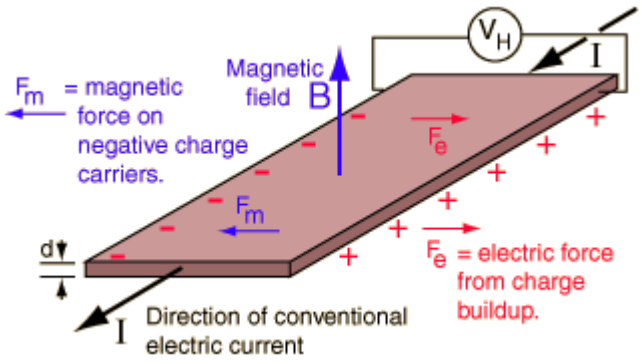

Figure 4: Schematic diagram of the Hall effect[16]

The same year, Geim et al. reported the electric field effect in ultra-thin graphite flakes (thickness down to few atomic layers including single-layer graphene)[17]. These flakes were prepared by mechanical exfoliation (repeated peeling with scotch-tape) of small mesas of highly oriented pyrolytic graphite (HOPG). In this work, Geim demonstrated that graphene offers ballistic transport (transport of charge carriers without any scattering) at sub-micrometer

distances, linear current-voltage (I-V) relationships, and huge sustainable currents (>10^8 Acm^{-2}). It must be noted that the similar electronic properties had already been demonstrated in low-dimensional graphitic structures such as carbon nanotubes (CNTs). Ballistic transport[18] and quantum interference effects[19] in CNTs had been observed at room and cryogenic temperatures, respectively. Simple CNT transistors[20] and interconnected logic circuits[21] had also been demonstrated. Therefore, CNTs were regarded as a promising candidate to succeed silicon in integrated circuits. However, because of the cylindrical structure of nanotubes, the realization of CNT-based electronics requires precise placement of a high density of carbon nanotubes on a substrate. The advantage of graphene over CNTs lies in its planar structure which facilitates the seamless integration of standard IC fabrication techniques into graphene-based electronics. Although the planar nanoscopic graphene ribbons had been predicted to share the exceptional electronic properties of CNTs[22], de Heer and Geim provided the first experimental evidence for this theoretical prediction. The electronic properties of graphene reported in these experimental studies offered the possibility of seamlessly integrated ballistic carrier devices and subsequently intensified the research on graphene. Andrew Geim and Konstantin Novoselov were later awarded the Nobel Prize in physics in 2010 "for groundbreaking experiments regarding the two-dimensional material graphene.[23]"

1.3 Growth of graphene

Currently, graphene samples are produced by one of the following methods:

1.3.1 Mechanical exfoliation from bulk graphite

In 2004, Geim et al. prepared flakes of graphene, as shown in Figure 5, by mechanical exfoliation (repeated peeling with scotch-tape) of small mesas of HOPG. Although labor-intensive and time-consuming, this method provides graphene flakes of high structural and electronic quality. Because of the relatively low cost and the simplicity of the process, this method is useful for producing graphene samples for fundamental research. However, this method cannot produce graphene films over wafer-scale areas. In addition, the process of mechanical exfoliation is not compatible with high volume production of electronic devices.

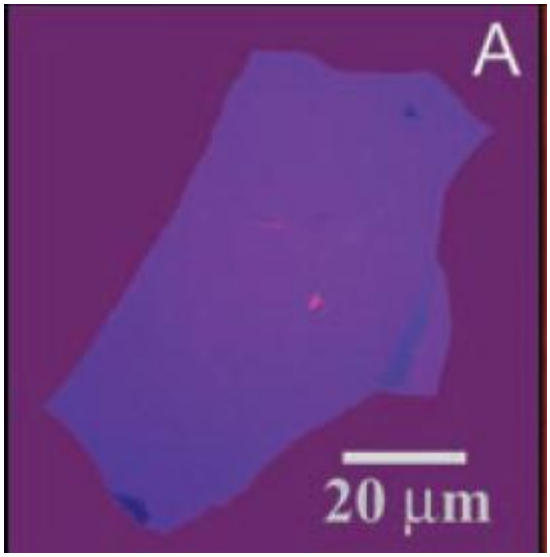

Figure 5: Photograph (in normal white light) of a multi-layer graphene flake with thickness ~3 nm on top of an oxidized Si[17]

1.3.2 Graphitization of silicon carbide (SiC)

In 2004, de Heer et al. grew ultrathin graphite films, typically composed of three layers, on the Si-face of 6H-SiC. In their experiments, the Si-face of 6H-SiC was heated to 1250-1450 °C in an ultra-high vacuum (UHV) chamber for 1-20 min (see Figure 6). Graphene layers formed by this

method on SiC substrates are commonly referred as epitaxial graphene (EG). The quality of the EG produced in UHV is poor due to the high sublimation rates at relatively low temperatures. Defects in EG grown in UHV can be attributed to the relatively low growth temperatures and the high graphitization rates in the non-equilibrium UHV sublimation process. Whereas increased growth temperature anneals vacancies and grain boundaries, the UHV growth method still leads to very high sublimation rates. There are number of ways to control the rate at which silicon sublimes that include supplying silicon through a vapor phase compound like silane[24] or flowing an inert gas over the hot silicon carbide surface[25].

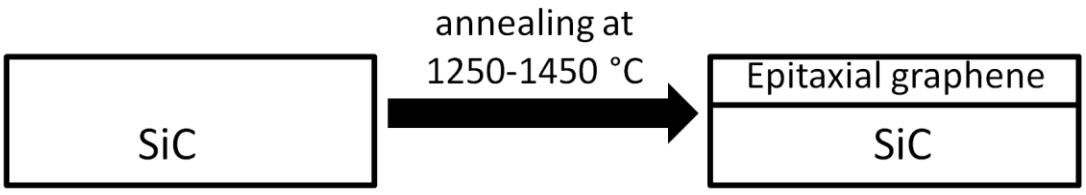

Figure 6: Schematic diagram of the graphitization of SiC

EG growth rate depends on the specific polar SiC crystal face — EG grows much slower on the Si-face than on the C-face SiC. On C-face SiC, controllable growth of multi-layer (10-20 layers) EG is possible. In multi-layer EG, graphene layers do not grow as AB stacked layers characteristic of graphite; instead, these graphene layers contain a high density of rotational stacking faults which cause the adjacent layers to decouple electronically[26]. Another important distinction between the EG grown on C- and Si- face SiC is the presence of a $(6\sqrt{3} \times 6\sqrt{3})R30°$ reconstructed interface layer in EG grown on the Si-face of SiC[27]; as a result of this interface layer, EG grown on the Si-face of SiC is electron-doped ($n \approx 10^{13}\ cm^{-2}$)[28].

This method has attracted widespread use because of the scalability of the process since high quality SiC wafers are available in sizes as large as 150 mm. The scalability of this process was demonstrated by IBM by successfully fabricating field-effect transistors (FETs) in EG (grown on the Si-face of semi-insulating SiC by annealing at 1450 °C) on a 2 inch wafer with a cutoff frequency of 100 GHz[29].

1.3.3 Synthesis of graphene on metal substrates

Growth of graphene on metal substrates such as Ni[30], Pd[31], Ru[32], Ir[33] or Cu[34] via thermal decomposition (~ 1000 °C) of hydrocarbons or solid-state carbon sources is a facile and readily accessible approach toward high quality graphene samples because of the simplicity of the process and the relatively low cost of the metal substrates. Graphene grown by this technique is referred to as CVD-graphene (see Figure 7). Growth of uniform single-layer graphene on copper foils over large areas (~30 inches) is evidence of the scalability of this technique[35]. However, this method requires an additional step of transferring the graphene film onto another substrate if devices are to be fabricated. Therefore, a reliable and scalable transfer process will facilitate the industrial applications of the graphene grown on metal substrates. The mechanism for the graphitization of these metal surfaces was previously proposed to be the diffusion and segregation of carbon atoms from the bulk to the surface during the annealing and cooling stages. Recently, Ruoff's group demonstrated that the growth of graphene on Ni occurs by segregation or precipitation of carbon atoms whereas graphene on Cu grows by a surface adsorption process[36].

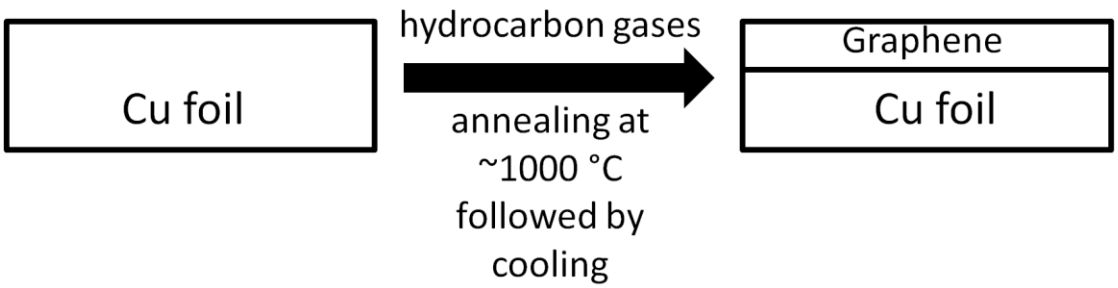

Figure 7: Schematic diagram of a typical CVD-graphene grown on Cu foil

1.3.4 Reduction of graphite oxide

Another commonly used method to grow graphene film is the reduction of exfoliated graphite oxide. This method consists of following steps:

Step 1: Oxidation of graphite

Graphite oxide (GO) is produced by an oxidative treatment of graphite such as the Hummers' method that consist of treating graphite with a water-free mixture of sulfuric acid, nitric acid, and potassium permanganate[37]. The oxygen moieties (see Figure 8[38]) render the graphene oxide layers of GO hydrophilic and water molecules can readily intercalate. Consequently, the interlayer spacing expands from 0.34 nm in graphite to 0.65−0.75 nm depending upon the water content of GO[39].

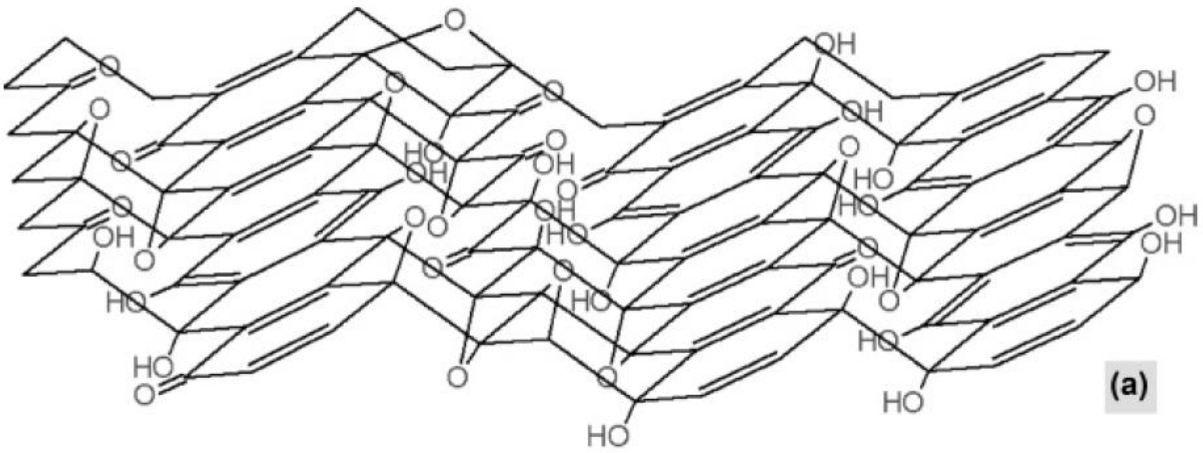

Figure 8: Structural model of GO[38]

Step 2: Exfoliation of GO

Rapid heating (>2000 °C/min) of GO to 1050 °C splits the graphite oxide into individual sheets by rapid evaporation of the intercalated water and evolution of gases produced by thermal pyrolysis of the oxygen-containing functional groups[39].

Step 3: Reduction of GO into graphene-like films

Exfoliated GO sheets are then reduced chemically by treating with reductants such as hydrazine[40], dimethylhydrazine[41], hydroquinone[42] and sodium borohydride[43], thermally by high-temperature annealing[44], photothermally by exposure to a pulsed Xenon flash[45], or photocalytically by ultraviolet assisted reduction in TiO_2 suspension[46].

Although this method is capable of producing wafer-scale graphene sheets, the reduction is not complete and also incorporates undesired species such as nitrogen into the graphite. As a result, the chemical composition and electrical properties of reduced GO are significantly inferior to those of pristine graphene.

1.3.5 Synthesis of graphene nanoribbons by unzipping CNTs

Graphene nanoribbons (GNRs) have been synthesized by unzipping the CNTs along their longitudinal directions as seen in Figure 9 by using one of following techniques:

1) chemical treatment with sulfuric acid (H_2SO_4) and potassium permanganate ($KMnO_4$)[47],

2) plasma etching[48],

3) intercalation of CNTs with alkali-metal atoms such as Li[49],

4) catalytic approach, in which metal nanoparticles ‘‘cut’’ the nanotube under hydrogen flow conditions[50], and

5) gas-phase oxidation that forms etch pits followed by solution-phase sonication to enlarge the pits and unzip the tubes[51].

Because of the mass production of CNTs, these techniques offer a promising alternative to the "top-down" approach of lithographically patterning the graphene films to fabricate GNRs. However, atomic control of edge chemistry and morphology remain as significant challenges.

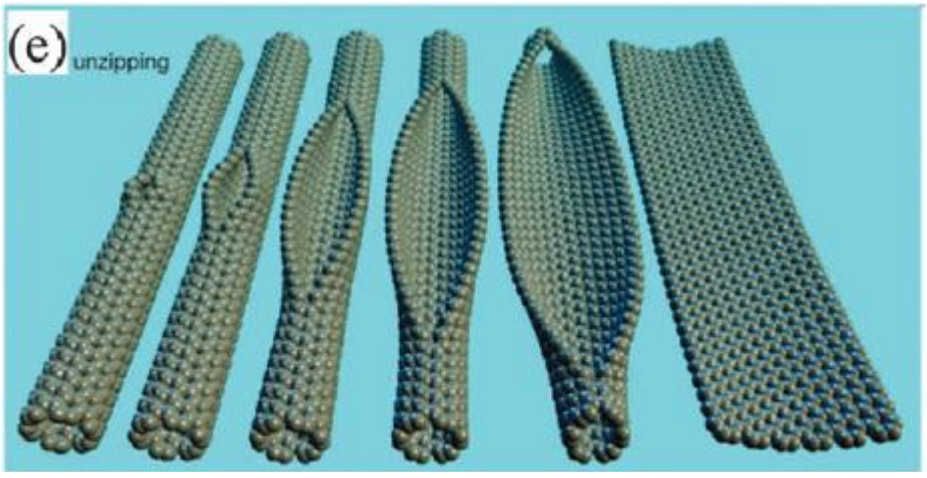

Figure 9: Schematic diagram of the unzipping of a CNT to form a GNR[2]

1.4 Properties of graphene

The relentless and rapid pace of scientific research on graphene has resulted in the discovery of several unique properties. Following is a description of some of the properties of graphene that have attracted significant attention.

1.4.1 Unusual electronic properties

Electrons in graphene behave as quasi-particles called "Dirac fermions"[52]; that is, the electrons in graphene mimic relativistic particles with zero rest mass and display an effective 'speed of light' equal to 10^6 ms^{-1}. "Dirac-fermions" are described by a Dirac-like equation rather than the Schrödinger equation. In addition, the quantum Hall effect (QHE) has been observed in graphene even at room temperature[53], which extends the previous temperature range for the QHE by a factor of 10.

1.4.2 Band structure of graphene

As seen in Figure 10[54], graphene is a zero-gap semiconductor. An energy gap (~ 0.1 eV) has been reported in lithographically patterned GNRs which are 10-100 nm wide[55]. In addition, chemically functionalized graphene also exhibit energy gap as large as 3 eV[56].

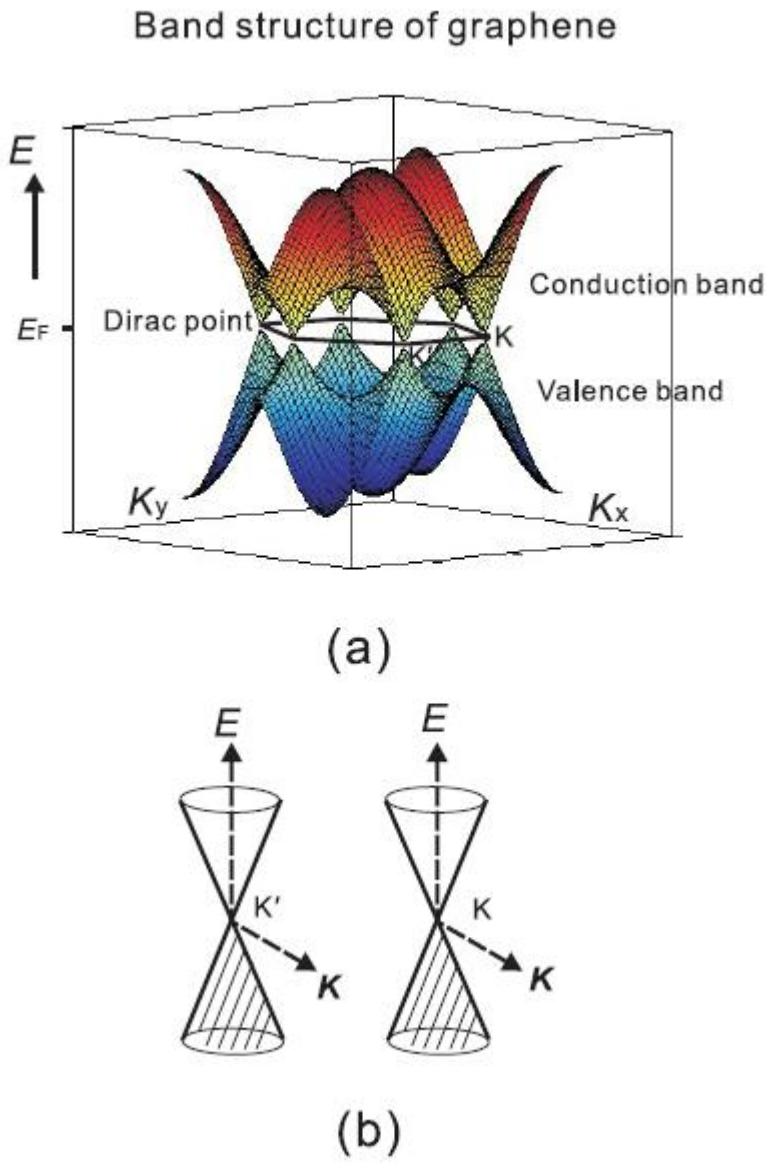

Figure 10: Band structure of graphene obtained by using the dispersion relation given by a simple nearest-neighbor tight-binding calculation
(a) Energy of the conduction and valence band as a function of wave vector K (b) Energy dispersion relation near the Dirac point (K, K')[54]

1.4.2 Thermal conductivity and carrier mobility

Phonon scattering in graphene is negligible. Since the low-energy phonons are generally involved in heat transfer, high thermal conductivity (~ 5300 $Wm^{-1}K^{-1}$) in graphene has been

demonstrated[57]. The mobility of charge carrier in graphene exceeds 15,000 $cm^2V^{-1}s^{-1}$ even under ambient conditions[17]. The observed mobility depends weakly on temperature which suggests that mobility at room temperature (300 K) is limited by impurity scattering. The mobility improves to 200,000 $cm^2V^{-1}s^{-1}$ in suspended graphene[58]. In graphene, mobility remains high even at high carrier concentration (>10^{12} cm^{-2}) in both electrically and chemically doped devices[59] which implies ballistic transport on the sub-micrometer scale (currently up to 0.3 μm) at room temperature.

1.5 Applications of graphene

The discovery of the unique properties of graphene has led to the development of graphene for a variety of applications. Following is a description of some of the recently demonstrated applications of graphene.

1.5.1 Transparent electrode for organic electronic devices

At present, Indium tin oxide (ITO) is the most commonly used transparent electrode material in organic electronic devices. ITO has a transparency greater than 90% at a wavelength of 550 nm, a low sheet resistance of 10–30 Ω sq.$^{-1}$, and a favorable work function of approximately 4.8 eV[60]. However, there are several limitations to using ITO as a transparent electrode material such as the ever-increasing cost of indium due to its scarcity, complicated processing requirements, difficulty in patterning, sensitivity to both acidic and basic environments, and high surface roughness. Furthermore, ITO is brittle which makes it unsuitable for touch screens and flexible displays.

In order to replace ITO as a transparent electrode, several alternative materials such as metallic nanowires[61], conductive polymers such as poly(3,4-ethylenedioxythiophene) (PEDOT) film[62], and CNT films[63] have been investigated. Among these materials, CNT films exhibit significant transparency across the entire visible light spectrum. One of the critical requirements for CNT films is that the density of nanotubes must be greater than the threshold for the formation of a percolation network. Moreover, the high electrical resistance at nanotube-nanotube junctions limits the conductive pathway within the films in spite of the high conductivity of individual CNTs[64]. Therefore, CNT films are not competitive with ITO as transparent electrodes for practical applications.

Recently, graphene has been demonstrated as a potential candidate to replace ITO as a transparent electrode material in organic electronic devices such as solar cells[65–67], organic light emitting diodes[68–70] , liquid crystal devices[71], touch-screens[35], and organic field-effect transistors[72–74] because of its transparency[75], low contact resistance with organic materials[73,74] , flexibility[67,76], and chemical and thermal stability[65,71]. The electrical resistance of graphene does not undergo significant variation up to a bending radius of 2.3 mm (approximate tensile strain of 6.5%) and the original resistance can be perfectly recovered after unbending[30]. Notably, the original resistance can be restored even for a bending radius of 0.8 mm (approximate tensile strain of 18.7%) thereby exhibiting extreme mechanical stability in comparison with conventional materials used in flexible electronics. Moreover, both longitudinal and transverse resistance appear stable up to 11% stretching and show only one order of magnitude change at 25% stretching[30]. Although research is still in the early stages, graphene already offers several potential advantages over conventional transparent electrodes. The excellent performance of various graphene-based electronic devices gives graphene a realistic chance of being competitive in transparent and flexible technologies.

1.5.2 Integrated circuits

The ballistic transport of charge carriers in graphene at room temperature offers the possibility of ultra-fast field effect transistors (FETs) with low power consumption without following the route of conventional scaling as dictated by Moore's law (see Figure 11[77]).

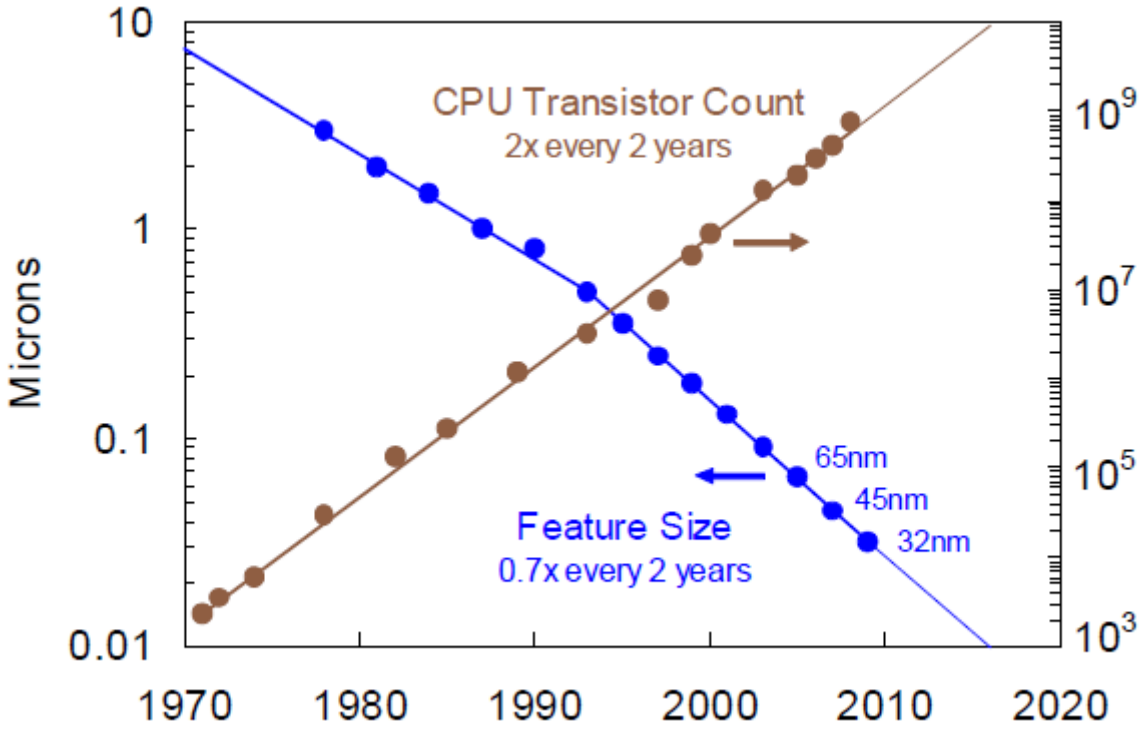

Figure 11: Moore's law: Decrease in the feature size (0.7 times) and increase in the CPU transistor count (2 times) every two years[77]

Toward this end, IBM has fabricated 100 GHz FETs (EG grown on 2 inch SiC wafers)[29] and 150 GHz FETs (CVD-graphene grown on Cu and then transferred to a wafer of diamond-like carbon)[78].

The ultra-high carrier mobility in graphene makes it an attractive material not only for switching devices such as transistors but also for interconnect layers, thereby enabling the prospect of a truly monolithic system. The viability of graphene as an alternative to more commonly used interconnect metals such as copper in future integrated circuits has been demonstrated[79]. Average resistivity of a GNR interconnect at a given line width (18 nm < W < 52 nm) is reported to be approximately three times that of a copper wire whereas the resistivity of the best GNR interconnect is comparable to that of copper wire[79].

1.5.3 Supercapacitors

Supercapacitors are energy-storage devices that store energy in electrochemical double layers whereas more ubiquitously used energy-storage devices like batteries store energy through electrochemical reactions. Ion flow is faster than redox reactions which enable supercapacitors to deliver higher power densities than batteries. On the other hand, batteries exhibit high energy densities of 20 to 150 $Whkg^{-1}$ whereas supercapacitors are limited to energy densities of 4 to 5 $Whkg^{-1}$. This means that supercapacitors cannot store large amounts of energy but can accept or release the energy more rapidly than batteries. An electrode that possesses larger surface area than that of a conventional supercapacitor electrode without sacrificing the high electrical conductivity will allow a combination of the power performance of supercapacitors with the high energy density of batteries. Toward this end, graphene has attracted considerable interest as an electrode material for supercapacitors[80,81] because of its excellent mechanical and electrical properties and exceptionally large specific surface area of 2630 m^2g^{-1} which is significantly higher than the surface area of activated carbons used in current electrochemical double layer capacitors[80].

1.5.4 Sensors

Detection of a single gas molecule by a graphene-based chemical sensor has been demonstrated[59]. This level of sensitivity that can resolve the smallest quantum of a measured entity has not been attained previously by any detection technique including solid-state gas sensors that are known for their exceptionally high sensitivity. Graphene-based sensors use the change in electrical conductivity of graphene to detect the adsorption of gas molecules which can act as acceptors or donors of electrons. This operating principle is similar to that of solid state sensors. The fundamental characteristic that limits the resolution of solid-state sensors is

fluctuations due to thermal motion of charges and defects[82] which leads to an intrinsic noise level that exceeds the sought-after signal from individual molecules by many orders of magnitude. However, graphene is an extremely low noise-material even in the limit of zero carriers[1] and even a few added electrons can cause a noticeable change in carrier concentration. In addition, graphene also allows four-point probe measurements on single crystal devices which ensure that any influence of the contact resistance in limiting sensitivity is eliminated. These features maximize the signal-to-noise ratio of graphene-based sensors to a level sufficient to detect changes in local concentration of less than one electron charge at room temperature.[59] The achieved sensitivity of graphene makes it an attractive candidate not only for chemical detectors but also for other applications where local probes sensitive to external charge, magnetic field, or mechanical strain are required.

1.5.5 Composite materials

The unique properties of graphene can be further utilized by incorporation with other functional materials. Graphene-based composites have already been demonstrated with inorganic nanostructures[83], organic crystals[84], polymers[85], metal-organic frameworks[86], biomaterials[87], and CNTs[88] for applications such as batteries[89], supercapacitors[90], fuel cells[91], photovoltaic devices[92], photocatalysis[93], sensing platforms[87], and Raman enhancement[94].

CHAPTER 2: PLASMA-FLUORINATION OF EPITAXIAL GRAPHENE

2.1 Introduction

2.1.1 Chemical functionalization of graphene

Chemical functionalization is an attractive method to tailor the electronic, chemical, and physical properties of graphene. Typical applications of chemical functionalization include band gap opening via functionalization with oxygen[95–97], hydrogen[98], and fluorine[56,99] and the production of graphene sheets by reduction of graphite oxide[40,42–46]. Graphene can be chemically functionalized via either covalent or non-covalent interactions. The covalent reactions usually result in the rehybridization of carbon atoms from sp^2 to sp^3 thereby disrupting the lattice while the non-covalent interactions preserve the planarity of graphene layers.

2.1.1.1 Covalent functionalization

Graphene consists of sp^2-hybridized carbon atoms and is therefore chemically unsaturated. Intrinsically, covalent addition to convert the carbons from sp^2 to sp^3 hybridization is possible. However, carbon atoms in the basal plane of graphene are protected by their π-conjugation system and their motion is constrained by surrounding carbon atoms. Therefore, covalent addition usually encounters large energy barriers and thus requires reactive chemical groups such as atomic hydrogen, fluorine, or oxygen as the reactants. Following is the description of some of the commonly used approaches to covalent functionalization.

1) Hydrogenation

Hydrogenation of free-standing graphene and graphene on oxidized silicon substrates has been investigated both experimentally and theoretically[98,100–104]. The supported graphene displays different structures and electronic properties before and after hydrogenation. Hydrogenation

changes the hybridization of carbon atoms from sp^2 to sp^3 resulting in elongated C–C bonds in the hydrogenated graphene. Hydrogen atoms react with both sides of the basal plane of pristine graphene. If only one side is hydrogenated, it can then be rolled to form CNTs because of the unbalanced external stress[105]. The semi-hydrogenated graphene possesses ferromagnetic semiconductor properties because partial hydrogenation can destroy the delocalized π bonding network of graphene[106]. The fully hydrogenated graphene called ‘‘graphane’’, which has been prepared by hydrogen plasma-treatment, has also been the subject of a number of studies because of its insulating properties[98]. Moreover, hydrogenation is reversible and the original metallic state and lattice structure can be restored by annealing[98].

2) Oxidation

As exemplified in Figure 8, GO contains a wide variety of oxygen functionalities such as carbonyl, carboxyl, and hydroxyl groups[107]. These oxygen-containing functional groups enable the control of graphene's hydrophilicity or organophilicity. For example, GO sheets are readily dispersed in organic solvents for further functionalization or mixing with organic matrices to form new nanocomposite materials. The following chemical routes have been reported for the synthesis of GO.

1) a one-step process — direct oxidation of graphene with strong oxidants such as concentrated sulfuric acid, concentrated nitric acid, or potassium permanganate[108].

2) a two-step process — oxidation of graphite through Hummers’ method[37] or electrochemical oxidation[109,110] followed by exfoliation of the GO[111].

3) a physicochemical process — fabrication of GO nanoribbons through lengthwise cutting and unraveling the side walls of multi- walled CNTs by oxidative processes[112,113].

3) Diazotization

Graphene has an electron-rich surface due to its network of delocalized π electrons. When electron-accepting moieties such as aryl diazonium salts react with graphene, electrons from the basal plane of graphene transfer to the reactant. Diazotization can be used to control the electrical conductivity of graphene because this process permits tuning of the surface potential of graphene via regiofunctionalization[114,115]. When nitrophenyl groups are attached to the surface of graphene, the resultant diazonium-functionalized graphene sheets are easily dispersed in polar aprotic solvents such as dimethylformamide, dimethylacetamide, and N-methylpyrrolidone. Nitro groups on the surface of diazotized graphene can be further reduced to amine. The amine groups enable subsequent graphene functionalization because amines can react with many other groups such as hydroxyl radicals, carboxyl groups, and acyl chlorides. For example, non-volatile memory devices have been fabricated by attaching gold nanoparticles to the surface of graphene through a π-conjugated molecular bridge — 4-mercapto-benzenediazonium tetrafluoroborate salt[116].

2.1.1.2 Non-covalent functionalization

Transition metals, ions, molecules, and other atomic clusters can be added onto the basal plane of graphene through complexation reactions or charge-transfer adsorption. Since these interactions do not convert the hybridization of carbon atoms from sp^2 to sp^3, the framework of sp^2-hybridized carbon atoms remains intact. Therefore, graphene functionalized by these methods can be highly conductive. Following is the description of some of the commonly reported methods of non-covalent functionalization

1) Adsorption of gas molecules

The delocalized π electrons of graphene are sensitive to adsorbates. As a result, molecules adsorbed on a graphene surface can change the local carrier concentration and also open a band gap due to the charge carrier transfer between graphene and the adsorbate[117–120]. As described earlier, graphene-based sensors that use the change in graphene's electrical conductivity to detect the adsorption of gas molecules have been demonstrated. An energy gap (~ 0.206 eV) can be opened in graphene via the controlled adsorption of water molecules[121]. Hence, the adsorption of gas molecules offers one approach to controlling the energy gap of graphene without disrupting the π-skeleton structure.

2) Interaction with conjugated compounds

Graphene is hydrophobic in nature and therefore aggregates easily in solution. Conjugated compounds such as 1-pyrenecarboxylic acid (PCA) [Figure 12 (a)[122]] enable the control of its surface energy and stable suspensions of individual graphene sheets can thereby be achieved[122–124]. Conjugated compounds can be attached to graphene sheets via non-covalent interactions such as π-π stacking (attractive, non-covalent interaction between aromatic rings) as shown in Figure 12 (b)[122].

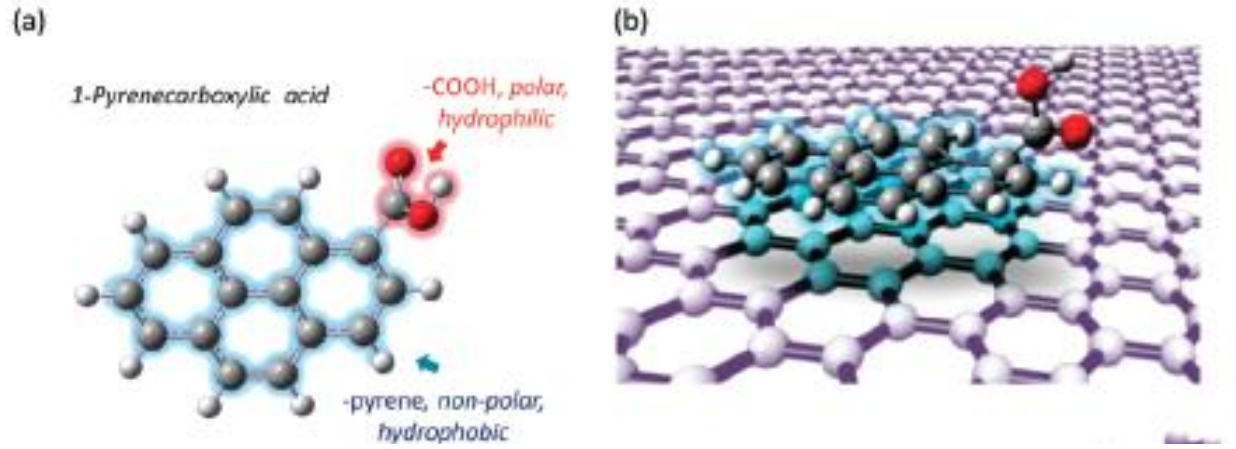

Figure 12: (a) Molecular structure of 1-pyrenecarboxylix acid (PCA) (b) π-π stacking interaction of PCA with graphitic surface[122]

Graphene dispersions have been prepared via exfoliation of graphite in N-methyl-pyrrolidone (NMP) where the energy required to exfoliate graphite is partially compensated by the strong interaction between graphene and NMP[125]. Non-covalent functionalization of GO with 1-pyrenebutyrate followed by reduction of the functionalized GO with hydrazine monohydrate can also be used to produce stable aqueous dispersions of graphene sheets[126]. The positively charged 5,10,15,20-tetrakis(1-methyl-4-pyridinio) porphyrin (TMPyP) molecules can be assembled onto the surfaces of graphene sheets to form complexes through electrostatic and π–π stacking interactions. TMPyP-graphene complexes are used as optical probes for rapid and selective detection of Cd^{2+} ions [127]. Conjugated molecules on graphene also affect the adsorption of metal nanoparticles in two different ways. First, conjugated molecules can weaken the interactions between the metal nanoparticles and graphene. Second, the conjugated molecules provide new reactive sites for the deposition of the nanoparticles[128]. Surfactants and biomolecules such as cetyltrimethylammonium bromide (CTAB)[129], sodium cholate (NaC)[124], sodium dodecyl benzenesulfonate (SDBS)[130] and tryptophan[131] have also been used to disperse graphene in

different solvents. These surfactants adsorb onto the electron-rich surfaces of graphene sheets and thereby permit solubilization of graphene. In large-scale production processes of graphene by electrolytic exfoliation of graphite in a poly(sodium-4-styrenesulfonate) (PPS) electrolyte, the π-π interactions between the aromatic rings of PPS and the graphene plane play a major role in its dispersion[132].

3) Interaction with transition-metal nanoparticles

Adsorption of transition-metal nanoparticles on the basal plane of graphene has been demonstrated[133–137]. These transition-metal nanoparticles, in combination with the excellent electrical conductivity and large surface area of graphene, have potential applications in catalysis and sensors[138,139]. Nanocomposites that consist of transition metals and graphene have been reported to outperform conventional transition-metal catalysts or transition-metal carbides[140–144]. For instance, Pt nanoparticles supported on reduced graphene oxide sheets showed a higher electrochemical surface area and oxygen reduction activity with improved stability than the commercial catalyst. TEM, XPS, and electrochemical characterization suggest that the improved performance can be attributed to smaller particle size and decrease in aggregation of Pt nanoparticles on the reduced graphene oxide sheets[141]. Likewise, in comparison with the widely-used Vulcan XC-72R carbon black catalyst supports, graphene-supported Pt and Pt–Ru nanoparticles demonstrate enhanced efficiency for both methanol and ethanol electro-oxidations[140].

2.1.2 Fluorination of graphene

As described earlier, pristine graphene does not have a band gap. Therefore, opening a band gap in graphene is an important goal for electronic applications. An energy gap (~ 0.1 eV) has been

reported in lithographically patterned GNRs which are 10-100 nm wide[55]. Chemical functionalization is another important technique for band gap engineering because of its scalability. Recently, production of fluorinated graphene with a band gap as large as 3.8 eV has been reported after the treatment of graphene with xenon difluoride (XeF_2) [56]. As seen in Figure 13**,** no photoluminescence emission was observed in pristine graphene because of the absence of a band gap. In contrast, the fluorinated graphene shows two distinct photoluminescence peaks at ~ 3.80 eV and ~ 3.65 eV which confirms the opening of a band gap in graphene.

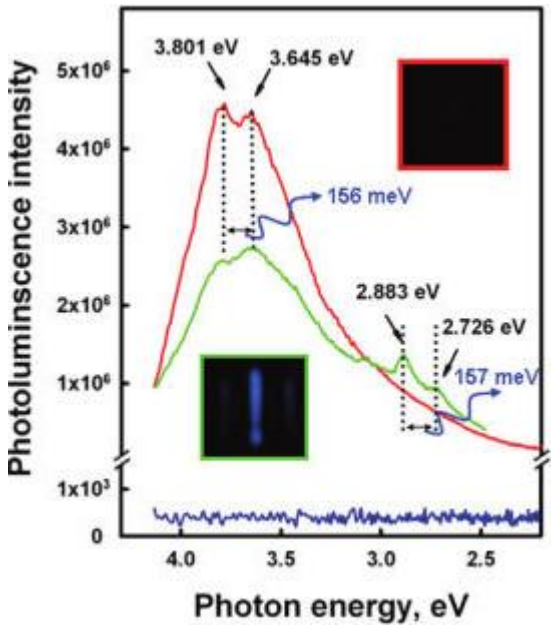

Figure 13: Room temperature photoluminescence emission of the pristine graphene and fluorinated graphene dispersed in acetone using 290 nm (4.275 eV) excitation[56]
Blue line represents pristine graphene while green and red lines represent graphene heat-treated with XeF_2 at 350 °C for 1 day and 3 days respectively.

In addition to opening a band gap, fabrication of graphene-based electronic devices requires uniform deposition of ultra-thin (2–30 nm) films of high-κ gate dielectrics such as Al_2O_3, HfO_2, and TiO_2. Atomic layer deposition (ALD) is a commonly used technique for the growth of high-quality ultrathin dielectric films. In general, ALD requires reactive species such as hydroxyl

groups on the surface to initiate the growth. However, the hydrophobic and chemically inert nature of the graphene surface inhibits direct deposition of thermal ALD oxides. To this end, several methods have been investigated to alter the surface chemistry to ensure that the graphene surface is amenable to ALD; these methods include deposition of a metal or an electron-beam physical vapor deposited oxide seed layer[145], an ozone pretreatment[146], or the use of a low-κ polymer seed layer[147]. The high electronegativity of fluorine suggests that it would be an appropriate reactive species candidate for enhancing the surface reaction of graphene with ALD precursors. As shown in Figure 14**,** an EG sample without fluorine functionalization prior to ALD exhibited large variations in oxide coverage while ALD after the fluorination results in a conformal deposition across the entire sample.

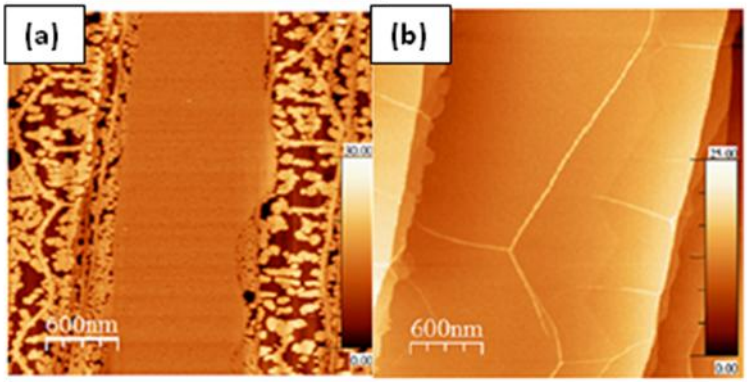

Figure 14: AFM (9 μm^2) images of the surface morphology of Al_2O_3 deposited on (a) pristine graphene and (b) graphene exposed to XeF_2 for 120 s [148]

In addition to facilitating electronic applications, fluorination of graphene also increases its hydrophobicity[149] which may enable biomedical applications. Furthermore, derivation of graphene sheets from graphite fluoride has also been demonstrated[150] which provides an alternative method for the production of graphene samples.

2.1.3 Plasma-fluorination of graphene

Graphite fluoride was first synthesized in 1934 by exposing graphite to molecular fluorine[151]; extensive literature on the fluorination of other graphitic structures such as buckyballs[152] and carbon nanotubes[153] is also available. The techniques currently used to produce fluorinated graphene include exposure to fluorine gas at high temperature (400-600 °C)[154,155] and to XeF_2 at room temperature[56,156]. However, fluorine gas is toxic and corrosive and XeF_2 hydrolyzes readily to form HF when exposed to air. In contrast, plasma-assisted fluorination using benign sources of fluorine such as sulfur hexafluoride (SF_6) can provide a safer and convenient alternative to F_2 and XeF_2 sources. Moreover, plasma etching using SF_6 is employed extensively in the fabrication of integrated circuits.

Plasmas used in surface modification are usually low-temperature non-equilibrium plasmas generated at a low or atmospheric pressure by igniting a gas discharge[157]. Plasmas are generated by supplying energy to electrons that produce ions and new electrons via inelastic collisions. The energy is supplied through an electric field generated by a power supply and applied to the low pressure gas. The electric field accelerates electrons in the plasma that then release the energy by ionization, excitation, and other collision processes **(**see Figure 15**).** The resultant plasmas therefore are partially ionized gases that contain chemically active species (neutral radicals and atoms/molecules in excited state), ions, electrons, and photons[157].

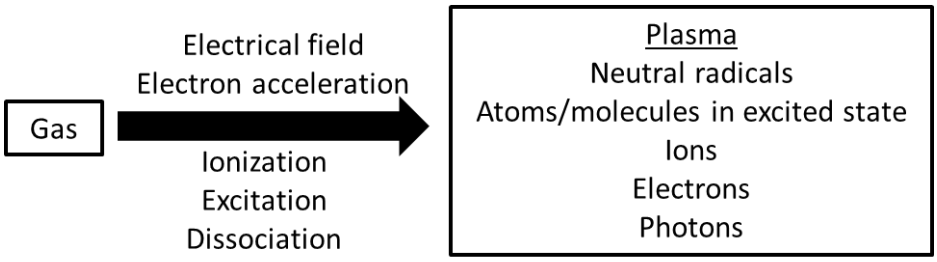

Figure 15: Schematic diagram of plasma-generation

Fluorination of graphene using SF_6 plasmas has been demonstrated. Specifically, electron beam generated plasmas have been successfully used to fluorinate single-layer graphene films grown on copper and then transferred to Si/SiO_2 substrates[158]. The fluorinated graphene film was subsequently characterized using x-ray photoelectron spectroscopy (XPS) and Raman spectroscopy, but the effect of fluorination on the electronic properties was not reported. Moreover, electron-beam technology requires high vacuum conditions, which can ultimately limit the industrial application of this method. Most recently, Yang et al. reported Raman studies characterizing the results of SF_6 plasma treatment of few-layer (1-3) graphene flakes, which were exfoliated from bulk graphite, in a reactive ion etch (RIE) reactor[159]. However, their work does not provide a description of chemical bonding in the resultant material and thus direct evidence of fluorination. Furthermore, the effect of SF_6 plasma treatment on the electronic properties was not discussed. Experimental results suggesting a thickness reduction of few-layer graphene sheets subjected to prolonged CF_4 plasma (RIE) treatment and only fluorine functionalization on the surface layer for shorter exposure times have also been reported[160].

The work discussed in this chapter investigates the SF_6 RIE plasma fluorination of both multi-layer (~20 layers) and single-layer graphene films, which were grown epitaxially on the carbon-face silicon carbide (SiC). Plasma fluorination of large-area epitaxial graphene films grown on

SiC offers a means of controlling electronic properties during device processing. In addition, the use of multi-layer graphene allows a more fundamental study of the extent of fluorination as a function of relative rates of epitaxial graphene fluorination and etching. Plasma-treated graphene films have been characterized by Raman spectroscopy, low energy electron diffraction (LEED), x-ray photoelectron spectroscopy, and ultra-violet photoelectron spectroscopy (UPS). Raman spectroscopy and LEED characterization verify that the sp^2 configuration of carbon atoms in graphene is not destroyed by plasma treatment while XPS confirms the incorporation of fluorine atoms in the SF_6 plasma-treated samples, where fluorination is limited to one or two layers at the surface and the concentration of fluorine can be changed by simply varying the plasma treatment time. UPS characterization reveals the modification in valence electronic states and work function of graphene after the SF_6 plasma-treatment, which may facilitate the application of graphene in optoelectronic devices. The thickness of graphene films grown on the carbon-face SiC can be controlled by the growth time; this unique growth characteristic has been exploited to fabricate a single or bi-layer fluorinated graphene on top of both the insulating substrate (SiC) and a conductive graphene film of desired thickness. The ability to generate a fluorinated graphene/graphene interface offers an approach to the formation of layered structures with graded or structured electronic properties that can be employed for device fabrication.

2.2 Experimental

2.2.1 Material

EG samples used in the study described in this chapter were grown on the C-face of a semi-insulating 4H-SiC by high-temperature annealing (~1600 °C) in an RF induction furnace [see Figure 16 (c)] in Professor Walt de Heer's lab using a confinement-controlled sublimation (CCS)[161] method developed at the Georgia Institute of Technology. As described earlier, the ability to control EG growth rates by controlling the sublimation rate of Si is critical to the growth of high-quality EG. In the CCS method, a SiC sample (~ 3.5 mm by 4.5 mm) is confined in a graphite enclosure with a calibrated leak either into a vacuum or an inert gas environment [see Figure 16 (b)]. This confinement reduces the rate at which Si atoms escape, thereby maintaining a high Si partial pressure which is not possible in an UHV system [see Figure 16 (a)]. As a result, this method allows the growth of EG in a regime that is near thermodynamic equilibrium. Using this method, EG growth over macroscopic areas can be controlled on both Si- and C- faces of SiC to grow either single- or multi- layer EG films [see Figure 16 (d)]. The principle of CCS can be understood from kinetic gas theory. EG growth rate is proportional to the rate of Si sublimation from the SiC surface because each Si atom that escapes the surface leaves behind one C atom. In thermodynamic equilibrium, the Si sublimation rate (n^-) and the Si condensation rate (n^+) at the SiC surface are equal, thereby mitigating EG growth. This condition will eventually be established in a "hermetically sealed" and nonreactive enclosure at any temperature after the enclosure surfaces have been passivated. In this system, graphite enclosure is passivated after several EG growth cycles. However, if the enclosure is not "hermetically sealed" but supplied with a calibrated leak [see Figure 16 (b)], then n^- will be greater than n^+

resulting in the EG growth at a rate $n^{gr} = n^{-} - n^{+}$. Consequently, EG growth rate can be controlled by controlling the size of the leak.

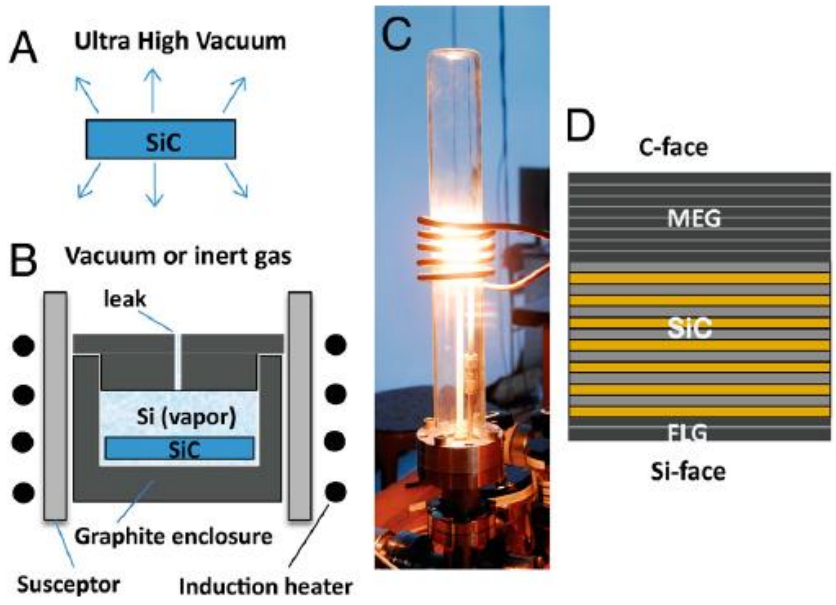

Figure 16: Growth of epitaxial graphene via confinement-controlled sublimation method[161] (A) SiC in UHV: sublimed Si is not confined resulting in rapid and non-equilibrium EG growth (B) The CCS method: sublimed Si is confined in a graphite enclosure resulting in the EG growth in a regime near thermodynamic equilibrium. Growth rate is controlled the enclosure aperture (leak) and the background gas pressure (C) Photograph of the RF induction furnace (D) Under CCS conditions, few layer graphite (FLG, from 1 to 10 layers) grows on the Si-face, and multilayer epitaxial graphene (MEG, from 1 to 100 layers) grows on the C-face

2.2.2 Method

EG samples were exposed to an SF_6 plasma generated in an RIE system. RIE is one of the simplest configurations of plasma-etch equipment. This configuration consists of a parallel plate hardware arrangement where the substrate is placed on a biased electrode (the cathode) facing a grounded electrode (see Figure 17 for the schematic of an RIE system[162]). Since only bias power is used for both plasma generation and the ion acceleration to the cathode, independent control of these two processes is not possible.

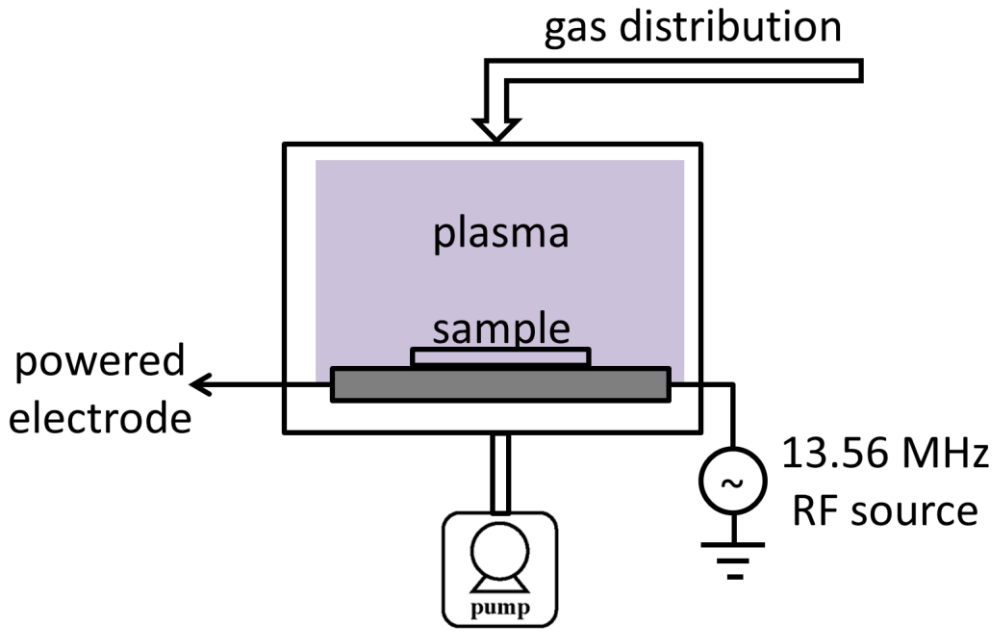

Figure 17: Schematic diagram of an RIE system[162]

The RIE system (Plasma-Therm RIE, see Figure 18 for its photograph) used in this study operates at a radio-frequency (rf) of 13.56 MHz and has an electrode diameter of 11 inches. An rf power of 50 W and an SF_6 partial pressure of 100 mTorr were used for all experiments. In order to minimize sputtering and structural damage to the surface of EG, pure SF_6 gas was used;

no other carrier gas was introduced into the system. All experiments have been carried out at room temperature.

Figure 18: Photograph of Plasma-Therm RIE in the Nanotechnology Research Center at Georgia Tech

2.2.3 Characterization

EG samples were characterized by XPS/UPS (Axis UltraDLD, Kratos Analytical) to determine elemental composition, confirm the existence of fluorine-carbon bonds, estimate the thickness of film, and measure the work function. The fluorinated EG samples were depth-profiled by argon ion-bombardment (3 keV) in a different XPS system (Thermo Scientific K-Alpha). All XPS spectra described in this thesis were collected using monochromatized AlKα radiation (energy=1486.6 eV) and UPS spectra were collected using He I radiation (energy=21.2 eV).

An ellipsometer (Horiba Jobin Yvon Auto SE) was also used to determine thickness of EG grown on C-face 4H-SiC.

Raman spectroscopy was used to investigate the change in graphitic structure of the EG after exposure to SF_6 plasmas. All Raman spectra described in this thesis were obtained with a confocal Raman microscope (JY Horiba LabRam HR800) using 532 nm laser excitation.

Low-energy electron diffraction (LEED) was used to investigate the effect of SF_6 plasmas on the surface structure of the EG after plasma exposure. All LEED patterns described in this thesis were obtained with a LK Technologies Model RVL2000 Reverse View LEED system.

2.3 Results and Discussions

Fluorination of EG via SF_6 plasma-treatment and its effect on the work function of EG films were investigated by exposing multi-layer EG to SF_6 plasmas for 30 s, 60 s, and 90 s under identical plasma conditions. Single-layer EG was subsequently plasma-treated for 30 s to demonstrate that single-layer EG can be successfully fluorinated rather than simply etched away by SF_6 plasma-treatments.

2.3.1 Multi-layer graphene

2.3.1.1 X-ray photoelectron spectroscopy

Evidence of fluorination

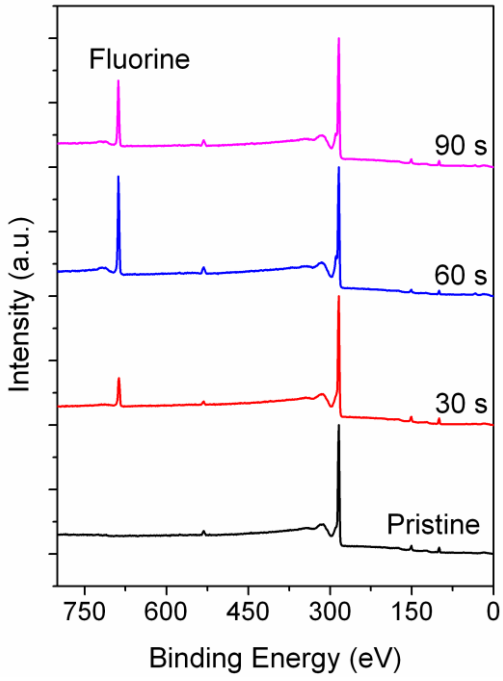

Figure 19: XPS survey spectra of SF_6 plasma-treated multi-layer EG (~20 layers)

The presence of fluorine in samples exposed to SF_6 plasmas is confirmed by the appearance of an F 1s peak at ~ 688 eV in the XPS survey spectra of fluorinated samples as shown in Figure

19. The fluorine concentration is 5.2±0.1 at. %, 14.1±1.5 at. %, and 9.5±1.2 at. % for EG samples exposed to SF_6 plasma for 30 s, 60 s, and 90 s respectively.

EG film thickness

The EG film thickness was calculated using a two-layer model assuming a thin continuous sheet of graphene with a thickness t on a semi-infinitely thick SiC substrate from the modified equation of Bierdmann et al.[163]

$$\frac{N_G}{N_{SiC}} = \frac{\rho_G * \lambda_e^G(E_{C\,1s})}{\rho_{SIC} * \lambda_e^{SiC}(E_{C\,1s})} \left[\frac{1 - \exp\left(\frac{-t}{\lambda_e^G(E_{C\,1s})}\right)}{\exp\left(\frac{-t}{\lambda_e^G(E_{C\,1s})}\right)} \right]$$

where

N_G = total intensity of C 1s peaks from graphene at ~ 284.5 eV

N_{SiC} = total intensity of C 1s peaks from graphene SiC at ~ 283.7 eV

ρ_G = carbon density in graphene (atoms per cm^3)

ρ_{SiC} = carbon density in SiC (atoms per $cm^{3)}$

λ_e^G = inelastic mean-free path for the C 1s photoelectron for graphene with kinetic energy of $E_{C\,1s}$

λ_e^{SiC} = inelastic mean-free path for the C 1s photoelectron for SiC with kinetic energy of $E_{C\,1s}$

The film thickness (Figure 20) calculated using this model shows that graphene sputtering during a 30 s plasma-treatment is negligible while approximately one layer of graphene may have been sputtered during 60 s and 90 s plasma treatments. However, this model assumes a continuous sheet of carbon atoms. Because of the incorporation of fluorine atoms in the EG film after the plasma-treatment, the decrease in EG film thickness after 60 s and 90 s plasma-treatment may also be attributed to the decrease in the intensity of C 1s peaks from graphene due to the emergence of C 1s peaks that are indicative of carbon-fluorine bonds at ~289.5 eV [Figure 21

(b)]. This alternate explanation of the decrease in the EG film thickness suggests that graphene sputtering during 60 s and 90 s plasma-treatment may also be negligible.

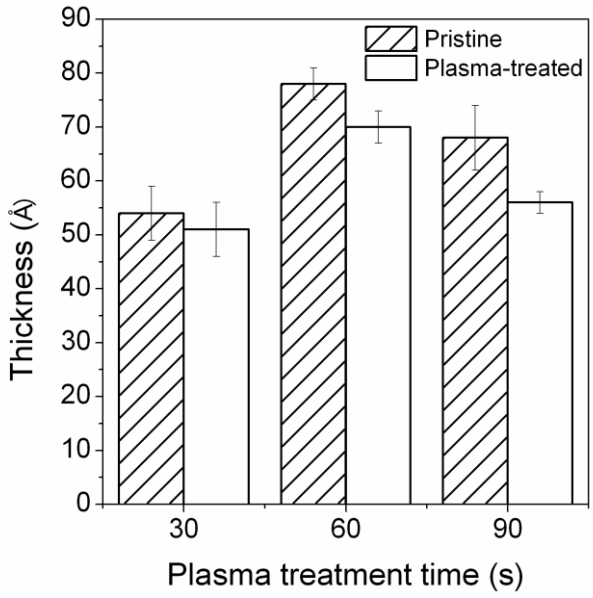

Figure 20: Thickness of pristine and SF_6 plasma-treated multi-layer EG (~20 layers)

Depth of fluorination

Depth of fluorination was determined by in-situ ion-bombardment to slowly remove graphene layers. After 15 s of argon ion- bombardment, the C/Si ratio of single and three-layer thick non-fluorinated EG films decreased from 1.9 to 1.0 and 3.0 to 1.9 respectively, thereby suggesting that one or two graphene layers were etched; thickness of these EG samples was determined by the ellipsometer. In addition, the fluorine concentration is below XPS detectability in all plasma-treated samples after 15 s of ion- bombardment under identical conditions. These data indicate that graphene fluorination under the conditions used in this study is limited to one or two surface layers irrespective of the treatment time.

Existence of C-F bonds

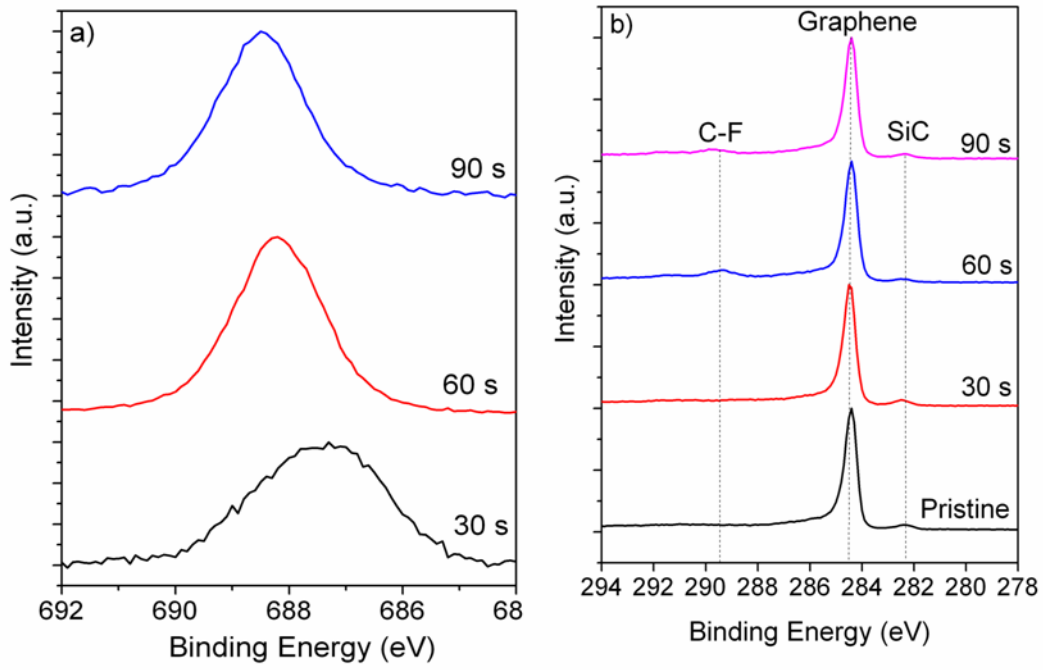

Figure 21: F 1s (a) and C 1s (b) XPS spectra of SF_6 plasma-treated multi-layer EG (~20 layers)

For samples exposed to the SF_6 plasma for 30 s, a F 1s peak at ~ 687.3 eV appears as shown in Figure 21 (a) which is characteristic of fluorine atoms bonded to carbon atoms in aromatic rings[164]. For samples exposed to an SF_6 plasma for 60 s and 90 s, the peaks in F 1s spectra [see Figure 21 (a)] are shifted by nearly 1 eV to 688.5 eV. A similar increase in the binding energy with an increase in degree of fluorination has also been reported in XPS studies of fluorobenzene[165]. The presence of carbon-fluorine bonds in 60 s and 90 s plasma-treated samples is corroborated by peaks at ~289.5 eV, which is indicative of carbon-fluorine bonds in aromatic rings[165], in the corresponding C 1s spectra as seen in Figure 21 (b). Absence of a peak at a similar binding energy in the C 1s spectrum of 30 s SF_6 plasma-treated sample [see Figure 21 (b)

], appears to contradict our earlier conclusion regarding the existence of fluorine-carbon bonds in the sample that was exposed to an SF_6 plasma for 30 s. However, this observation can be attributed to signal attenuation of the characteristic peak in C 1s spectra as a result of the lower fluorine content.

Graphitic nature of carbon atoms

C 1s spectra of both pristine and fluorinated EG are dominated by the peak at ~ 284.5 eV, which is characteristic of graphitic carbon[166]. There is no shift in the position and width of this peak after plasma treatment, which indicates that the chemical environment of the graphitic carbon was not altered significantly in spite of the incorporation of fluorine moieties. The peak at ~ 282.3 eV is characteristic of carbidic carbon — carbon atoms bound to silicon atoms in the silicon carbide substrate[166].

2.3.1.2 Raman spectroscopy

The Raman spectrum of graphene is dominated by the features of graphitic carbon, the G and D peaks at ~ 1580 cm^{-1} and ~ 1350 cm^{-1}, respectively. The G peak, a bond-stretching vibration of a pair of sp^2-hybridized carbon atoms, is Raman active in both aromatic rings and olefinic chains[167]. The D peak is a breathing vibration of a 6-member aromatic ring. The D peak becomes Raman active only in polycrystalline graphite and its intensity is inversely proportional to the effective crystalline size[167]. Raman spectra of all EG samples before and after plasma-treatment, as shown in Figure 22, consist of a G peak at ~ 1583 cm^{-1}. Retention of the G peak at ~1583 cm^{-1} in the Raman spectrum of fluorinated EG films as seen in Figure 22 suggests that the skeleton of sp^2-hybridized carbon atoms remains intact after plasma exposure. The emergence of the D peak at ~1350 cm^{-1} is an indication of the polycrystallinity of fluorinated graphene. Ion-bombardment

during plasma treatment most likely results in the formation of smaller graphite domains, which enhances the Raman activity of the D peak. In addition to the graphite phonon modes, several SiC characteristic bands at ~1480 cm^{-1}, 1520 cm^{-1}, 1620 cm^{-1}, 1688 cm^{-1}, and 1718 cm^{-1} appear in the Raman spectra of both plasma-treated and pristine EG. Other than the appearance of the D peak, no overall changes are observed in the Raman spectra after plasma treatment.

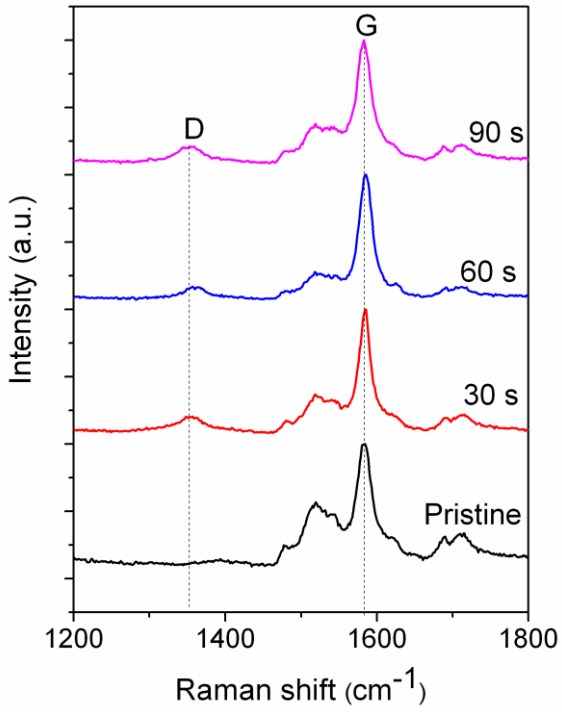

Figure 22: Raman spectra of SF_6 plasma-treated multi-layer EG (~20 layers)

The position and width of a single Lorentzian peak fitted around the G mode after the plasma treatment do not undergo significant changes as shown in Table 1**.** In addition, there is no splitting of the G peak, which is an indication that bond alteration has not occurred. These observations suggest that little to no change in the energy of bond-stretching vibration of sp^2 sites after the plasma treatment takes place; such results imply that the chemical environment of

the sp^2 graphene sites was not altered significantly by the plasma treatment. These Raman studies are consistent with our earlier conclusion from XPS characterization that the sp^2-hybridized carbon skeleton of graphene remains intact upon plasma fluorination.

Table 1: Position and width of a single Lorentzian peak fitted around the G mode (see Figure 22) of multi-layer EG films before and after plasma-treatment

Treatment time (s)	G peak position (cm^{-1})		G peak width (cm^{-1})	
	Before plasma treatment	After plasma treatment	Before plasma treatment	After plasma treatment
30	1583±0.5	1584±1.0	17±2.5	17±1.2
60	1583±2.0	1585±0.8	20±1.7	16±1.4
90	1584±0.4	1583±0.6	21±4.0	19±2.1

2.3.1.3 Ultra-violet photoelectron spectroscopy

Spectral features

The effect of SF_6 plasma treatments on the electronic properties of graphene was investigated using UPS. Figure 23 indicates that the UPS spectrum of EG before plasma treatment consists of peaks at ~3.0 eV (labeled A) and ~13.6 eV (labeled B) below the Fermi level (labeled E_F) which can be attributed to photoelectrons emitted from the 2p-π and the mixed 2s-2p hybridized states respectively[168]. Retention of both peaks in the UPS spectra of plasma-treated samples suggests that the sp^2-hybridized carbon skeleton of graphene is preserved after the plasma treatment. A feature at ~ 10 eV (labeled C) appears in the UPS spectra of samples plasma-treated for 60 s and 90 s, which can be attributed to the photoelectrons emitted from fluorine 2p-like

states[168]. Emergence of this peak after plasma-treatment confirms the existence of fluorine containing moieties while its absence in the sample that was plasma-treated for only 30 s can be explained by the lower fluorine concentration.

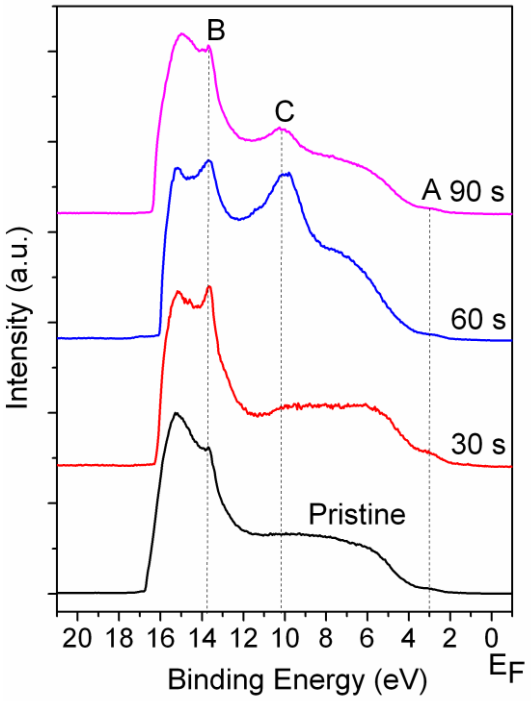

Figure 23: UPS spectra of SF_6 plasma-treated multi-layer EG (~20 layers)

Increase in work function

From UPS spectra, the work function of graphene can be estimated by subtracting the width of the photoelectron spectrum from the photon energy. The work function of multi-layer EG prior to the SF_6 plasma-treatment is estimated to be 4.40±0.05 eV. The decrease in the width of the photoelectron spectra after an SF_6 plasma-treatment (see Figure 23) indicates that the work function has increased; the work function of fluorinated EG has increased by 0.64±0.05 eV, 0.71±0.06 eV, and 0.48±0.05 eV for samples exposed to SF_6 plasma for 30 s, 60 s, and 90 s respectively. Since the work function is the energy difference between the Fermi and the vacuum

levels and no shift in the Fermi edge was observed, the increased work function can be attributed to the creation of a surface dipole by incorporation of the highly electronegative fluorine containing moieties. An electrical double layer with a negatively charged outer surface is generated, which produces a dipole field at the surface that opposes electron escape from the surface, thereby increasing the work function[169].

Lack of correlation between the increase in work function and fluorine concentration

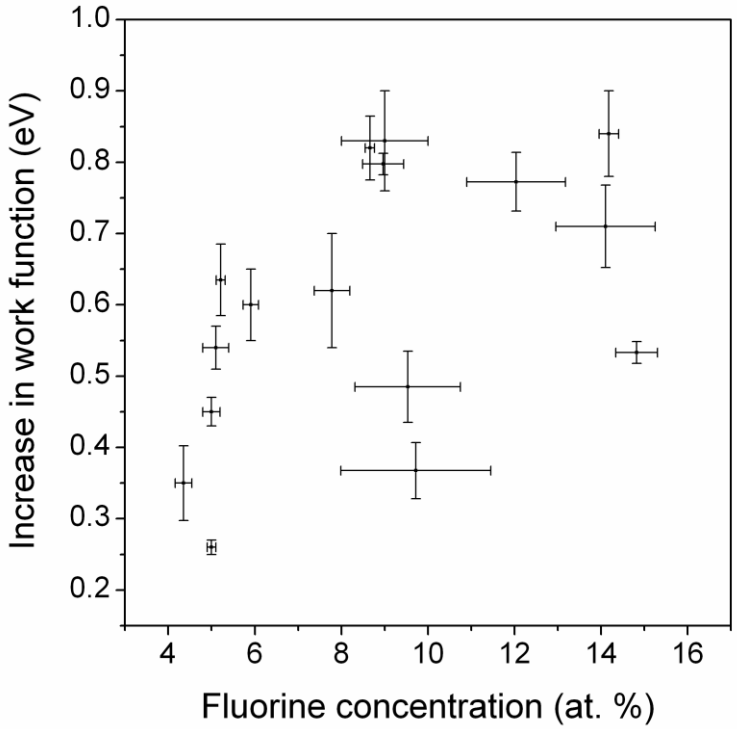

Figure 24: Increase in work function as a function of fluorine concentration

Plasma-treatment involves ion bombardment of sample surfaces; the surface defects created by the ion bombardment have been reported to induce changes in work function[169–172]. Because a number of parameters (e.g., crystal orientation, measurement technique, ion-bombardment energy) affect work function measurements, these results do not establish a quantitative relationship between surface defects and the change in work function. Since the synergy between

the effects of fluorine adsorption and the surface defects generated by ion bombardment may govern the sign and magnitude of change in the work function, the magnitude of the increase in work function does not correlate with the fluorine concentration as shown in Figure 24 (data used in this plot were generated by SF_6 plasma-treatment of EG samples of various thicknesses). The relationship between the change in work function of graphene and fluorine concentration can be elucidated by isolating the two effects, fluorine adsorption and surface defects, from each other and studying each effect separately. The results of our subsequent studies to investigate these effects separately will be discussed in Chapter 3. Nevertheless, the observed increase in work function after the plasma-treatment of EG indicates the utility of SF_6 plasma treatments for modification of the electron emission characteristics of graphene. Furthermore, retention of the characteristic features of graphene in the valence-band spectra corroborates our previous conclusions drawn from XPS and Raman studies that the sp^2-hybridized carbon skeleton of graphene survives the plasma-treatment.

2.3.1.4 Low-energy electron diffraction

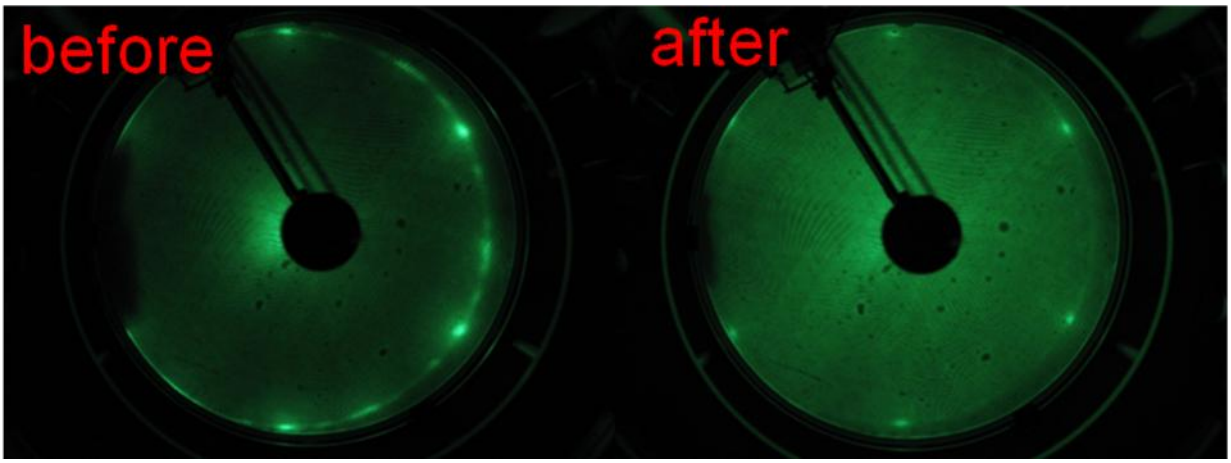

Figure 25: LEED patterns of multi-layer EG (~4 layers) grown on the C-face of 4H-SiC before and after exposure to SF_6 plasma for 60 s collected at electron energies of 52.9 eV and 53.9 eV respectively

Figure 25 shows LEED patterns of multi-layer EG grown on the C-face of 4H-SiC before and after plasma fluorination. The LEED pattern before fluorination contains the "bright spots" and “arcs” that are attributed to the hexagonal lattice of graphene layers and the rotational stacking between the graphene layers respectively[161]. Retention of these features in the LEED pattern after the fluorination indicates that the hexagonal lattice of the graphene remains intact after the fluorination. The attenuation of the intensity after the fluorination may be due to scattering of electrons from the defects generated by the plasma-treatment. This data is in agreement with our conclusion previously drawn from Raman and photoelectron spectroscopy data. Since the planarity of graphene layers is preserved, we can infer that fluorination is dominant at the edges of the domains generated by the plasma-treatment. Alternatively, the fluorine atoms may be intercalated between the graphene layers which will also leave the framework of sp^2-hybridized carbon atoms unperturbed.

2.3.2 Single-layer graphene

Studies on the plasma-fluorination of multi-layer EG demonstrated that graphene films can be fluorinated with negligible etching using a 30 s plasma treatment time. Therefore, a plasma treatment time of 30 s was used to demonstrate that single-layer EG films can be fluorinated by exposure to SF_6 plasmas. Preservation of the G peak in the Raman spectrum [Figure 26 (a)] of EG film after plasma-treatment suggests that the graphene film is not etched and the sp^2-hybridized carbon skeleton survives the plasma treatment. Emergence of the D peak in the Raman spectrum [Figure 26 (a)] accounts for the polycrystallinity generated by ion bombardment. Fluorine content in the plasma-treated sample is 7.8±0.4 %; the peak at ~ 687 eV in the F 1s spectrum [Figure 26 (b)] and the peak at ~288.5 eV in the C 1s spectrum [Figure 26

(c)] suggest the existence of carbon-fluorine bonds. From the UPS spectra [see Figure 26 (d)], a 0.62±0.08 eV increase in work function after the plasma-treatment is estimated.

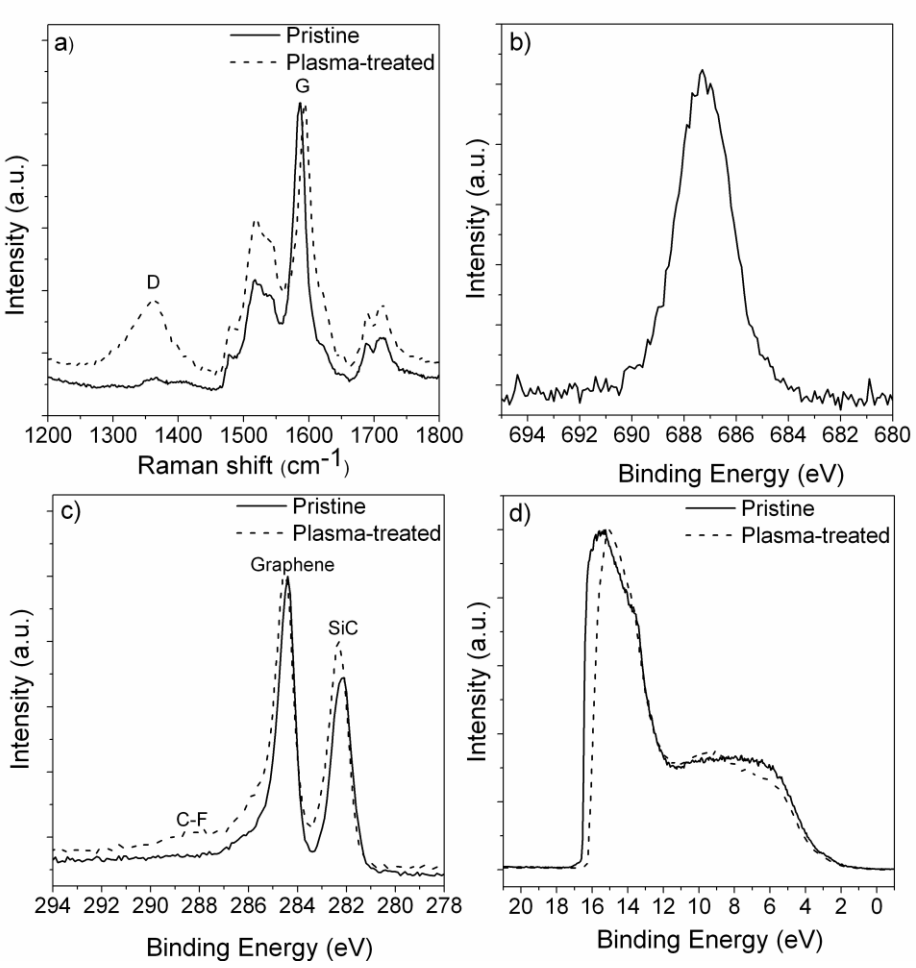

Figure 26: Raman (a) , XPS F 1s (b), XPS C 1s (c), and UPS (d) spectrum of fluorinated single-layer EG

In addition to confirming the viability of SF_6 plasma to fluorinate single-layer EG films, results on this single-layer EG film also allow further insight into the experiments on multi-layer EG films. From the XPS, UPS, and Raman studies of multi-layer EG, we inferred that the sp^2 configuration of graphene remains intact after the plasma treatment and the fluorination is limited to one or two surface layers. Such conclusions lead to the question of whether these spectroscopic studies are influenced by the contribution of the EG layers underneath the surface

modified layer. XPS and Raman studies of single-layer EG clarify this issue. Retention of the G peak in the Raman spectrum [Figure 26 (a)] and the graphene peak in the C 1s XPS spectrum [Figure 26 (c)] of the single-layer EG without any significant change in the peak position and width validate the conclusions drawn from our studies of multi-layer EG. Furthermore, our conclusions pose another intriguing question concerning the existence of carbon-fluorine bonds: if the sp^2 configuration of graphene is not disrupted by plasma-treatment, then how is fluorine bonded to carbon atoms? A plausible scenario is the confinement of fluorination to the carbon atoms at the edges of graphite domains generated by ion-bombardment. If carbon-fluorine bonds exist only at the edges, the basal plane of graphene does not undergo chemical modification which is manifested in the spectroscopic characterization of plasma-treated samples. A subsequent question emerges on whether the carbon-fluorine bonds lead to sp^3 rehybridization of carbon atoms at the edges of graphite domains. The observed shift of work function requires a surface dipole perpendicular to the basal plane of graphene which is not possible if the carbon-fluorine bonds are coplanar with the basal plane of graphene. Therefore, the carbon atoms at the edges most likely rehybridize to sp^3 configuration and the carbon-fluorine bonds are out of plane.

2.4 Conclusion

Due to the ubiquitous presence of plasma technology in the semiconductor industry, plasma-enabled processing of graphene may facilitate the integration of the technological infrastructure of the semiconductor industry into graphene-based electronics. Toward this end, this study demonstrates that an SF_6 RIE plasma can fluorinate both multi-layer and single-layer EG films without disruption of the sp^2-hybridized carbon framework of EG. Fluorine content in the sample can be altered by simply varying the plasma treatment time and the fluorination is limited to only one or two surface layers. In addition, we have demonstrated the ability of plasma-assisted fluorination to modify the electron emission characteristics of graphene; therefore, SF_6 plasma treatment facilitates the application of graphene as an electrode for optoelectronic devices. The ability to control the thickness of EG on carbon-face SiC was exploited to fabricate one or two layers of fluorinated graphene both on top of the insulating substrate (SiC) and on a conductive graphene film of desired thickness. Since the semiconducting properties of fluorinated graphene have been reported previously, a fluorinated graphene/graphene interface also offers the possibility of fabricating bottom-gated epitaxial graphene devices.

CHAPTER 3: EFFECT OF THE POLARITY OF CARBON-FLUORINE BONDS ON THE WORK FUNCTION OF PLASMA-FLUORINATED EPITAXIAL GRAPHENE

3.1 Introduction

3.1.1 Structure and operation of organic electronic devices

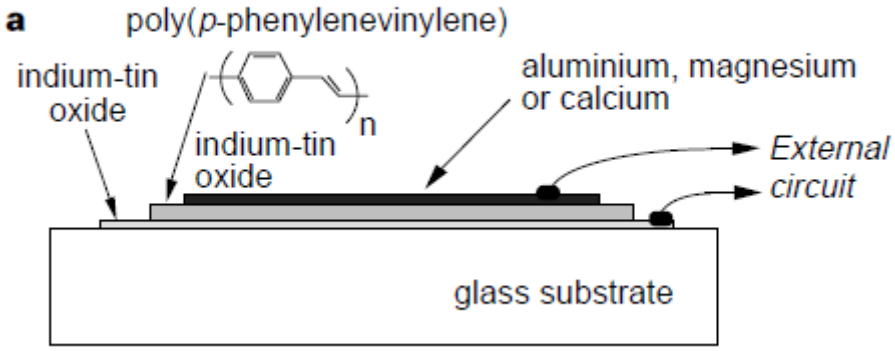

Figure 27: Schematic diagram of a single-layer polymer diode[173]

As described in Chapter 1, graphene has been demonstrated as a potential candidate to replace ITO as a transparent electrode in organic electronic devices. Figure 27 shows the schematic of a single-layer polymer electroluminescent diode. This device structure is representative of other organic electronic devices such as multilayer diodes and organic solar cells. This device consists of an emission layer (organic polymer) sandwiched between positive and negative electrodes. Indium tin oxide (ITO) is typically used as the hole-injecting electrode and it functions as a transparent electrode that allows the light generated within the diode to leave the device. The positive electrode is usually a thermally evaporated metal.

Operation of a typical organic light emitting diode (OLED) described above consists of following steps:

1) injection of electrons and holes from the electrodes after the diode is biased sufficiently,

2) formation of neutral bound excited states called excitons within the organic layer, and

3) decay of excitons that result in the emission of photons.

The operating principle of an organic solar cell is similar to that of an OLED. The process of conversion of light into electricity by an organic solar cell can be described by the following steps: absorption of photons leading to the formation of an exciton, exciton dissociation or charge separation, and charge transport within the organic layer to the respective electrodes.

3.1.2 Work function engineering in organic electronic devices

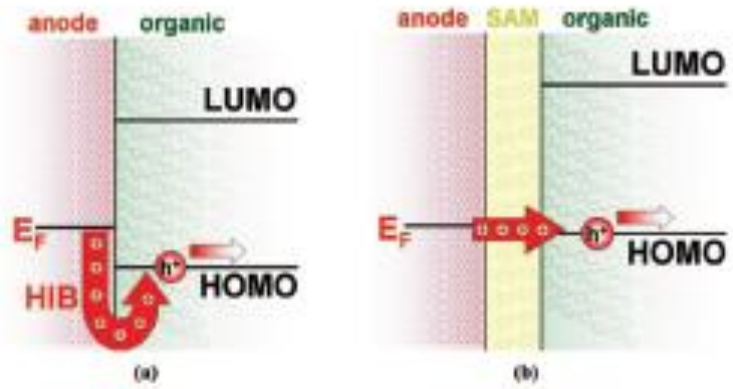

Figure 28: Schematic energy-level diagram at an electrode/organic interface in organic electronic devices [174]

Figure 28 (a) shows the position of the highest occupied molecular orbital (HOMO) and the lowest unoccupied molecular orbital (LUMO) with respect to the Fermi level (E_F) and Figure 28 (b) shows the reduction in hole-injection barrier after the treatment of the electrode with a

suitable self-assembled monolayer (SAM) for an organic electronic device. At the anode, holes are injected into the occupied states of the organic semiconductor. As seen in Figure 28 (a), the energy offset between the Fermi level (E_F) and the highest occupied molecular orbital (HOMO) is commonly termed the hole-injection barrier (HIB)[175,176] because holes must overcome this energy barrier before current can flow. This barrier gives rise to an undesirable onset voltage below which the device remains inactive. At the cathode, a similar scenario is encountered for electrons. To improve the performance of organic electronic devices, charge-injection barriers must be optimized. Traditionally, this issue has been addressed by choosing materials with a high work function (Φ) for the anode (low E_F) and low-Φ metals (high E_F) for the cathode and by using organic semiconductors with matching energy levels. More recently, however, SAMs of dipolar organic molecules have been used to control the work function of electrodes to reduce the charge-injection barriers [see Figure 28 (b)] and minimize the onset voltages[177–179]**.** This approach affords more flexibility for optimization of the active device components with regard to other device parameters.

3.1.3 Work function engineering of graphene

As already described in this chapter, the ability to engineer the work function of graphene is critical to facilitate its application as a transparent electrode material. Several approaches have been reported to modify the work function of graphene. For instance, the work function of graphene can be tuned by $AuCl_3$ doping[180]. Immersion of the CVD-graphene films into an $AuCl_3$ solution results in the formation of Au particles on the surface of graphene films by spontaneous reduction of metal ions. Graphene becomes p-doped due to the charge transfer from graphene during the reduction of Au^{III} to Au particles. By controlling the immersion time, the surface

potential of graphene films can be altered by up to 0.5 eV. Photovoltaic devices based on n-type silicon interfacing with graphene films were fabricated to demonstrate the benefit of an electrode with tunable work function. Similarly, the application of SAMs to control the work function of graphene electrodes (between 3.9 to 4.5 eV) for high-performance organic field effect transistors (OFETs) has also been demonstrated[181]. The work function of graphene electrodes can be controlled by functionalizing the surface of SiO_2 substrates with SAMs. Electron-donating NH_2-terminated SAMs induce strong n-doping in graphene while CH_3-terminated SAMs neutralize the p-doping induced by SiO_2 substrates. Likewise, a method for controlling the work function of graphene by using a small amount of aluminum has also been developed[182]. Deposition of less than 0.6 nm of aluminum is sufficient to control the work function of graphene between 3.77 and 4.40 eV. More recently, an increase in the work function of graphene has been demonstrated by chemical doping using six metal chlorides ($AuCl_3$, $IrCl_3$, $MoCl_3$, $OsCl_3$, $PdCl_2$, and $RhCl_3$) as the p-dopants[183]; the work function of graphene increases from 4.2 eV to 5.0, 4.9, 4.8, 4.68, 5.0, and 5.14 eV after treatment of graphene with 20 mM $AuCl_3$, $IrCl_3$, $MoCl_3$, $OsCl_3$, $PdCl_2$, and $RhCl_3$ respectively. In another study, a decrease in the work function of graphene (from 4.2 to 3.4 eV) was achieved via chemical doping using four different metal carbonates, Li_2CO_3, K_2CO_3, Rb_2CO_3, and Cs_2CO_3.[184] The resultant decrease in the work function has been attributed to the spontaneous electron donation from the metal ions to a specific energy level of graphene. Our previous studies on the plasma-fluorination of epitaxial graphene (EG) also revealed an increase in EG work function after an SF_6 plasma-treatment; however, the work function could not be varied in a predictable manner[185]. Our study also established that in addition to the incorporation of fluorine moieties on the surface, SF_6 plasma-treatment of EG introduced structural defects due

to ion-bombardment in plasma-fluorinated EG without disrupting the framework of sp^2-hybridized carbon atoms. Therefore, further studies to investigate the effect of chemical and physical components of plasma-fluorination on the work function of graphene and thereby obtain improved understanding of the interaction between fluorine and carbon atoms in graphene were performed. In this chapter, the findings of our subsequent investigation to controllably modify the work function of graphene are described; we demonstrate that the work function of fluorinated graphene is controlled by the polarity of carbon-fluorine bonds which depends upon the nature of the chemical bond (ionic, semi-ionic, or covalent) between fluorine and carbon.

3.2 Experimental

EG samples described in this chapter were grown on 4H-SiC by high-temperature (~ 1600 °C) annealing in an RF furnace; EG growth on the Si-face 4H-SiC is limited to few layers (one or two layers) while the growth of multi-layer EG is possible on the C-face 4H-SiC.

EG samples were fluorinated by an SF_6 plasma-treatment in an RIE system. This system (Plasma-Therm RIE) operates at a radio-frequency (rf) of 13.56 MHz and has an electrode diameter of 11 inches. All experiments were carried out at room temperature with an rf power of 50 W and an SF_6 partial pressure of 100 mTorr.

Fluorinated EG samples were characterized by XPS to determine elemental composition, compare the polarity of carbon-fluorine bonds, and measure the thickness of the films, and by UPS to estimate the work function. XPS and UPS spectra were collected using monochromatized AlKα radiation (1486.6 eV) and He I radiation (21.2 eV) respectively in an XPS/UPS system (Axis UltraDLD, Kratos Analytical). Raman spectroscopy (JY Horiba LabRam HR800, 532 nm laser excitation) was used to investigate the graphitic structure of the EG after SF_6 plasma-treatment.

3.3 Results and Discussion

Effect of fluorination versus structural defects

In order to isolate the effect of structural defects introduced by SF_6 plasma-treatment on the work function of EG from the effect of fluorine incorporation, a multi-layer EG sample (~ 2 layers) was fluorinated and then annealed at 1000 °C in a vacuum chamber with a base pressure of ~ 8.4 e-8 Torr for 30 minutes. Prior to annealing, the fluorine concentration was 9.0±1.0 at. %. The work function of EG was calculated from UPS spectra by subtracting the width of photoelectron spectrum from the photon energy; the work function of fluorinated EG was 5.23±0.07 eV. The fluorine concentration dropped below the XPS detectability limit after annealing as indicated by the disappearance of the F 1s peak at ~ 688 eV (Figure 29).

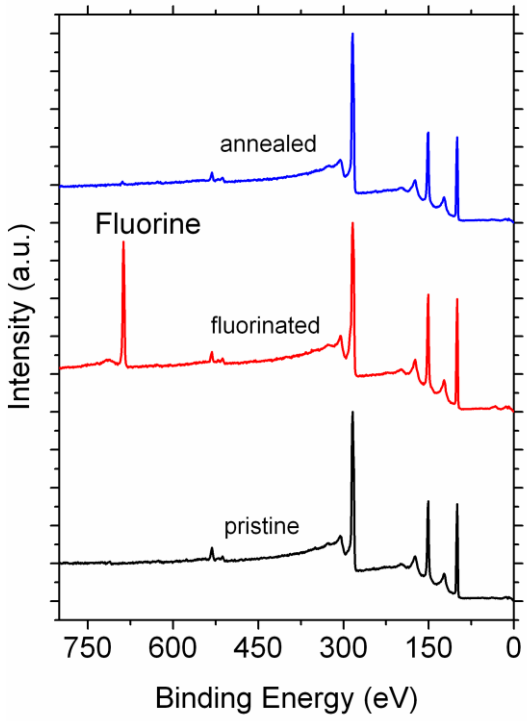

Figure 29: XPS survey spectra of SF_6 plasma-treated multi-layer EG (~ 2 layers) grown on C-face of 4H-SiC

After annealing, the work function decreased to 4.44±0.01 eV which is equal to the work function of EG prior to the SF_6 plasma-treatment [Figure 30 (a)]. Retention of the Raman D peak at ~ 1350 cm^{-1} after annealing [Figure 30 (b)] demonstrates that structural defects introduced by the SF_6 plasma-treatment still exist after annealing, thereby indicating that the structural defects may not affect the EG work function.

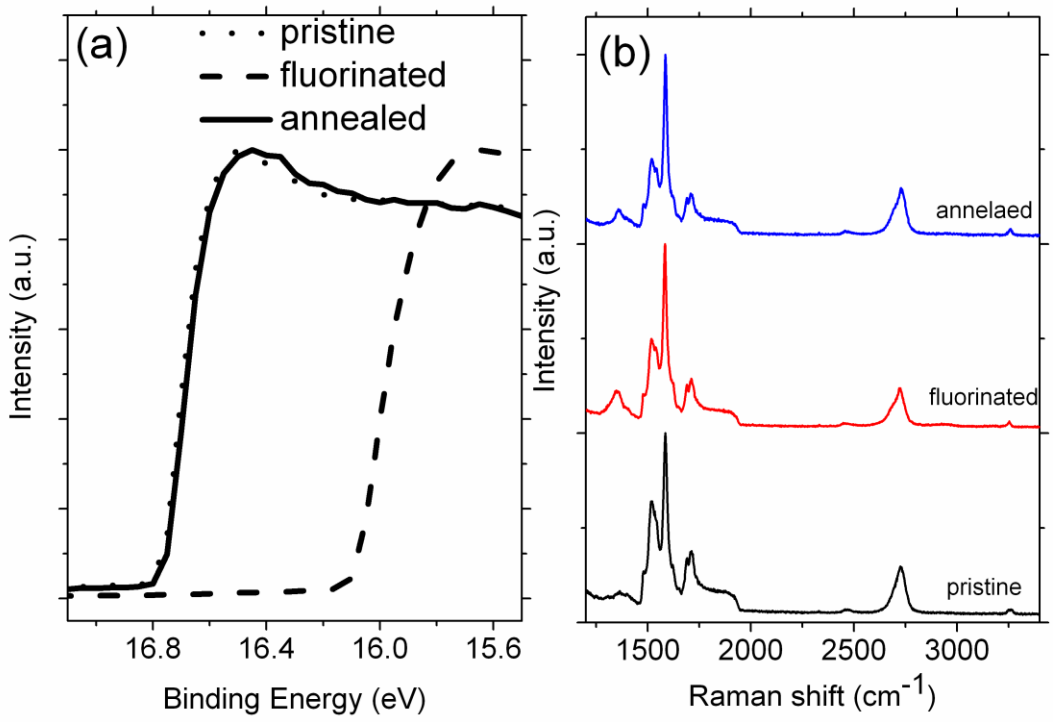

Figure 30: UPS (a) and Raman (b) spectra of fluorinated multi-layer EG (~ 2 layers) grown on C-face 4H-SiC

These data suggest that the increase in work function of EG after the SF_6 plasma-treatment is predominantly due to the adsorption of fluorine atoms and therefore the effects of ion bombardment (physical processes) on the work function of plasma-fluorinated EG are negligible. This conclusion offers an alternative and more detailed explanation of our previously reported studies where an understanding of the lack of correlation between fluorine concentration and work function of fluorinated EG was not apparent. Further insight into these observations can be

obtained from additional analysis of the F 1s XPS spectra of fluorinated EG which indicates that the polarity of carbon-fluorine bonds controls the work function of fluorinated EG.

Polarity of carbon-fluorine bonds

Fluorine atoms are covalently bonded to carbon atoms in polytetrafluoroethyelene (PTFE) while ionic bonding exists between fluorine and metal atoms. Therefore, the binding energies of F 1s peaks for PTFE[186] (~ 690 eV) and NiF_2[187] (~ 685 eV) can be used as references for covalent and ionic bonding respectively (see Figure 31) to compare the polarity of carbon-fluorine bonds in fluorinated EG. The relative proportion of ionic and covalent carbon-fluorine bonds in fluorinated EG can then be calculated by peak-fitting the F 1s spectra.

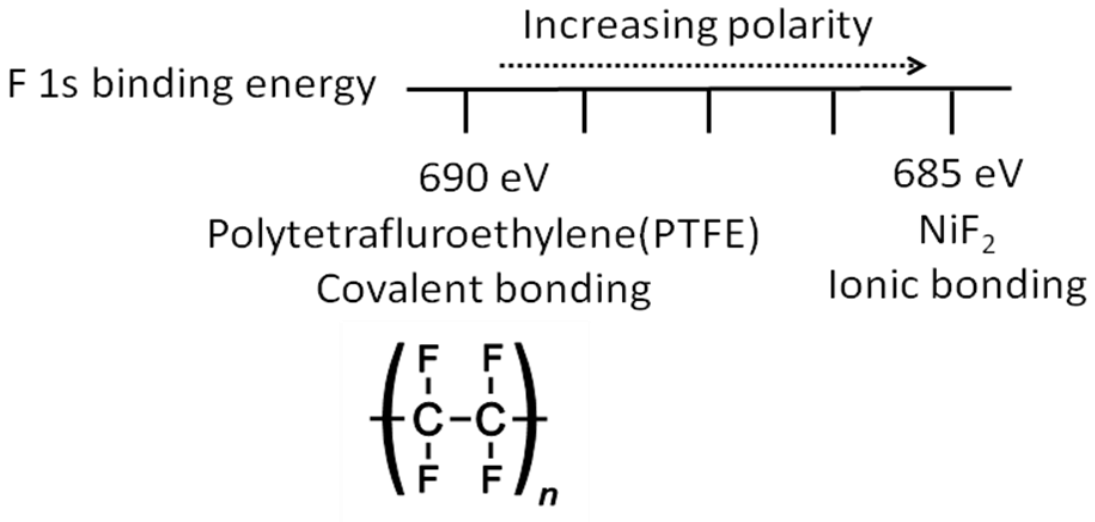

Figure 31: Polarity of carbon-fluorine bonds

Effect of the polarity of carbon-fluorine bonds

The effect of carbon-fluorine bond polarity on EG work function was observed on both multi-layer (~ 20 layers) EG grown on C-face 4H-SiC and few-layer EG grown on Si-face 4H-SiC. UPS and F 1s XPS spectra of three multi-layer (~ 20 layers) EG samples grown in the same batch and then simultaneously exposed to the SF_6 plasma for 30 s are shown in Figure 32.

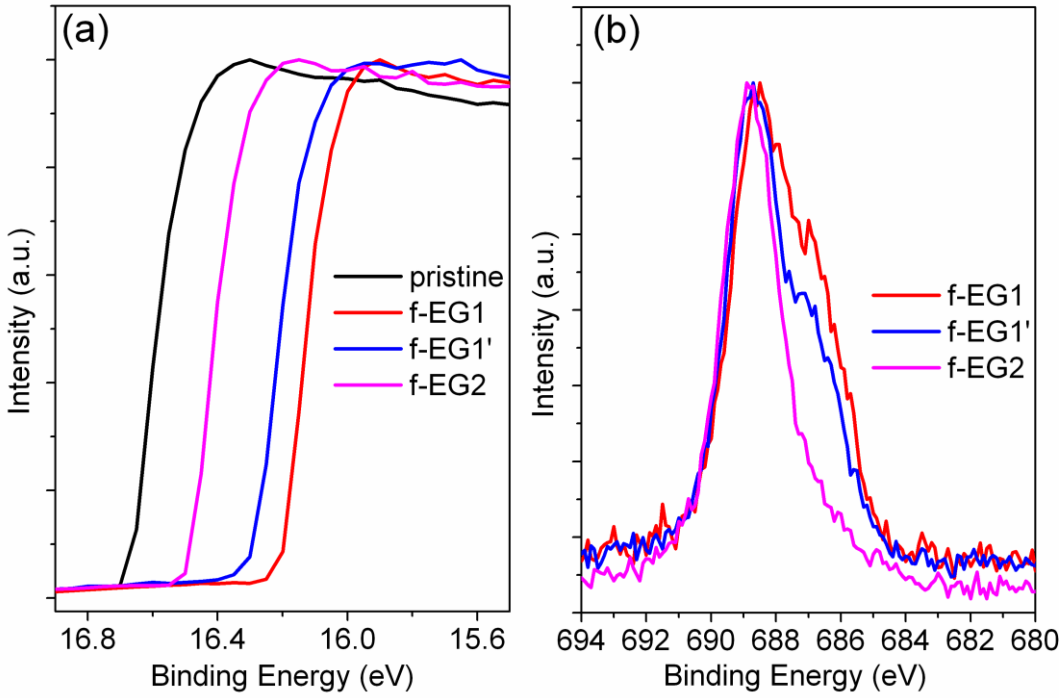

Figure 32: UPS (a) and F 1s XPS (b) spectra of SF_6 plasma-treated multi-layer EG (~20 layers) grown on C-face 4H-SiC

All fluorinated EG samples have similar fluorine concentrations. Specifically, the fluorine concentration of sample 1 (f-EG1) is 5.1±0.3 at. %, sample 2 (f-EG2) is 5.0±0.1 at. %, and sample 3 (f-EG1') is 5.0±0.2 at. %; however, the increases in work function are different. The work function of f-EG1 and f-EG1' increased by 0.54±0.03 eV and 0.45±0.02 eV respectively after the SF6 plasma-treatment while the work function of the f-EG2 increased only by 0.26±0.01 eV as shown in Figure 32 (a). These data are summarized in Table 2.

Table 2: Summary of XPS/UPS data of SF_6 plasma-treated multi-layer EG

	f-EG1	f-EG2	f-EG1’
F 1s (at. %)	5.1±0.3	5.0±0.1	5.0±0.2
Increase in work function (eV)	0.54±0.03	0.26±0.01	0.45±0.02

These data reiterate our inability to correlate directly the increase in work function of fluorinated EG with fluorine concentration. This lack of direct correlation can be explained by the F 1s spectra of fluorinated EG. As shown in Figure 32 (b), the F 1s peak for f-EG1 appear at ~ 688.5 eV which is a characteristic peak of fluorine atoms bonded to carbon atoms while the F 1s peak for f-EG1’ and f-EG2 appears at ~ 688.8 eV. Moreover, the F 1s spectrum of f-EG1 is broader and the area under the curve at binding energies below 688 eV is greater than that of f-EG1’and f-EG2. Peak-fitting these F 1s spectra confirm that f-EG1 has the largest proportion of fluorine atoms with binding energy lower than 688 eV (Table 3 compares the areas under the curve).

Table 3: Comparison of the area under the Gaussian/Lorentzian (30% Lorentzian) curves used to peak-fit F 1s spectra of multi-layer EG after the SF_6 plasma-treatment shown in Figure 32 (b)

f-EG1		f-EG2		f-EG1'	
Binding Energy (eV)	Area %	Binding Energy (eV)	Area %	Binding Energy (eV)	Area %
686.3	27	686.6	15	686.2	17
687.6	30	687.9	23	687.5	32
688.6	21	688.8	30	688.8	33
689.4	22	689.5	32	689.5	19

These data suggest that carbon-fluorine bonds in f-EG1 are the most ionic in nature and the carbon-fluorine bonds in f-EG2 are the least ionic. The polarity of carbon-fluorine bond in these samples correlates with the magnitude of increase in work function: the highest increase in work function was observed in f-EG1 while f-EG2 exhibited the lowest increase in work function. An increase in the polarity of carbon-fluorine bonds results in an increase in the surface dipole moment which in turn results in an increase in the work function of f-EG1 relative to that of f-EG2 as shown in Figure 32. From these observations, we conclude that the work function of fluorinated EG is controlled by the polarity of carbon-fluorine bonds as well as by the fluorine concentration. These results are consistent with the effect of carbon-fluorine bond polarity on graphite properties such as surface energy and electrical conductivity. That is, carbon-fluorine bonds in fluorine-intercalated graphite are ionic compared to the covalent bonds in graphite

fluoride; therefore, fluorine-intercalated graphite is more conductive and hydrophilic than graphite fluoride[188]. A similar relationship between the work function and carbon-fluorine bond polarity was also observed on few-layer EG grown in the same batch and then simultaneously exposed to the SF_6 plasma for 30 s.

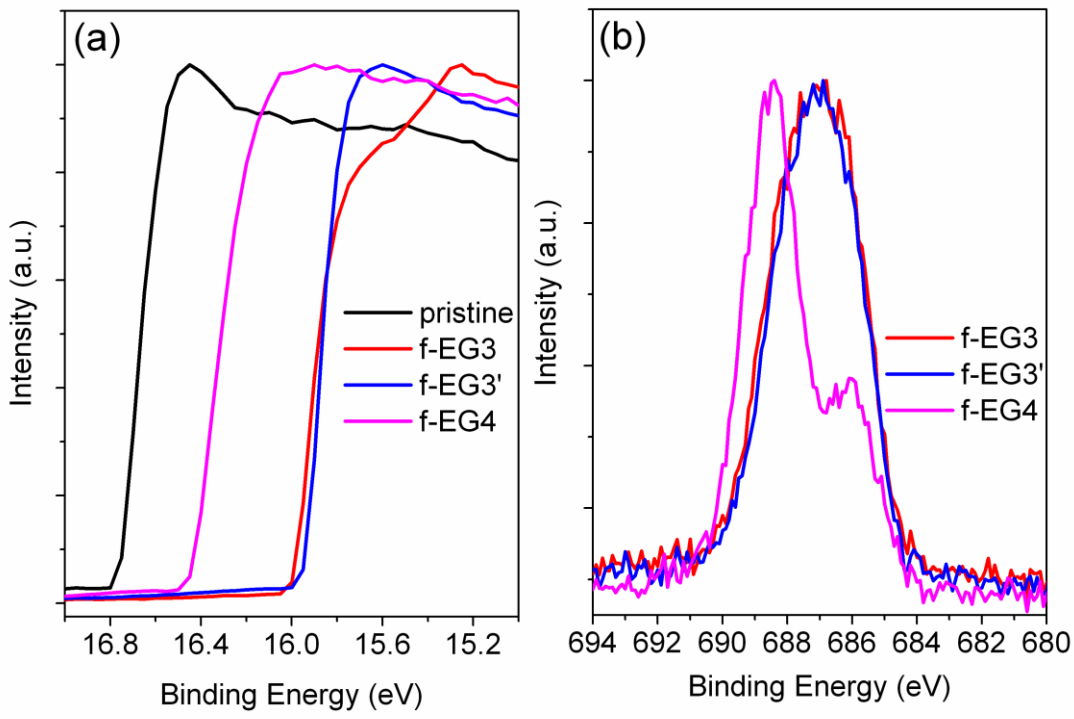

Figure 33: UPS (a) and F 1s XPS (b) spectra of SF_6 plasma-treated few-layer EG grown on Si-face 4H-SiC

The fluorine concentrations of f-EG3, f-EG3', and f-EG4 are 9.0±0.3 at. %, 8.7±0.1 at. %, and 9.7±1.7 at. % respectively. However, the work function of f-EG3 and f-EG3' increased by 0.80±0.01 eV and 0.82±0.04 eV respectively while the work function of f-EG4 increased by only 0.37±0.04 eV as shown in Figure 33 (a). These data are summarized in Table 4.

Table 4: Summary of XPS/UPS data of SF_6 plasma-treated few-layer EG

	f-EG3	f-EG4	f-EG3’
F 1s (at. %)	9.0±0.3	9.7±1.7	8.7±0.1
Increase in work function (eV)	0.80±0.01	0.37±0.04	0.82±0.04

F 1s peaks appear at ~ 687 eV for f-EG3 and f-EG3’ respectively and at ~ 688.5 eV for f-EG4 as shown in Figure 33 (b) which indicates that the carbon-fluorine bonds in f-EG3 and f-EG3’ are more ionic in nature than the carbon-fluorine bonds in f-EG4. Furthermore, the magnitude of increase in work function can be correlated with the area under the curve at binding energies below 688 eV (Table 5 compares the areas under the curve) which reinforces the conclusion drawn from the analysis of photoelectron spectra of EG grown on the C-face SiC.

Table 5: Comparison of the area under the Gaussian/Lorentzian (30% Lorentzian) curves used to peak-fit F 1s spectra of few-layer EG after the SF_6 plasma-treatment shown in Figure 33 (b)

f-EG3		f-EG4		f-EG3'	
Binding Energy (eV)	Area %	Binding Energy (eV)	Area %	Binding Energy (eV)	Area %
685.4	9			685.4	17
686.3	30	685.9	27	686.1	11
687.5	45	687.1	10	687.1	49
688.7	16	688.4	44	688.2	23
		689.5	19		

As seen in Figure 34, C 1s XPS spectra of multi-layer EG (f-EG1 and f-EG2) and few-layer EG (f-EG3 and f-EG4) consist of the graphitic peak at ~284.4 eV and 284.7 eV respectively; since there is no shift in the binding energy of the graphitic peak, we can dismiss the effect of charging artifacts on the measurement of work function.

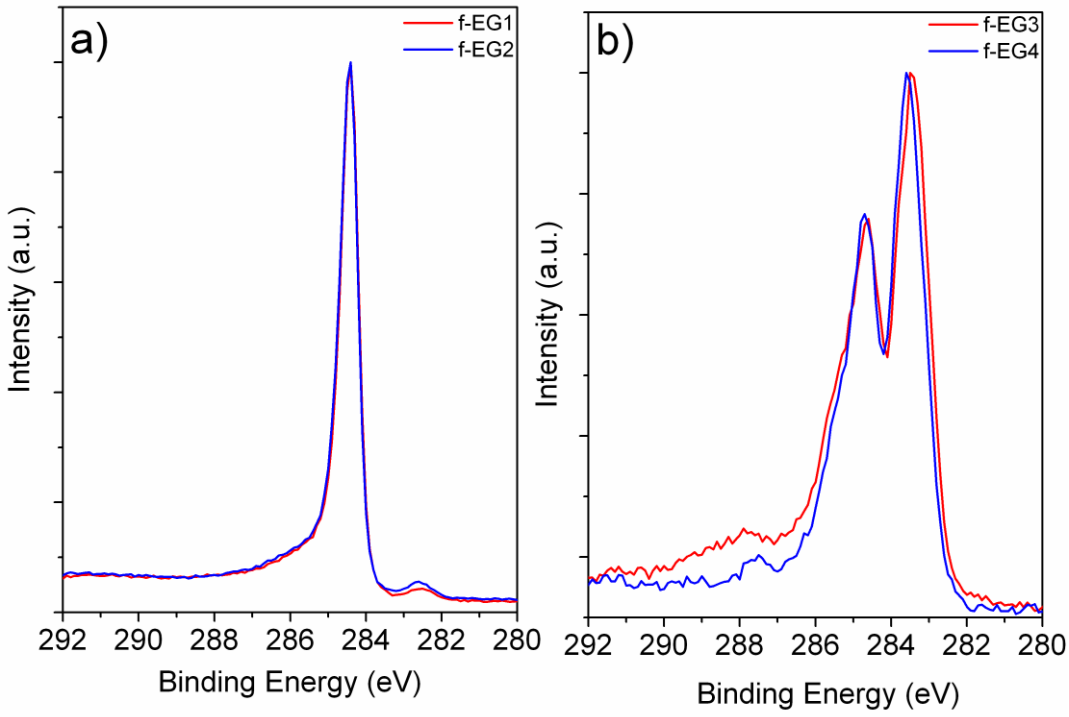

Figure 34: C 1s XPS spectra of SF_6 plasma treated (a) multi-layer and (b) few-layer EG

Although the fluorinated EG samples described above have similar fluorine concentrations, the carbon-fluorine bond polarities are different. Previously reported studies on graphite have shown that a lower concentration of fluorine results in ionic bonding between carbon and fluorine atoms and the bonding becomes more covalent as the fluorine concentration increases[189]. However, the fluorinated EG described in this report displays different polarities in spite of similar fluorine concentrations. Subsequent studies that focus on understanding this discrepancy in the polarity of carbon-fluorine bonds will be presented in Chapter 4. However, we should note here that the role of bi- or multi-layer EG film homogeneity may be important since controllable growth of homogenous bi- or multi-layer EG films is extremely challenging. Furthermore, fluorination of EG may be affected by defects such as cracks, holes, and pucker structures which are formed due

to the complicated surface modification of SiC during graphitization, which includes diffusion of Si from the SiC substrate to the surface of the graphene film and complex reconstructions at the interface between the graphene film and SiC[54]. Additional questions that require attention relate to how fluorine atoms interact with EG; that is, are the fluorine atoms adsorbed on the basal plane or is the fluorination confined to the edges of the graphite domains generated by the plasma-treatment? Given the observation of ionic bonding between fluorine and carbon atoms in fluorinated EG, intercalation of fluorine atoms between the graphene layers must also be considered. Whereas most intercalates bond ionically with carbon atoms in graphene layers, fluorine intercalation in graphite can exhibit three types of bonding: 1) purely ionic bonding where the sp^2-hybridization of carbon atoms in graphene is maintained, or 2) purely covalent bonding resulting in sp^3 rehybridization, or 3) a mixture of ionic and covalent bonding[189]. Our XPS studies do not permit definitive answers to these questions since XPS quantification averages over an area of a few hundred microns. Thus, atomic-scale characterization methods such as scanning tunneling microscopy (STM) must be invoked. A thorough understanding of the interaction between fluorine atoms and EG will provide the detailed insight needed to control the polarity of carbon-fluorine bonds in fluorinated EG.

3.4 Conclusions

In summary, we have established that the work function of fluorinated graphene can be tuned by controlling the polarity of carbon-fluorine bonds. Although the work function modification approach described in this study was limited to EG, our results will be applicable to graphene structures in general. That is, we present the possibility of ionic bonding as a viable approach to functionalize graphene without disrupting the framework of sp^2-hybridized carbon atoms and thereby control graphene properties such as work function, surface energy, and electrical conductivity.

CHAPTER 4: LOCAL WORK FUNCTION MEASUREMENTS OF PLASMA-FLUORINATED EPITAXIAL GRAPHENE

4.1 Introduction

The ability to control the work function of graphene is critical to its successful implementation as a transparent electrode material in organic electronic devices. Toward this end, modification of the work function of epitaxial graphene (EG) via plasma-fluorination has been demonstrated[185]. Our studies have also established the dependence of the work function of fluorinated EG on the polarity of carbon-fluorine bonds which is controlled by the nature of chemical bonding (ionic, semi-ionic, or covalent) between carbon and fluorine atoms[190]. However, the factors that determine the polarity of carbon-fluorine bonds in fluorinated EG are not apparent. Previously reported studies on graphite have shown that a lower concentration of fluorine results in ionic bonding between carbon and fluorine atoms and the bonding becomes more covalent as the fluorine concentration increases[189]. In contrast, carbon-fluorine bonds in the fluorinated EG described in our earlier study display different polarities in spite of similar fluorine concentrations. Understanding the factors that control the polarity of carbon-fluorine bonds in fluorinated EG will provide a novel technique to tune the electrical properties of graphene by controlling C-F bond polarity.

An EG surface can display inhomogeneity in film thickness and other defects which may affect its work function and rate of fluorination. For instance, the work function difference between single- and bi- layer EG grown on Si-face 6H-SiC has been reported be ~135 meV (see Figure 35[191]).

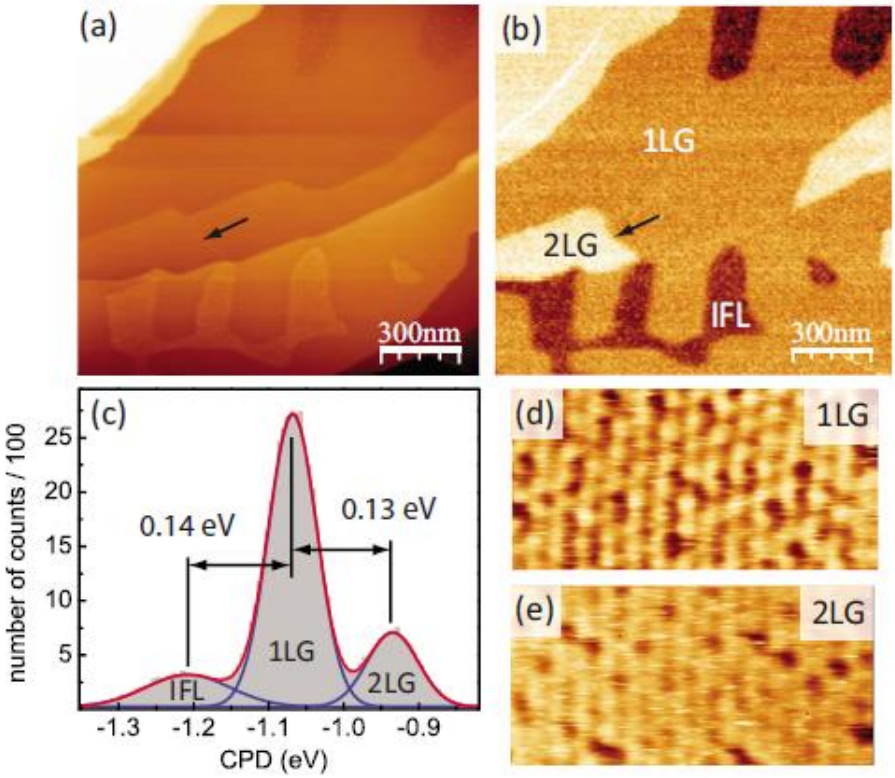

Figure 35: SKPM studies of EG grown on Si-face SiC[191]
(a) Surface topography of EG grown on the Si-face of SiC. (b) CPD map identifying the interface layer (IFL), single-layer graphene (1 LG), and bi-layer graphene (2 LG). The arrows in (a) and (b) indicate the position of a boundary between single and bilayer regions of graphene which is hardly visible in the topography image due to coincidence with a compensating step of the SiC substrate. (c) Histogram of the CPD map. (d) and (e) High-resolution topography images revealing the 6 x 6 superstructure on adjacent single and bilayer films, respectively. Note that (d) and (e) have equal z-range: 0.33 nm.

This difference in work function is attributed to n-doping from the underlying SiC substrate due to the presence of a $(6\sqrt{3} \times 6\sqrt{3})R30°$ reconstructed interface layer (see Figure 36)[27]. Likewise, Norris et al. had determined that the Fermi levels of the first four layers of EG grown on C-face 4H-SiC are 360, 215, 140, and 93 meV above the Dirac point respectively[192].

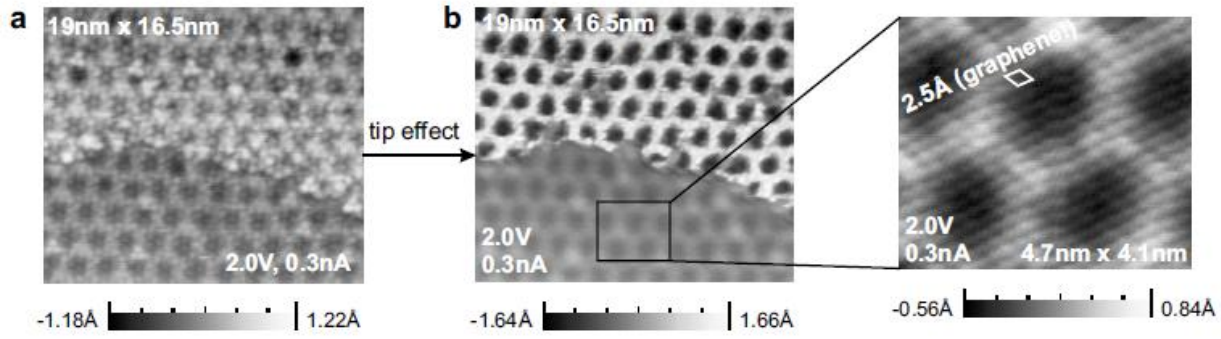

Figure 36: Atomically resolved STM images of the (6√3 x 6√3) R30 ° reconstruction on 4H-SiC (0001) showing (6 x 6) corrugations with two different contrasts for two different tip conditions shown in panels (a) and (b). Only for the tip condition in panel (b) can graphene on top of the (6√3 x 6√3) R30 ° reconstruction be resolved (lower part of the STM image)[27]

In addition, surface of multi-layer EG grown on C-face SiC contains step-edges, pits, and pleats (see Figure 37[54]) which are formed due to the complicated surface modification of SiC during graphitization, which includes diffusion of Si from the SiC substrate to the surface of graphene film and complex reconstructions at the interface between the graphene film and SiC[54].

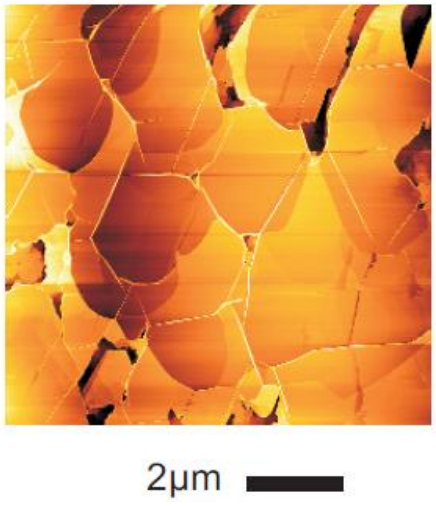

Figure 37: An AFM image of a typical multi-layer (≥10 layers) graphene film grown on C-face 4H-SiC[54]

The effect of these topographical features on the work function of fluorinated EG is not well-understood. In this chapter, we describe the results of local work function measurements of plasma-fluorinated EG by using scanning Kelvin probe microscopy (SKPM); we demonstrate that the increase in the EG work function after plasma-fluorination is independent of the surface topography, but non-uniformity in plasma density may result in non-uniform fluorination.

4.2 Experimental

EG samples were grown on 4H-SiC by high-temperature (~1600 °C) annealing in an RF furnace; EG growth on the Si-face 4H-SiC is limited to few layers (one or two layers) while the growth of multi-layer EG is possible on the C-face 4H-SiC[161]**.**

EG samples were fluorinated by an SF_6 plasma-treatment in an RIE system. This system (Plasma-Therm RIE) operates at a radio-frequency (rf) of 13.56 MHz and has an electrode diameter of 11 inches. All experiments were carried out at room temperature with an rf power of 50 W and an SF_6 partial pressure of 100 mTorr.

Fluorinated EG samples were characterized by XPS to determine elemental composition and by UPS to estimate the work function. XPS and UPS spectra were collected using monochromatized AlKα radiation (1486.6 eV) and He I radiation (21.2 eV) respectively in an XPS/UPS system (Axis UltraDLD, Kratos Analytical). Thickness of the multi-layer EG was determined by an ellipsometer (Horiba Jobin Yvon Auto SE). SKPM measures the contact potential difference (CPD) between a conducting atomic force microscopy (AFM) tip and the sample thereby mapping the CPD between the tip and the sample with a spatial resolution in the nanometer range; surface topography data are generated simultaneously via AFM. Since CPD is equal to the difference between the work function of the sample and the tip, the local work function of EG before and after fluorination can be measured from the CPD distribution. SKPM measurements thus allow investigation of the relationship between the surface topography and the work function of the fluorinated EG. In this study, SKPM measurements were performed under ambient conditions using a PtIr5 (an approximately 25 nm thick double layer of chromium and platinum iridium5) coated n^+-silicon tip (XE-70, Park Systems). Figure 38 shows the schematic diagram of the SKPM system used in this study[193]. A 1000 mV ac voltage was applied to the tip

at the resonance frequency (~75 kHz) with the tip positioned 12 nm above the EG surface. The total cantilever deflection that represents the electrostatic force between the tip and the sample can be analyzed in terms of its three separate parts: dc component, ac component with a frequency of ω, and ac component with a frequency of 2ω. A lock-in amplifier separates the frequency ω component from the total output signal. During the scan, the dc offset potential (V_{DC}) is controlled by a feedback loop such that the ω signal measured by the lock-in amplifier is zero. This value of V_{DC} that zeros the ω component of the electrostatic force between the tip and the sample is a measure of the CPD.

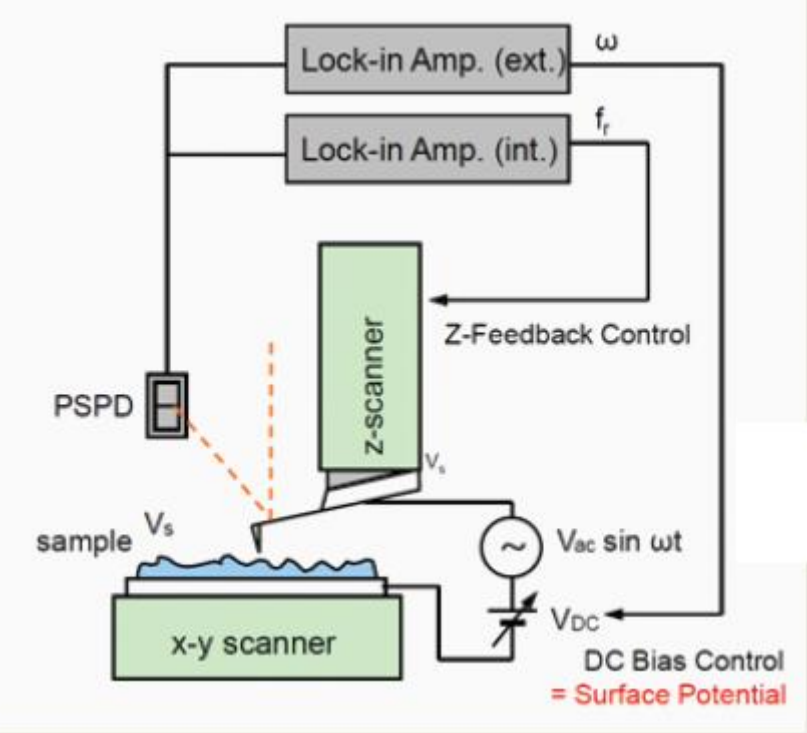

Figure 38: Schematic diagram of the scanning Kelvin probe microscopy of the Park System's XE-series[193]

4.3 Results and Discussions

4.3.1 Few-layer EG grown on Si-face 4H-SiC

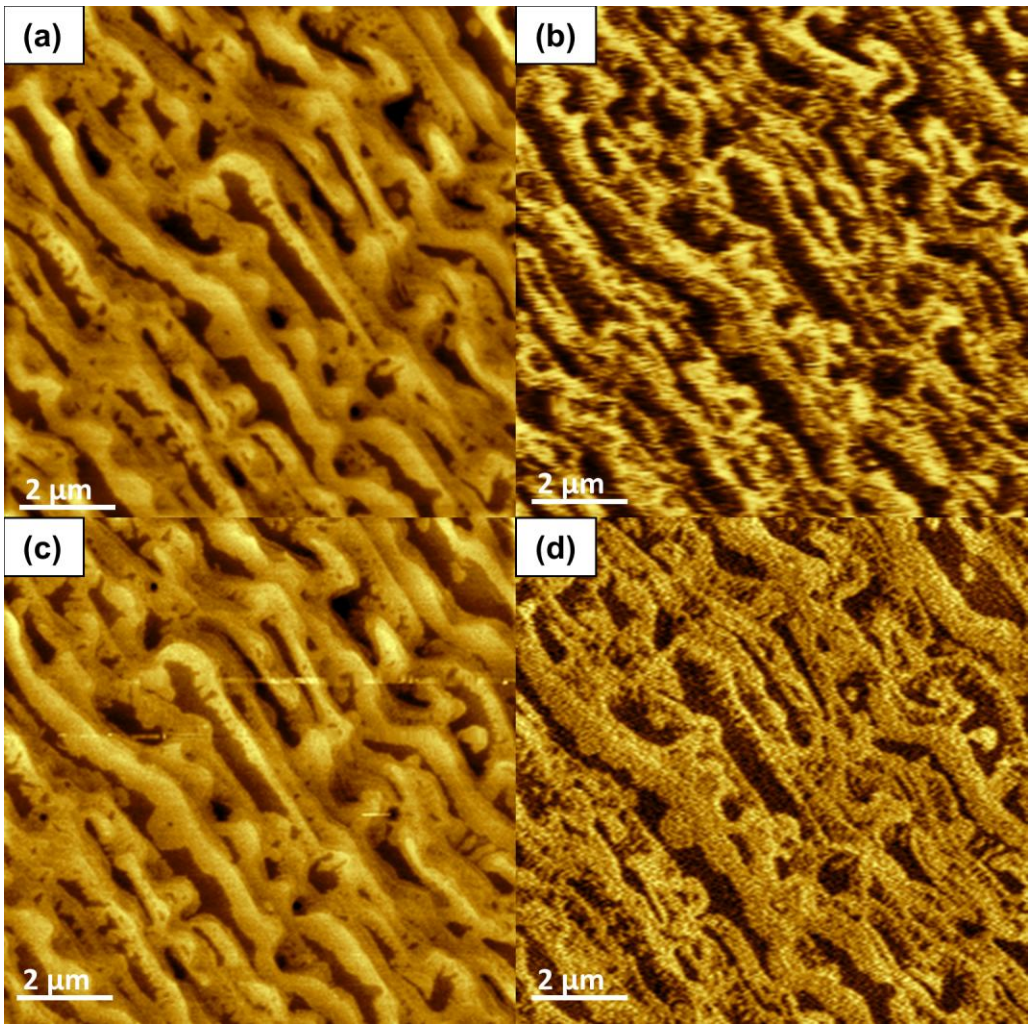

Figure 39: SKPM studies of SF_6 plasma-treated few-layer EG grown on the Si-face of 4H-SiC Surface topography (a) and CPD map (b) before fluorination. Surface topography (c) and CPD map (d) after the fluorination

SKPM studies scanned a (10 µm)^2 region. Surface topography of few-layer EG is shown in Figure 39 (a) and rms roughness (calculated by averaging 5 randomly chosen 0.1-0.3 µm^2 regions) of regions with similar height is ~ 0.70 nm. Regions of different CPD observed is in

Figure 39 (b) and the spread in potential between these regions is 77±45 mV [See Figure 40 (a) for the CPD histogram of few-layer EG before the fluorination and

Table 6 for parameters of the Gaussian curves used to peak-fit the CPD histogram].

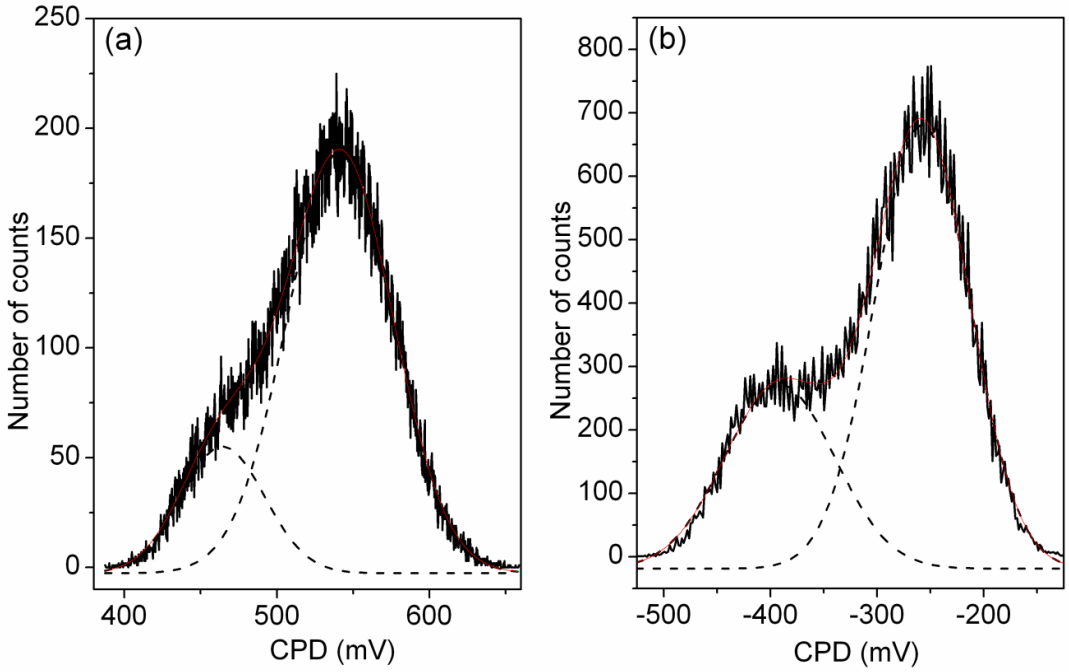

Figure 40: CPD histogram of few- layer EG grown on Si-face 4H-SiC (a) before and (b) after fluorination

Based on the Fermi levels of EG layers determined by Norris et al.[192], the regions of different CPD can be interpreted as the regions of bi- and tri- layer EG. The rms CPD variation (calculated by averaging 5 randomly chosen 0.1-0.3 μm^2 regions) over the region of similar thickness is ~ 20 mV which indicates the uniformity of carrier concentration. After SF_6 plasma exposure for 30 s, the fluorine concentration was determined to be ~7 at. % by XPS and the work function increased by ~ 650 meV as shown in Figure 41(a).

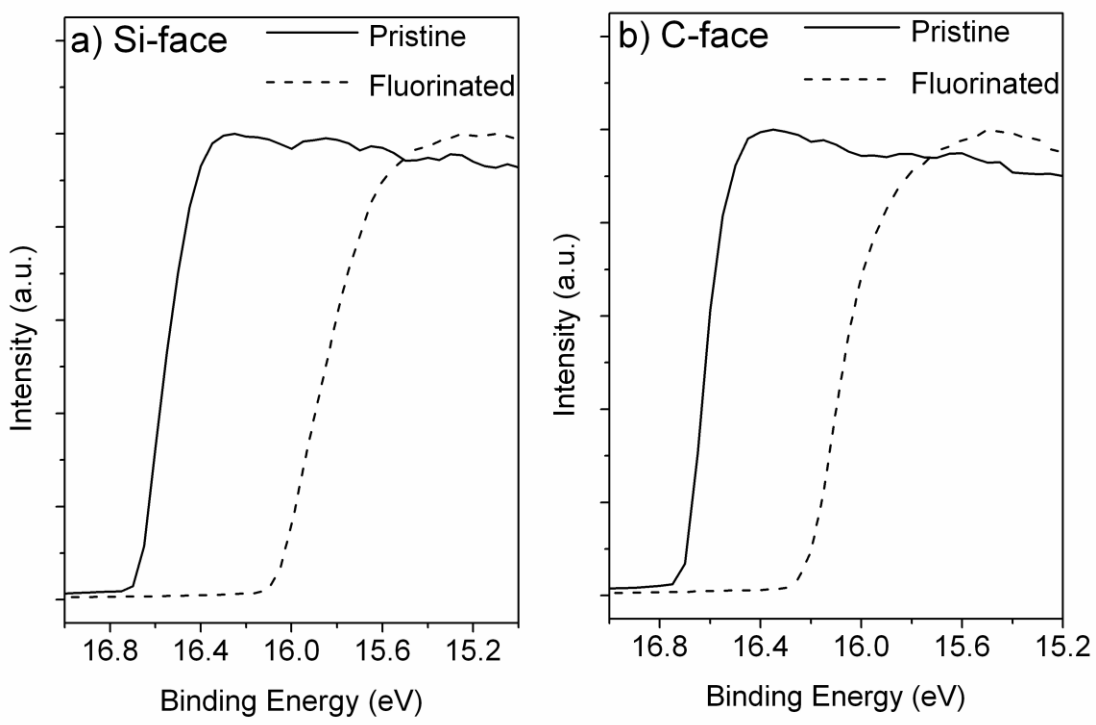

Figure 41: UPS spectra of pristine and fluorinated EG: (a) few-layer EG grown on Si-face 4H-SiC and (b) multi-layer (~10 layers) EG grown on C-face 4H-SiC

The SKPM scan was then repeated over the same (10 μm) ^{2} region shown in Figure 39 (a). Figure 39 (c) shows that the topographical features of the EG surface remain intact after the fluorination and the rms surface roughness (calculated by averaging 5 randomly chosen 0.1-0.3 μm2 regions) of the region with similar thickness is ~ 0.60 nm which suggest that the plasma-treatment is not deleterious to the EG surface. The regions of different CPD observed in Figure 39 (d) are similar to the CPD map of EG prior to fluorination as shown in Figure 39 (b) and the spread in CPD between these regions is 133±68 mV **[**See Figure 40 (b) for the CPD histogram of few-layer EG after the fluorination and

Table 6 for parameters of the Gaussian curves used to peak-fit the CPD histogram]. Thus, fluorination does not change the CPD distribution in spite of the increase in work function**.** From

these data, we can infer that the rate of fluorination does not correlate with EG thickness. The rms CPD variation over a region of similar thickness in fluorinated EG is ~30 mV which demonstrates the uniform carrier concentration in fluorinated EG and thereby confirms the uniformity of fluorination.

Table 6: Parameters of the Gaussian curves used to peak-fit the CPD histogram shown in Figure 40

	Peak 1		Peak 2			
	Mean (mV)	Standard Deviation (mV)	Mean (mV)	Standard Deviation (mV)	Difference in CPD (mV)	Standard Deviation (mV)
Figure 40 (a)	541	35	464	28	77	45
Figure 40 (b)	-258	45	-391	51	133	68

4.3.2 Multi-layer EG grown on C-face 4H-SiC

Figure 42 compares SKPM images on a (10 μm)^2 region of multi-layer EG (~10 layers) before and after fluorination.

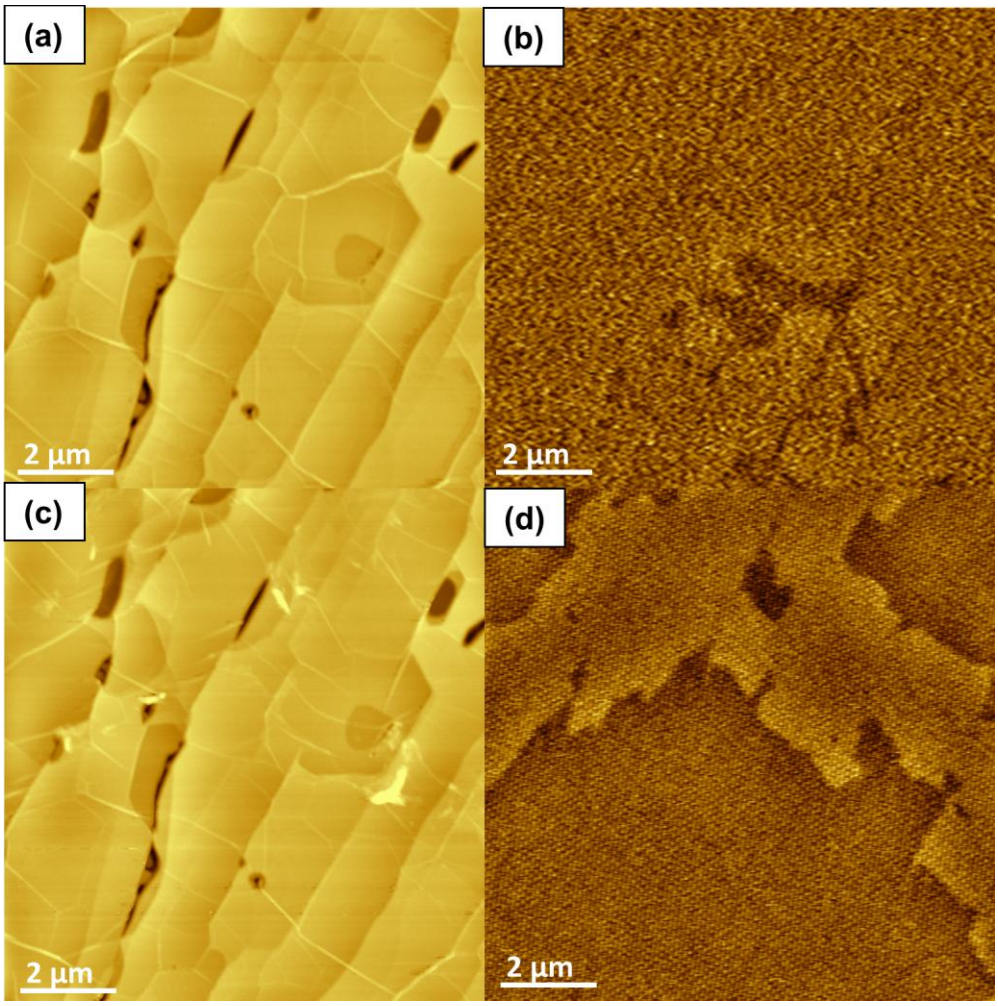

Figure 42: SKPM studies of SF_6 plasma-treated multi-layer EG (~10 layers) grown on the C-face of 4H-SiC Surface topography (a) and CPD map (b) before fluorination. Surface topography (c) and CPD map (d) after fluorination

Figure 42 (a) shows that the EG surface consists of characteristic topographical features of multi-layer EG, including steps, a network of pleats that bound the flat tile-like facets of graphene, and pits. The rms surface roughness (calculated by averaging 5 randomly chosen ~0.3 μm^2 regions) of the flat regions between the step-edges is ~0.60 nm. Unlike the few-layer EG grown on Si-

face 4H-SiC, the CPD of multi-layer EG is independent of variation in topographical features [Figure 42(b)]; the CPD distribution is nearly uni-modal [See Figure 43 (a) for the CPD histogram of multi-layer EG before the fluorination and

Table 7 for parameters of the Gaussian curves used to peak-fit the CPD histogram] and rms CPD variation over the entire scanned $(10\ \mu m)^2$ region is ~30 mV.

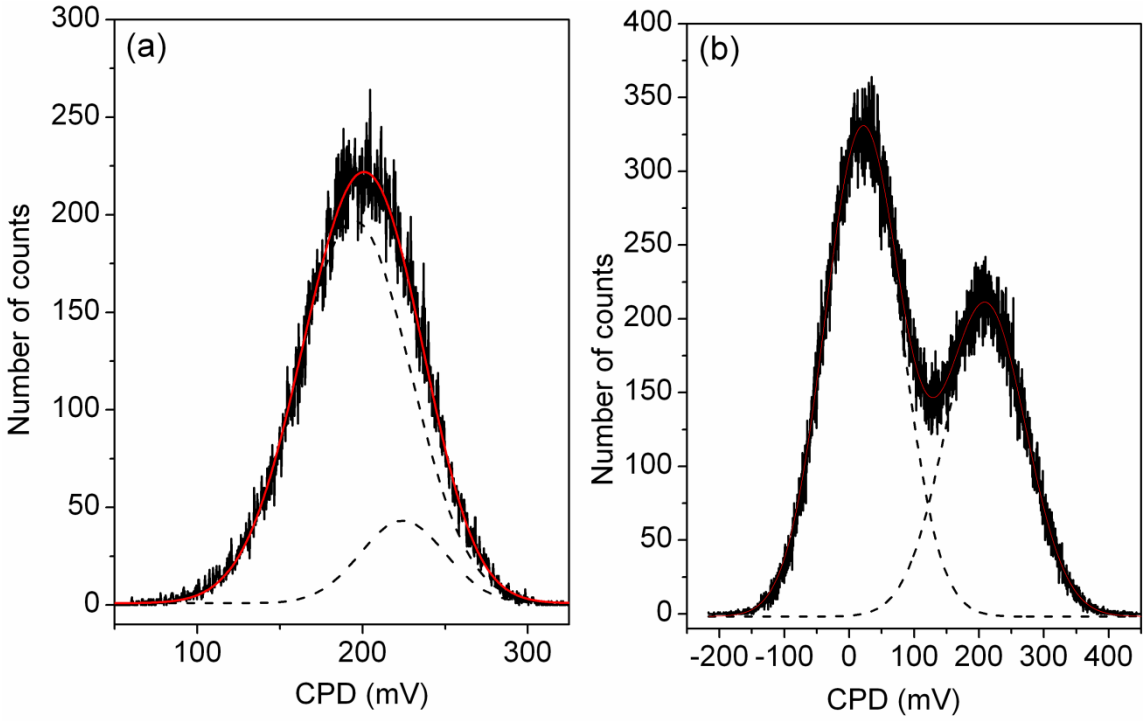

Figure 43: CPD histogram of multi-layer EG grown on C-face 4H-SiC (a) before and (b) after fluorination

It must be noted that the multi-layer EG grown on C-face 4H-SiC does not have the interface layer. Furthermore, additional layers of graphene in multi-layer EG may also screen the effect of substrate-induced doping. For this reason, the CPD of multi-layer EG is independent of the EG thickness. After SF_6 plasma exposure for 30 s, fluorinated EG contains ~8 at. % fluorine atoms and the increase in work function is ~560 meV as shown in UPS spectra in Figure 41 (b). The majority of the topographical features remain intact after EG fluorination [Figure 42 (c)] and the

rms surface roughness in the flat regions between the step-edges remains ~0.60 nm. These data are in agreement with observations from few-layer EG studies that plasma-treatment does not damage the EG surface. However, we also observe the disappearance of some of the pleats and the formation of new pleats along with a few bright and irregularly-shaped spots. During the plasma-treatment, the uppermost layer of EG in this region may have been etched away due to a non-uniformity in plasma density. Indeed, local plasma non-uniformities can originate from gradients in the local concentration of fluorine radicals[194], fluctuation in ion-fluxes[195], or non-uniformities in voltage distribution across the electrode area[196]. At this time, we cannot ascribe the results to any one of these phenomena. Because of the removal of the uppermost graphene layer, all topographical features associated with those layers disappear and new topographical features associated with the layer underneath the etched layer emerge. In contrast with non-fluorinated EG, regions of different CPD are evident after the fluorination [Figure 42(d)] and the region with higher CPD corresponds to the region that consists of newly-formed pleats and bright and irregular spots. The CPD distribution is bimodal and the spread in CPD is 189±85 mV [See Figure 43 (b) for the CPD histogram of multi-layer EG after the fluorination and Table 7 for parameters of the Gaussian curves used to peak-fit the CPD histogram]; the rms CPD variation (calculated by averaging 5 randomly chosen ~ 2 μm^2 regions) over the region of similar CPD in fluorinated EG is ~ 50 mV.

Table 7: Parameters of the Gaussian curves used to peak-fit the CPD histogram shown in Figure 43

	Peak 1		Peak 2			
	Mean (mV)	Standard Deviation (mV)	Mean (mV)	Standard Deviation (mV)	Difference in CPD (mV)	Standard Deviation (mV)
Figure 43 (a)	194	34	224	26	30	43
Figure 43 (b)	21	58	210	62	189	85

These data indicate a non-uniform increase in work function after plasma-treatment which is consistent with our previously reported difference in work function of fluorinated EG layers that had been exposed to SF_6 plasma simultaneously[190]. The non-uniformity in work function observed in the EG sample shown in Figure 42 (d) can be explained if a local fluorine concentration gradient exists. XPS studies cannot corroborate this assumption since XPS quantification averages over an area of a few hundred microns. Alternatively, the non-uniformity in work function can be attributed to a difference in the polarity of carbon-fluorine bonds in the regions with different CPD. Previously, C_{60}-functionalized scanning tunneling microscopy (STM) tips have been used to distinguish ionic and covalent carbon-fluorine bonds on graphite; this distinction is established by the differences induced by each bonding configuration in the surrounding local density of states on the graphite surface[197]. We expect that STM characterization of fluorinated EG may provide further insight into this local work function gradient.

4.4 Conclusions

In summary, SKPM studies of fluorinated EG demonstrate that the increase in the work function after SF_6 plasma-treatment is independent of the surface topography and the plasma-treatment is not detrimental to the EG surface. There is also a possibility of non-uniform fluorination which may result from the non-uniformities in plasma density. The fact that the plasma-treatment can functionalize graphene with negligible surface damage highlights the feasibility of plasma-chemistry treatments as a facile approach for the chemical functionalization of graphene.

CHAPTER 5: CONCLUSIONS AND FUTUTRE WORK

5.1 Conclusions

Graphene is a single layer of sp^2-hybridized carbon atoms. The discovery of unique properties of graphene has led to the development of graphene for a variety of applications like integrated circuits, organic electronic devices, supercapacitors, sensors, and composite materials. The ability to engineer the properties of graphene is critical to facilitate the realization of these applications. Toward this end, chemical functionalization of graphene has emerged as an attractive method to control its physical, chemical, and electronic properties. Typical applications of chemical functionalization include band gap opening via functionalization with oxygen, hydrogen, and fluorine and the production of graphene sheets by reduction of graphite oxide. Recently, fluorinated graphene has garnered significant attention as a wide band gap semiconductor and a high-quality insulator. Fluorination of graphene therefore offers the ability to tune its electronic properties. Furthermore, fluorination of graphene enhances its surface reactivity thereby improving the uniformity of the atomic layer deposition of ultra-thin films of high-κ dielectrics. Derivation of graphene sheets from graphite fluoride has also been demonstrated. Since fluorination of graphene increases its hydrophobicity, biomedical applications of graphene could also be enabled. This thesis describes the results of our investigation of the fluorination of graphene using reactive ion etch (RIE) plasma and our subsequent efforts to engineer the work function of graphene via fluorination for optoelectronic applications. The findings of our studies have established plasma technology as a facile approach for the fluorination of graphene without the disruption of its lattice and surface topography. The work function of graphene can be modified via plasma-fluorination and our studies indicate that

the increase in its work function depends on the polarity of carbon-fluorine bonds in addition to its fluorine concentrations.

Due to the ubiquitous presence of plasma technology in the semiconductor industry, plasma-enabled processing of graphene may facilitate the integration of the technological infrastructure of the semiconductor industry into graphene-based electronics. Toward this end, our initial studies demonstrated that an SF_6 RIE plasma can fluorinate both multi-layer and single-layer EG films without disruption of sp^2-hybridized carbon framework of EG. Fluorine content in the sample can be altered by simply varying the plasma treatment time and the fluorination is limited to only one or two surface layers. In addition, we have demonstrated the ability of plasma-assisted fluorination to modify the work function of graphene; therefore, SF_6 plasma treatment facilitates the application of graphene as an electrode for organic electronic devices. The ability to control the thickness of EG on carbon-face SiC was exploited to fabricate one or two layers of fluorinated graphene both on top of the insulating substrate (SiC) and the conductive graphene film of desired thickness. Since the semiconducting properties of fluorinated graphene have been reported, a fluorinated graphene/graphene interface also offers the possibility of fabricating bottom-gated EG devices.

Work function engineering of graphene is critical to facilitate its application as a transparent electrode material in organic electronic devices. Initial studies on the plasma-fluorination of EG revealed an increase in the work function of EG after an SF_6 plasma-treatment; however, the work function could not be varied in a predictable manner. Subsequent investigations to controllably modify the work function of EG has established that the work function of fluorinated graphene may be tuned by controlling the polarity of carbon-fluorine bonds which

depends upon the nature of the chemical bonds (ionic, semi-ionic, or covalent) between fluorine and carbon atoms. Although the work function modification approach described in this thesis was applied to EG, our results will be applicable to graphene structures in general. That is, we present the possibility of ionic bonding as a viable approach to functionalize graphene without disrupting the framework of sp^2-hybridized carbon atoms and thereby control graphene properties such as work function, surface energy, and electrical conductivity.

Although the dependence of the work function of fluorinated graphene on the polarity of carbon-fluorine bonds was established, the factors that determine the polarity of carbon-fluorine bonds in fluorinated graphene were not apparent. Therefore, further studies to investigate the effect of the surface topography of EG on the work function of plasma-fluorinated EG were performed using SKPM. The results of the SKPM studies of fluorinated EG demonstrate that the increase in the work function after SF_6 plasma-treatment is independent of the surface topography and the plasma-treatment is not detrimental to the EG surface. There is also a possibility of non-uniform fluorination which may result from the non-uniformities in plasma density. The fact that the plasma-treatment can functionalize graphene with negligible surface damage highlights the feasibility of plasma-chemistry treatments as a facile approach for the chemical functionalization of graphene.

In summary, the work described in this thesis has established the viability of plasma technology for the chemical functionalization of graphene without the disruption of its lattice and surface topography. Work function of graphene can be modified via plasma-fluorination and the increase in its work function depends on the polarity of carbon-fluorine bonds in addition to its fluorine concentration.

5.2 Future work

This thesis describes plasma-fluorination as an attractive method for the work function engineering of graphene. A detailed understanding of the plasma-fluorinated EG developed by employing a diverse set of characterization techniques presents several opportunities for further research that require controlled surface modification of graphene.

Factors that control the polarity of carbon-fluorine bonds have not yet been determined. Previously, C_{60}-functionalized STM tips have been used to distinguish ionic and covalent carbon-fluorine bonds on graphite; this distinction is established by the differences induced by each bonding configuration in the surrounding local density of states on the graphite surface. We expect that STM characterization of fluorinated EG may provide further insight into the understanding of the factors that control the carbon-fluorine bond polarity.

All of our experiments were performed on EG which is not suitable for certain applications, including the fabrication of organic electronic devices that require graphene to be placed on an arbitrary substrate. Because of its transferability, CVD-graphene is more suitable for such applications. Simultaneous exposure of EG and CVD-graphene to SF_6 plasma will allow investigation of the differences in reaction chemistry between the two graphene samples. We expect the findings of our studies on EG to be applicable to graphene structures in general, but the surface topography of CVD-graphene is different than that of EG. Specifically, CVD-graphene is polycrystalline — multiple graphene crystals connected by grain boundaries[198]. Theoretical investigations of polycrystalline graphene have revealed enhanced reactivity at the grain boundaries in graphene due to an inhomogeneous strain[199]. Therefore, we anticipate the CVD-graphene to be more reactive than EG.

Realization of graphene-based transistors requires the uniform and pin-hole free deposition of ultra-thin films (~10 nm) of high-κ dielectrics on graphene. The uniform deposition of these films is typically achieved via atomic layer deposition (ALD) which requires surface reaction with ALD precursors to initiate the nucleation of the film. However, pristine graphene is hydrophobic and chemically inert — there are no dangling bonds on the surface of defect-free graphene. For this reason, uniform ALD of ultra-thin films of high-κ dielectrics on pristine graphene is challenging. To this end, the quality of ALD of ultra-thin films can be improved by enhancing the surface reactivity of graphene via plasma-fluorination which incorporates fluorine moieties that can react with ALD precursors.

Nanoscale reduction of graphene oxide by using heated AFM tips has been demonstrated[200]. However, the reduction of graphene oxide is not complete; reduced graphene oxide contains residual oxygen and structural defects. In contrast, plasma-fluorinated EG described in this thesis retains the framework of sp^2-hybridized carbon atoms as well its surface morphology. Furthermore, fluorination of graphene can be reversed via thermal annealing. Therefore, nanoscale annealing of fluorinated graphene with heated AFM tips affords an alternate opportunity for non-lithographic nano-patterning of graphene.

APPENDIX
AUTHOR'S PUBLICATIONS

[1] S.D. Sherpa, G. Levitin, and D.W. Hess, Applied Physics Letters 101, 111602 (2012).

[2] S.D. Sherpa, S.A. Paniagua, G. Levitin, S.R. Marder, M.D. Williams, and D.W. Hess, Journal of Vacuum Science & Technology B: Microelectronics and Nanometer Structures 30, 03D102 (2012).

REFERENCES

[1] A.K. Geim and K.S. Novoselov, Nature Materials **6**, 183 (2007).

[2] L. Yan, Y.B. Zheng, F. Zhao, S. Li, X. Gao, B. Xu, P.S. Weiss, and Y. Zhao, Chemical Society Reviews **41**, 97 (2012).

[3] H.P. Boehm, R. Setton, and E. Stumpp, Carbon **24**, 241 (1986).

[4] A.D. McNaught and A. Wilkinson, *IUPAC in Compendium of Chemical Terminology*, 2nd ed. (Blackwell Scientific, Oxford, 1997).

[5] P.R. Wallace, Physical Review **71**, 622 (1947).

[6] H.P. Boehm, A. Clauss, G.O. Fischer, and U. Hofmann, Zeitschrift Für Naturforschung **17**, 150 (1962).

[7] A.E. Morgan and G.A. Somorjai, Surface Science **12**, 405 (1968).

[8] J.W. May, Surface Science **17**, 267 (1969).

[9] J.C. Hamilton and J.. M. Blakely, Surface Science **91**, 199 (1980).

[10] J.M. Blakely, J.S. Kim, and H.C. Potter, Journal of Applied Physics **41**, 2693 (1970).

[11] J.C. Hamilton and J.M. Blakely, Journal of Vacuum Science and Technology **15**, 559 (1978).

[12] A.J. Van Bommel, J.E. Crombeen, and A. Van Tooren, Surface Science **48**, 463 (1975).

[13] D.V. Badami, Carbon **3**, 53 (1965).

[14] D.R. Dreyer, R.S. Ruoff, and C.W. Bielawski, Angewandte Chemie **49**, 9336 (2010).

[15] C. Berger, Z. Song, T. Li, X. Li, A.Y. Ogbazghi, R. Feng, Z. Dai, A.N. Marchenkov, E.H. Conrad, P.N. First, and W.A. de Heer, Journal of Physical Chemistry B **108**, 19912 (2004).

[16] "Hall Effect." http://hyperphysics.phy-astr.gsu.edu/hbase/magnetic/hall.html. 1 March 2013.

[17] K.S. Novoselov, A.K. Geim, S. V. Morozov, D. Jiang, Y. Zhang, S. V. Dubonos, I. V. Grigorieva, and A.A. Firsov, Science **306**, 666 (2004).

[18] S. Frank, P. Poncharal, Z.L. Wang, and W.A. de Heer, Science **280**, 1744 (1998).

[19] S.J. Tans, M.H. Devoret, H. Dai, A. Thess, R.E. Smalley, L.J. Geerligs, and C. Dekker, Nature **386**, 474 (1997).

[20] S.J. Tans, A.R.M. Verschueren, and C. Dekker, Nature **393**, 49 (1998).

[21] A. Bachtold, P. Hadley, T. Nakanishi, and C. Dekker, Science **294**, 1317 (2001).

[22] K. Nakada, M. Fujita, G. Dresselhaus, and M.S. Dresselhaus, Physical Review B **54**, 17954 (1996).

[23]"The Nobel Prize in Physics 2010." Nobelprize.org. 4 Feb 2013

[24] R.M. Tromp and J.B. Hannon, Physical Review Letters **102**, 106104 (2009).

[25] K. V. Emtsev, A. Bostwick, K. Horn, J. Jobst, G.L. Kellogg, L. Ley, J.L. McChesney, T. Ohta, S.A. Reshanov, J. Röhrl, E. Rotenberg, A.K. Schmid, D. Waldmann, H.B. Weber, and T. Seyller, Nature Materials **8**, 203 (2009).

[26] J. Hass, F. Varchon, J. Millán-Otoya, M. Sprinkle, N. Sharma, W. de Heer, C. Berger, P. First, L. Magaud, and E. Conrad, Physical Review Letters **100**, 125504 (2008).

[27] C. Riedl and U. Starke, Physical Review B **76**, 245406 (2007).

[28] T. Ohta, A. Bostwick, T. Seyller, K. Horn, and E. Rotenberg, Science **313**, 951 (2006).

[29] Y.-M. Lin, C. Dimitrakopoulos, K.A. Jenkins, D.B. Farmer, H.-Y. Chiu, A. Grill, and P. Avouris, Science **237**, 662 (2010).

[30] K.S. Kim, Y. Zhao, H. Jang, S.Y. Lee, J.M. Kim, K.S. Kim, J.-H. Ahn, P. Kim, J.-Y. Choi, and B.H. Hong, Nature **457**, 706 (2009).

[31] S.-Y. Kwon, C. V. Ciobanu, V. Petrova, V.B. Shenoy, J. Bareño, V. Gambin, I. Petrov, and S. Kodambaka, Nano Letters **9**, 3985 (2009).

[32] P.W. Sutter, J.-I. Flege, and E.A. Sutter, Nature Materials **7**, 406 (2008).

[33] J. Coraux, A.T. N'Diaye, C. Busse, and T. Michely, Nano Letters **8**, 565 (2008).

[34] X. Li, W. Cai, J. An, S. Kim, J. Nah, D. Yang, R. Piner, A. Velamakanni, I. Jung, E. Tutuc, S.K. Banerjee, L. Colombo, and R.S. Ruoff, Science **324**, 1312 (2009).

[35] S. Bae, H. Kim, Y. Lee, X. Xu, J.-S. Park, Y. Zheng, J. Balakrishnan, T. Lei, H.R. Kim, Y. Il Song, Y.-J. Kim, K.S. Kim, B. Ozyilmaz, J.-H. Ahn, B.H. Hong, and S. Iijima, Nature Nanotechnology **5**, 574 (2010).

[36] X. Li, W. Cai, L. Colombo, and R.S. Ruoff, Nano Letters **9**, 4268 (2009).

[37] W.S. Hummers and R.E. Offeman, Journal of the American Chemical Society **80**, 1339 (1958).

[38] T. Szabo, O. Berkesi, P. Forgo, K. Josepovits, Y. Sanakis, D. Petridis, and I. Dekany, Chemistry of Materials **18**, 2740 (2006).

[39] H.C. Schniepp, J.-L. Li, M.J. McAllister, H. Sai, M. Herrera-Alonso, D.H. Adamson, R.K. Prud'homme, R. Car, D.A. Saville, and I.A. Aksay, The Journal of Physical Chemistry B **110**, 8535 (2006).

[40] S. Stankovich, D.A. Dikin, R.D. Piner, K.A. Kohlhaas, A. Kleinhammes, Y. Jia, Y. Wu, S.T. Nguyen, and R.S. Ruoff, Carbon **45**, 1558 (2007).

[41] S. Stankovich, D.A. Dikin, G.H.B. Dommett, K.M. Kohlhaas, E.J. Zimney, E.A. Stach, R.D. Piner, S.T. Nguyen, and R.S. Ruoff, Nature **442**, 282 (2006).

[42] G. Wang, J. Yang, J. Park, X. Gou, B. Wang, H. Liu, and J. Yao, The Journal of Physical Chemistry C **112**, 8192 (2008).

[43] Y. Si and E.T. Samulski, Nano Letters **8**, 1679 (2008).

[44] Y. Zhu, M.D. Stoller, W. Cai, A. Velamakanni, R.D. Piner, D. Chen, and R.S. Ruoff, ACS Nano **4**, 1227 (2010).

[45] L.J. Cote, R. Cruz-Silva, and J. Huang, Journal of the American Chemical Society **131**, 11027 (2009).

[46] G. Williams, B. Seger, and P. V Kamat, ACS Nano **2**, 1487 (2008).

[47] D. V Kosynkin, A.L. Higginbotham, A. Sinitskii, J.R. Lomeda, A. Dimiev, B.K. Price, and J.M. Tour, Nature **458**, 872 (2009).

[48] L. Jiao, L. Zhang, X. Wang, G. Diankov, and H. Dai, Nature **458**, 877 (2009).

[49] A.G. Cano-Márquez, F.J. Rodríguez-Macías, J. Campos-Delgado, C.G. Espinosa-González, F. Tristán-López, D. Ramírez-González, D.A. Cullen, D.J. Smith, M. Terrones, and Y.I. Vega-Cantú, Nano Letters **9**, 1527 (2009).

[50] L. Ci, Z. Xu, L. Wang, W. Gao, F. Ding, K.F. Kelly, B.I. Yakobson, and P.M. Ajayan, Nano Research **1**, 116 (2008).

[51] L. Jiao, X. Wang, G. Diankov, H. Wang, and H. Dai, Nature Nanotechnology **5**, 321 (2010).

[52] K.S. Novoselov, A.K. Geim, S. V Morozov, D. Jiang, M.I. Katsnelson, I. V Grigorieva, S. V Dubonos, and A.A. Firsov, Nature **438**, 197 (2005).

[53] Y. Zhang, Y.-W. Tan, H.L. Stormer, and P. Kim, Nature **438**, 201 (2005).

[54] X. Li, Epitaxial Graphene Films on SiC: Growth, Characterization, and Devices, Georgia Institute of Technology, 2008.

[55] M. Han, B. Özyilmaz, Y. Zhang, and P. Kim, Physical Review Letters **98**, 206805 (2007).

[56] K.-J. Jeon, Z. Lee, E. Pollak, L. Moreschini, A. Bostwick, C.-M. Park, R. Mendelsberg, V. Radmilovic, R. Kostecki, T.J. Richardson, and E. Rotenberg, ACS Nano **5**, 1042 (2011).

[57] A.A. Balandin, S. Ghosh, W. Bao, I. Calizo, D. Teweldebrhan, F. Miao, and C.N. Lau, Nano Letters **8**, 902 (2008).

[58] K.I. Bolotin, K.J. Sikes, Z. Jiang, M. Klima, G. Fudenberg, J. Hone, P. Kim, and H.L. Stormer, Solid State Communications **146**, 351 (2008).

[59] F. Schedin, A.K. Geim, S. V Morozov, E.W. Hill, P. Blake, M.I. Katsnelson, and K.S. Novoselov, Nature Materials **6**, 652 (2007).

[60] S. Pang, Y. Hernandez, X. Feng, and K. Müllen, Advanced Materials **23**, 2779 (2011).

[61] J.-Y. Lee, S.T. Connor, Y. Cui, and P. Peumans, Nano Letters **8**, 689 (2008).

[62] Y.-M. Chang, L. Wang, and W.-F. Su, Organic Electronics **9**, 968 (2008).

[63] Z. Wu, Z. Chen, X. Du, J.M. Logan, J. Sippel, M. Nikolou, K. Kamaras, J.R. Reynolds, D.B. Tanner, A.F. Hebard, and A.G. Rinzler, Science **305**, 1273 (2004).

[64] P.W. Chiu, G.T. Kim, G. Gu, G. Philipp, and S. Roth, in *AIP Conference Proceedings* (AIP, 2001), p. 368.

[65] X. Wang, L. Zhi, and K. Müllen, Nano Letters **8**, 323 (2008).

[66] X. Wang, L. Zhi, N. Tsao, Z. Tomović, J. Li, and K. Müllen, Angewandte Chemie **47**, 2990 (2008).

[67] L. Gomez De Arco, Y. Zhang, C.W. Schlenker, K. Ryu, M.E. Thompson, and C. Zhou, ACS Nano **4**, 2865 (2010).

[68] P. Matyba, H. Yamaguchi, G. Eda, M. Chhowalla, L. Edman, and N.D. Robinson, ACS Nano **4**, 637 (2010).

[69] G. Jo, M. Choe, C.-Y. Cho, J.H. Kim, W. Park, S. Lee, W.-K. Hong, T.-W. Kim, S.-J. Park, B.H. Hong, Y.H. Kahng, and T. Lee, Nanotechnology **21**, 175201 (2010).

[70] J. Wu, M. Agrawal, H.A. Becerril, Z. Bao, Z. Liu, Y. Chen, and P. Peumans, ACS Nano **4**, 43 (2010).

[71] P. Blake, P.D. Brimicombe, R.R. Nair, T.J. Booth, D. Jiang, F. Schedin, L.A. Ponomarenko, S. V Morozov, H.F. Gleeson, E.W. Hill, A.K. Geim, and K.S. Novoselov, Nano Letters **8**, 1704 (2008).

[72] W. Liu, B.L. Jackson, J. Zhu, C.-Q. Miao, C.-H. Chung, C.-H. Chung, Y.-J. Park, K. Sun, J. Woo, and Y.-H. Xie, ACS Nano **4**, 3927 (2010).

[73] C.-A. Di, D. Wei, G. Yu, Y. Liu, Y. Guo, and D. Zhu, Advanced Materials **20**, 3289 (2008).

[74] S. Pang, H.N. Tsao, X. Feng, and K. Müllen, Advanced Materials **21**, 3488 (2009).

[75] R.R. Nair, P. Blake, A.N. Grigorenko, K.S. Novoselov, T.J. Booth, T. Stauber, N.M.R. Peres, and A.K. Geim, Science **320**, 1308 (2008).

[76] D.I. Son, T.W. Kim, J.H. Shim, J.H. Jung, D.U. Lee, J.M. Lee, W. Il Park, and W.K. Choi, Nano Letters **10**, 2441 (2010).

[77] K.J. Kuhn, *Moore's Law Past 32nm : Future Challenges in Device Scaling* (2010).

[78] Y. Wu, Y. Lin, A.A. Bol, K.A. Jenkins, F. Xia, D.B. Farmer, Y. Zhu, and P. Avouris, Nature **472**, 74 (2011).

[79] R. Murali, K. Brenner, Y. Yang, T. Beck, and J.D. Meindl, IEEE Electron Device Letters **30**, 611 (2009).

[80] M.D. Stoller, S. Park, Y. Zhu, J. An, and R.S. Ruoff, Nano Letters **8**, 3498 (2008).

[81] M.F. El-Kady, V. Strong, S. Dubin, and R.B. Kaner, Science **335**, 1326 (2012).

[82] P. Dutta and P. Horn, Reviews of Modern Physics **53**, 497 (1981).

[83] S. Wu, Z. Yin, Q. He, X. Huang, X. Zhou, and H. Zhang, The Journal of Physical Chemistry C **114**, 11816 (2010).

[84] S. Wang, B.M. Goh, K.K. Manga, Q. Bao, P. Yang, and K.P. Loh, ACS Nano **4**, 6180 (2010).

[85] X. Qi, K.-Y. Pu, H. Li, X. Zhou, S. Wu, Q.-L. Fan, B. Liu, F. Boey, W. Huang, and H. Zhang, Angewandte Chemie **49**, 9426 (2010).

[86] M. Jahan, Q. Bao, J.-X. Yang, and K.P. Loh, Journal of the American Chemical Society **132**, 14487 (2010).

[87] C. Lu, H. Yang, C. Zhu, X. Chen, and G. Chen, Angewandte Chemie **121**, 4879 (2009).

[88] X. Dong, B. Li, A. Wei, X. Cao, M.B. Chan-Park, H. Zhang, L.-J. Li, W. Huang, and P. Chen, Carbon **49**, 2944 (2011).

[89] Z.-S. Wu, W. Ren, L. Wen, L. Gao, J. Zhao, Z. Chen, G. Zhou, F. Li, and H.-M. Cheng, ACS Nano **4**, 3187 (2010).

[90] W. Shi, J. Zhu, D.H. Sim, Y.Y. Tay, Z. Lu, X. Zhang, Y. Sharma, M. Srinivasan, H. Zhang, H.H. Hng, and Q. Yan, Journal of Materials Chemistry **21**, 3422 (2011).

[91] Y. Li, L. Tang, and J. Li, Electrochemistry Communications **11**, 846 (2009).

[92] Z. Yin, S. Wu, X. Zhou, X. Huang, Q. Zhang, F. Boey, and H. Zhang, Small **6**, 307 (2010).

[93] J. Liu, H. Bai, Y. Wang, Z. Liu, X. Zhang, and D.D. Sun, Advanced Functional Materials **20**, 4175 (2010).

[94] X. Ling, L. Xie, Y. Fang, H. Xu, H. Zhang, J. Kong, M.S. Dresselhaus, J. Zhang, and Z. Liu, Nano Letters **10**, 553 (2010).

[95] S. Gilje, S. Han, M. Wang, K.L. Wang, and R.B. Kaner, Nano Letters **7**, 3394 (2007).

[96] Z. Luo, P.M. Vora, E.J. Mele, A.T.C. Johnson, and J.M. Kikkawa, Applied Physics Letters **94**, 111909 (2009).

[97] X. Wu, M. Sprinkle, X. Li, F. Ming, C. Berger, and W. de Heer, Physical Review Letters **101**, 026801 (2008).

[98] D.C. Elias, R.R. Nair, T.M.G. Mohiuddin, S. V Morozov, P. Blake, M.P. Halsall, A.C. Ferrari, D.W. Boukhvalov, M.I. Katsnelson, A.K. Geim, and K.S. Novoselov, Science **323**, 610 (2009).

[99] S.-H. Cheng, K. Zou, F. Okino, H.R. Gutierrez, A. Gupta, N. Shen, P.C. Eklund, J.O. Sofo, and J. Zhu, Physical Review B **81**, 205435 (2010).

[100] S. Ryu, M.Y. Han, J. Maultzsch, T.F. Heinz, P. Kim, M.L. Steigerwald, and L.E. Brus, Nano Letters **8**, 4597 (2008).

[101] A. Savchenko, Science (New York, N.Y.) **323**, 589 (2009).

[102] A.K. Singh, E.S. Penev, and B.I. Yakobson, ACS Nano **4**, 3510 (2010).

[103] J. Sofo, A. Chaudhari, and G. Barber, Physical Review B **75**, 153401 (2007).

[104] T. Wassmann, A. Seitsonen, A. Saitta, M. Lazzeri, and F. Mauri, Physical Review Letters **101**, 096402 (2008).

[105] D. Yu and F. Liu, Nano Letters **7**, 3046 (2007).

[106] J. Zhou, Q. Wang, Q. Sun, X.S. Chen, Y. Kawazoe, and P. Jena, Nano Letters **9**, 3867 (2009).

[107] J. Chattopadhyay, A. Mukherjee, C.E. Hamilton, J. Kang, S. Chakraborty, W. Guo, K.F. Kelly, A.R. Barron, and W.E. Billups, Journal of the American Chemical Society **130**, 5414 (2008).

[108] K.S. Subrahmanyam, S.R.C. Vivekchand, A. Govindaraj, and C.N.R. Rao, Journal of Materials Chemistry **18**, 1517 (2008).

[109] J.W. Peckett, P. Trens, R.D. Gougeon, A. Pöppl, R.K. Harris, and M.J. Hudson, Carbon **38**, 345 (2000).

[110] M.J. Hudson, F.R. Hunter-Fujita,, J.W. Peckett, and P.M. Smith, Journal of Materials Chemistry **7**, 301 (1997).

[111] Z. Luo, Y. Lu, L.A. Somers, and A.T.C. Johnson, Journal of the American Chemical Society **131**, 898 (2009).

[112] D. V Kosynkin, A.L. Higginbotham, A. Sinitskii, J.R. Lomeda, A. Dimiev, B.K. Price, and J.M. Tour, Nature **458**, 872 (2009).

[113] L. Jiao, L. Zhang, X. Wang, G. Diankov, and H. Dai, Nature **458**, 877 (2009).

[114] A. Sinitskii, A. Dimiev, D.A. Corley, A.A. Fursina, D. V Kosynkin, and J.M. Tour, ACS Nano **4**, 1949 (2010).

[115] R. Sharma, J.H. Baik, C.J. Perera, and M.S. Strano, Nano Letters **10**, 398 (2010).

[116] P. Cui, S. Seo, J. Lee, L. Wang, E. Lee, M. Min, and H. Lee, ACS Nano **5**, 6826 (2011).

[117] R.K. Joshi, H. Gomez, F. Alvi, and A. Kumar, The Journal of Physical Chemistry C **114**, 6610 (2010).

[118] N. Jung, N. Kim, S. Jockusch, N.J. Turro, P. Kim, and L. Brus, Nano Letters **9**, 4133 (2009).

[119] T.O. Wehling, K.S. Novoselov, S. V Morozov, E.E. Vdovin, M.I. Katsnelson, A.K. Geim, and A.I. Lichtenstein, Nano Letters **8**, 173 (2008).

[120] W. Zhang, C.-T. Lin, K.-K. Liu, T. Tite, C.-Y. Su, C.-H. Chang, Y.-H. Lee, C.-W. Chu, K.-H. Wei, J.-L. Kuo, and L.-J. Li, ACS Nano **5**, 7517 (2011).

[121] F. Yavari, C. Kritzinger, C. Gaire, L. Song, H. Gulapalli, T. Borca-Tasciuc, P.M. Ajayan, and N. Koratkar, Small **6**, 2535 (2010).

[122] X. An, T. Simmons, R. Shah, C. Wolfe, K.M. Lewis, M. Washington, S.K. Nayak, S. Talapatra, and S. Kar, Nano Letters **10**, 4295 (2010).

[123] Y. Liang, D. Wu, X. Feng, and K. Müllen, Advanced Materials **21**, 1679 (2009).

[124] M. Lotya, P. J King, U. Khan, S. De, and J. N Coleman, ACS Nano **4**, 3155 (2010).

[125] Y. Hernandez, V. Nicolosi, M. Lotya, F.M. Blighe, Z. Sun, S. De, I.T. McGovern, B. Holland, M. Byrne, Y.K. Gun'Ko, J.J. Boland, P. Niraj, G. Duesberg, S. Krishnamurthy, R. Goodhue, J. Hutchison, V. Scardaci, A.C. Ferrari, and J.N. Coleman, Nature Nanotechnology **3**, 563 (2008).

[126] Y. Xu, H. Bai, G. Lu, C. Li, and G. Shi, Journal of the American Chemical Society **130**, 5856 (2008).

[127] Y. Xu, L. Zhao, H. Bai, W. Hong, C. Li, and G. Shi, Journal of the American Chemical Society **131**, 13490 (2009).

[128] X. Wang, S.M. Tabakman, and H. Dai, Journal of the American Chemical Society **130**, 8152 (2008).

[129] S. Vadukumpully, J. Paul, and S. Valiyaveettil, Carbon **47**, 3288 (2009).

[130] M. Lotya, Y. Hernandez, P.J. King, R.J. Smith, V. Nicolosi, L.S. Karlsson, F.M. Blighe, S. De, Z. Wang, I.T. McGovern, G.S. Duesberg, and J.N. Coleman, Journal of the American Chemical Society **131**, 3611 (2009).

[131] J. Guo, L. Ren, R. Wang, C. Zhang, Y. Yang, and T. Liu, Composites Part B: Engineering **42**, 2130 (2011).

[132] G. Wang, B. Wang, J. Park, Y. Wang, B. Sun, and J. Yao, Carbon **47**, 3242 (2009).

[133] Z. Jin, D. Nackashi, W. Lu, C. Kittrell, and J.M. Tour, Chemistry of Materials **22**, 5695 (2010).

[134] P. V. Kamat, The Journal of Physical Chemistry Letters **1**, 520 (2010).

[135] I. V Lightcap, T.H. Kosel, and P. V Kamat, Nano Letters **10**, 577 (2010).

[136] M. Machida, T. Mochimaru, and H. Tatsumoto, Carbon **44**, 2681 (2006).

[137] K. Vinodgopal, B. Neppolian, I. V. Lightcap, F. Grieser, M. Ashokkumar, and P. V. Kamat, The Journal of Physical Chemistry Letters **1**, 1987 (2010).

[138] J.L. Johnson, A. Behnam, S.J. Pearton, and A. Ural, Advanced Materials **22**, 4877 (2010).

[139] H. Wang, J.T. Robinson, G. Diankov, and H. Dai, Journal of the American Chemical Society **132**, 3270 (2010).

[140] L. Dong, R.R.S. Gari, Z. Li, M.M. Craig, and S. Hou, Carbon **48**, 781 (2010).

[141] R. Kou, Y. Shao, D. Wang, M.H. Engelhard, J.H. Kwak, J. Wang, V. V. Viswanathan, C. Wang, Y. Lin, Y. Wang, I.A. Aksay, and J. Liu, Electrochemistry Communications **11**, 954 (2009).

[142] Y. Li, L. Tang, and J. Li, Electrochemistry Communications **11**, 846 (2009).

[143] G.M. Scheuermann, L. Rumi, P. Steurer, W. Bannwarth, and R. Mülhaupt, Journal of the American Chemical Society **131**, 8262 (2009).

[144] E. Yoo, T. Okata, T. Akita, M. Kohyama, J. Nakamura, and I. Honma, Nano Letters **9**, 2255 (2009).

[145] M.J. Hollander, M. Labella, Z.R. Hughes, M. Zhu, K.A. Trumbull, R. Cavalero, D.W. Snyder, X. Wang, E. Hwang, S. Datta, and J.A. Robinson, Nano Letters **11**, 3601 (2011).

[146] B. Lee, S.-Y. Park, H.-C. Kim, K. Cho, E.M. Vogel, M.J. Kim, R.M. Wallace, and J. Kim, Applied Physics Letters **92**, 203102 (2008).

[147] D.B. Farmer, H.-Y. Chiu, Y.-M. Lin, K.A. Jenkins, F. Xia, and P. Avouris, Nano Letters **9**, 4474 (2009).

[148] V. Wheeler, N. Garces, L. Nyakiti, R. Myers-Ward, G. Jernigan, J. Culbertson, C. Eddy, and D. Kurt Gaskill, Carbon **50**, 2307 (2012).

[149] R. Hatada and K. Baba, Nuclear Intsruments and Methods in Physics Research B **148**, 655 (1999).

[150] K.A. Worsley, P. Ramesh, S.K. Mandal, S. Niyogi, M.E. Itkis, and R.C. Haddon, Chemical Physics Letters **445**, 51 (2007).

[151] O. Ruff, O. Bretschneider, and F. Ebert, Zeitschrift Für Anorganische Und Allgemeine Chemie **217**, 1 (1934).

[152] R. Taylor, J.H. Holloway, E.G. Hope, A.G. Avent, G.J. Langley, T.J. Dennis, J.P. Hare, H.W. Kroto, and D.R.M. Walton, Journal of the Chemical Society, Chemical Communications 665 (1992).

[153] E.T. Mickelson and C.B. Huffman, Chemical Physics Letters **296**, 188 (1998).

[154] S.-H. Cheng, K. Zou, F. Okino, H.R. Gutierrez, A. Gupta, N. Shen, P.C. Eklund, J.O. Sofo, and J. Zhu, Physical Review B **81**, 205435 (2010).

[155] F. Withers, M. Dubois, and A. Savchenko, Physical Review B **82**, 073403 (2010).

[156] J.T. Robinson, J.S. Burgess, C.E. Junkermeier, S.C. Badescu, T.L. Reinecke, F.K. Perkins, M.K. Zalalutdniov, J.W. Baldwin, J.C. Culbertson, P.E. Sheehan, and E.S. Snow, Nano Letters **10**, 3001 (2010).

[157] A. Grill, *Cold Plasma in Materials Fabrication: From Fundamentals to Applications* (IEEE Press, Piscataway, NJ, 1994).

[158] M. Baraket, S.G. Walton, E.H. Lock, J.T. Robinson, and F.K. Perkins, Applied Physics Letters **96**, 231501 (2010).

[159] H. Yang, M. Chen, H. Zhou, C. Qiu, L. Hu, F. Yu, W. Chu, S. Sun, and L. Sun, The Journal of Physical Chemistry C **115**, 16844 (2011).

[160] C. Shen, G. Huang, Y. Cheng, R. Cao, F. Ding, U. Schwingenschlögl, and Y. Mei, Nanoscale Research Letters **7**, 268 (2012).

[161] W.A. de Heer, C. Berger, M. Ruan, M. Sprinkle, X. Li, Y. Hu, B. Zhang, J. Hankinson, and E. Conrad, Proceedings of the National Academy of Sciences of the United States of America **108**, 16900 (2011).

[162] C.-M. Zetterling, editor, *Process Technology for Silicon Carbide Devices* (INSPEC, The Institution of Electrical Engineers, London, 2002), p. 88.

[163] L. Biedermann, M. Bolen, M. Capano, D. Zemlyanov, and R. Reifenberger, Physical Review B **79**, 125411 (2009).

[164] S. Hoste, D.F. Van De Vondel, and G.P. Van Der Kelen, Journal of Electron Spectroscopy and Related Phenomena **17**, 191 (1979).

[165] D.T. Clark, D. Kilcast, D.B. Adams, and W.K.R. Musgrave, Journal of Electron Spectroscopy and Related Phenomena **1**, 227 (1972).

[166] E. Rollings, G.-H. Gweon, S.Y. Zhou, B.S. Mun, J.L. McChesney, B.S. Hussain, A.V. Fedorov, P.N. First, W.A. de Heer, and A. Lanzara, Journal of Physics and Chemistry of Solids **67**, 2172 (2006).

[167] F. Tuinstra, The Journal of Chemical Physics **53**, 1126 (1970).

[168] C. Bittencourt, G. Van Lier, X. Ke, I. Suarez-Martinez, A. Felten, J. Ghijsen, G. Van Tendeloo, and C.P. Ewels, ChemPhysChem **10**, 920 (2009).

[169] T. Leung, C. Kao, W. Su, Y. Feng, and C. Chan, Physical Review B **68**, 195408 (2003).

[170] M. Chelvayohan, Journal of Physics C: Solid State Physics **16**, L323 (1983).

[171] J.A. Dillon and H.E. Farnsworth, Journal of Applied Physics **29**, 1195 (1958).

[172] R. Lawson and G. Carter, Vacuum **18**, 205 (1968).

[173] R.H. Friend, R.W. Gymer, A.B. Holmes, J.H. Burroughes, R.N. Marks, C. Taliani, D.D.C. Bradley, D.A. Dos Santos, J.L. Bredas, M. Logdlund, and W.R. Salaneck, Nature **397**, 121 (1999).

[174] G. Heimel, L. Romaner, E. Zojer, and J.-L. Bredas, Accounts of Chemical Research **41**, 721 (2008).

[175] H. Ishii, K. Sugiyama, E. Ito, and K. Seki, Advanced Materials **11**, 605 (1999).

[176] A. Kahn, N. Koch, and W. Gao, Journal of Polymer Science Part B: Polymer Physics **41**, 2529 (2003).

[177] I. Campbell, S. Rubin, T. Zawodzinski, J. Kress, R. Martin, D. Smith, N. Barashkov, and J. Ferraris, Physical Review B **54**, R14321 (1996).

[178] B. de Boer, A. Hadipour, M.M. Mandoc, T. van Woudenbergh, and P.W.M. Blom, Advanced Materials **17**, 621 (2005).

[179] C. Ganzorig, K.-J. Kwak, K. Yagi, and M. Fujihira, Applied Physics Letters **79**, 272 (2001).

[180] Y. Shi, K.K. Kim, A. Reina, M. Hofmann, L.-J. Li, and J. Kong, ACS Nano **4**, 2689 (2010).

[181] J. Park, W.H. Lee, S. Huh, S.H. Sim, S. Bin Kim, K. Cho, B.H. Hong, and K.S. Kim, The Journal of Physical Chemistry Letters **2**, 841 (2011).

[182] Y. Yi, W.M. Choi, Y.H. Kim, J. Won Kim, and S.J. Kang, Applied Physics Letters **98**, 013505 (2011).

[183] K.C. Kwon, K.S. Choi, and S.Y. Kim, Advanced Functional Materials **22**, 4724 (2012).

[184] K.C. Kwon, K.S. Choi, B.J. Kim, J.-L. Lee, and S.Y. Kim, The Journal of Physical Chemistry C **116**, 26586 (2012).

[185] S.D. Sherpa, S.A.. Paniagua, G. Levitin, S.R. Marder, M.D. Williams, and D.W. Hess, Journal of Vacuum Science & Technology B: Microelectronics and Nanometer Structures **30**, 03D102 (2012).

[186] D.T. Clark, W.J. Feast, D. Kilcast, and W.K.R. Musgrave, Journal of Polymer Science Part A: Polymer Chemistry **11**, 389 (1973).

[187] C.D. Wagner, W.M. Riggs, L.E. Davis, J.F. Moulder, and G.E. Mullenberg, *Handbook of X-ray Photoelectron Spectroscopy* (1979), p. 55344.

[188] T. Nakajima, *Fluorine-Carbon and Fluoride-Carbon Materials* (Marcel Dekker, New York, 1995), p. 25.

[189] T. Mallouk, B.L. Hawkins, M.P. Conrad, K. Zilm, G.E. Maciel, and N. Bartlett, Philosophical Transactions of the Royal Society A: Mathematical, Physical and Engineering Sciences **314**, 179 (1985).

[190] S.D. Sherpa, G. Levitin, and D.W. Hess, Applied Physics Letters **101**, 111602 (2012).

[191] T. Filleter, K. V. Emtsev, T. Seyller, and R. Bennewitz, Applied Physics Letters **93**, 133117 (2008).

[192] D. Sun, C. Divin, C. Berger, W.A. de Heer, P.N. First, and T.B. Norris, Physical Review Letters **104**, 136802 (2010).

[193] "Scanning Kelvin Probe Microscopy - Surface Potential Imaging with the XE-Series Atomic Force Microscope from Park Systems." Azonano.com/article.aspx?ArticleID=2555. 14 Feb 2013.

[194] A.G. Nagy, Journal of The Electrochemical Society **131**, 1871 (1984).

[195] A. Perret, P. Chabert, J.-P. Booth, J. Jolly, J. Guillon, and P. Auvray, Applied Physics Letters **83**, 243 (2003).

[196] L. Sansonnens, A. Pletzer, D. Magni, A.A. Howling, C. Hollenstein, and J.P.M. Schmitt, Plasma Sources Science and Technology **6**, 170 (1997).

[197] K.F. Kelly, E.T. Mickelson, R.H. Hauge, J.L. Margrave, and N.J. Halas, Proceedings of the National Academy of Sciences of the United States of America **97**, 10318 (2000).

[198] A.W. Tsen, L. Brown, R.W. Havener, and J. Park, Accounts of Chemical Research **XXX**, (2012).

[199] B. Wang, Y. Puzyrev, and S.T. Pantelides, Carbon **49**, 3983 (2011).

[200] Z. Wei, D. Wang, S. Kim, S.-Y. Kim, Y. Hu, M.K. Yakes, A.R. Laracuente, Z. Dai, S.R. Marder, C. Berger, W.P. King, W.A. de Heer, P.E. Sheehan, and E. Riedo, Science **328**, 1373 (2010).

VITA
SONAM DORJE SHERPA

Sonam is originally from Nepal. He finished his high school studies in Nepal and then came to the United States in 2002 for his undergraduate studies. He spent three semesters at Southern Arkansas University and then transferred to Louisiana State University (LSU) to study chemical engineering. He received his bachelors' degree in chemical engineering from LSU in May 2007 and graduated with magna cum laude honors. He started his doctoral studies in chemical engineering at Georgia Institute of Technology in the fall of 2008.

In his spare time, Sonam likes to watch and play soccer. As an avid soccer fan, he reads the tactical analysis of recently played soccer matches and follows the tactical evolutions in the game of soccer. Sonam is also a movie buff. Some of his favorite movies include Field of Dreams, Kramer v Kramer, and Moneyball. Lately, he has developed interest in reading and cooking.